



UNIVERSIDAD AUTÓNOMA
DE AGUASCALIENTES

CENTRO DE CIENCIAS BÁSICAS

DEPARTAMENTO DE MATEMÁTICAS Y FÍSICA

TESIS

STRUCTURE-PRESERVING METHODS FOR RIESZ
SPACE-FRACTIONAL SINE-GORDON EQUATIONS

PRESENTA

Luis Fernando Martínez Álvarez

PARA OPTAR POR EL GRADO DE MAESTRO EN CIENCIAS EN
MATEMÁTICAS APLICADAS

TUTOR

Dr. Jorge Eduardo Macías-Díaz

COMITÉ TUTORAL

Dr. José Villa Morales
Dr. Manuel Ramírez Aranda

Aguascalientes, Ags., 16 de Febrero de 2018



UNIVERSIDAD AUTONOMA DE AGUASCALIENTES

FORMATO DE CARTA DE VOTO APROBATORIO

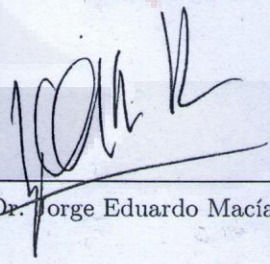
M. en C. José de Jesús Ruiz Gallegos
DECANO DEL CENTRO DE CIENCIAS BÁSICAS
PRESENTE

Por medio de la presente, en mi calidad de tutor designado del estudiante **LUIS FERNANDO MARTÍNEZ ÁLVAREZ** con ID 108447 quien realizó la tesis titulada: **STRUCTURE-PRESERVING METHODS FOR RIESZ SPACE-FRACTIONAL SINE-GORDON EQUATIONS**, y con fundamento en el Artículo 175, Apartado II del Reglamento General de Docencia, me permito emitir el **VOTO APROBATORIO**, para que él pueda proceder a imprimirla, y así continuar con el procedimiento administrativo para la obtención del grado.

Pongo lo anterior a su digna consideración y, sin otro particular por el momento, me permito enviarle un cordial saludo.

ATENTAMENTE
"Se Lumen Proferre"

Aguascalientes, Ags., a 12 de Enero de 2018


Dr. Jorge Eduardo Macías-Díaz

- c.c.p.- Interesado
- c.c.p.- Secretaría de Investigación y Posgrado
- c.c.p.- Jefatura del Depto. de Matemáticas y Física
- c.c.p.- Consejero Académico
- c.c.p.- Minuta Secretario Técnico





UNIVERSIDAD AUTÓNOMA
DE AGUASCALIENTES

FORMATO DE CARTA DE VOTO APROBATORIO

M. en C. José de Jesús Ruiz Gallegos
DECANO DEL CENTRO DE CIENCIAS BÁSICAS
PRESENTE

Por medio de la presente, en mi calidad de sinodal designado del estudiante **LUIS FERNANDO MARTÍNEZ ÁLVAREZ** con ID 108447 quien realizó la tesis titulada: **STRUCTURE-PRESERVING METHODS FOR RIESZ SPACE-FRACTIONAL SINE-GORDON EQUATIONS**, y con fundamento en el Artículo 175, Apartado II del Reglamento General de Docencia, me permito emitir el **VOTO APROBATORIO**, para que él pueda proceder a imprimirla, y así continuar con el procedimiento administrativo para la obtención del grado.

Pongo lo anterior a su digna consideración y, sin otro particular por el momento, me permito enviarle un cordial saludo.

ATENTAMENTE

“Se Lumen Proferre”

Aguascalientes, Ags., a 12 de Enero de 2018

Dr. Manuel Ramírez Aranda

- c.c.p.- Interesado
- c.c.p.- Secretaría de Investigación y Posgrado
- c.c.p.- Jefatura del Depto. de Matemáticas y Física
- c.c.p.- Consejero Académico
- c.c.p.- Minuta Secretario Técnico





UNIVERSIDAD AUTÓNOMA
DE AGUASCALIENTES

FORMATO DE CARTA DE VOTO APROBATORIO

M. en C. José de Jesús Ruiz Gallegos
DECANO DEL CENTRO DE CIENCIAS BÁSICAS
PRESENTE

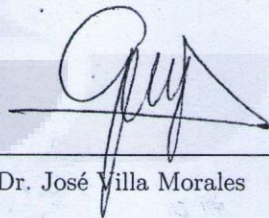
Por medio de la presente, en mi calidad de sinodal designado del estudiante **LUIS FERNANDO MARTÍNEZ ÁLVAREZ** con ID 108447 quien realizó la tesis titulada: **STRUCTURE-PRESERVING METHODS FOR RIESZ SPACE-FRACTIONAL SINE-GORDON EQUATIONS**, y con fundamento en el Artículo 175, Apartado II del Reglamento General de Docencia, me permito emitir el **VOTO APROBATORIO**, para que él pueda proceder a imprimirla, y así continuar con el procedimiento administrativo para la obtención del grado.

Pongo lo anterior a su digna consideración y, sin otro particular por el momento, me permito enviarle un cordial saludo.

ATENTAMENTE

“Se Lumen Proferre”

Aguascalientes, Ags., a 12 de Enero de 2018



Dr. José Villa Morales

- c.c.p.- Interesado
- c.c.p.- Secretaría de Investigación y Posgrado
- c.c.p.- Jefatura del Depto. de Matemáticas y Física
- c.c.p.- Consejero Académico
- c.c.p.- Minuta Secretario Técnico





UNIVERSIDAD AUTÓNOMA
DE AGUASCALIENTES

LUIS FERNANDO MARTÍNEZ ÁLVAREZ
MAESTRÍA EN CIENCIAS CON OPCIÓN A LA COMPUTACIÓN Y
MATEMÁTICAS APLICADAS
PRESENTE.

Estimado alumno:

Por medio de este conducto me permito comunicar a Usted que habiendo recibido los votos aprobatorios de los revisores de su trabajo de tesis y/o caso práctico titulado: **“STRUCTURE-PRESERVING METHODS FOR RIESZ SPACE-FRACTIONAL SINE-GORDON EQUATIONS”**, hago de su conocimiento que puede imprimir dicho documento y continuar con los trámites para la presentación de su examen de grado.

Sin otro particular me permito saludarle muy afectuosamente.

ATENTAMENTE

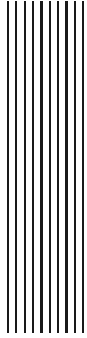
Aguascalientes, Ags., a 15 de enero de 20118

“Se lumen proferre”

EL DECANO

M. en C. JOSÉ DE JESÚS RUÍZ GALLEGOS

c.c.p.- Archivo.

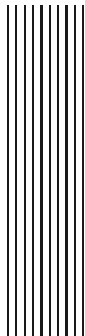


Acknowledgments

Firstly, I gratefully thank my institution, the Universidad Autónoma de Aguascalientes, for allowing me to continue with my education as a professional, and for providing me with the opportunity to conclude my studies in the master in sciences program in applied mathematics. Secondly, I would like to express my sincere gratitude to my advisor, Dr. Jorge Eduardo Macías-Díaz, for his continuous support during my master's studies and related research, for his patience, motivation, and immense knowledge. His guidance helped me throughout my research and the development of this thesis. I could not have imagined having a better advisor and mentor for my studies. Finally, I must express my most profound gratitude to my parents and friends for providing me with unfailing support and continuous encouragement throughout my years of study and through this stage of my life. This accomplishment would not have been possible without them.

Thank you!

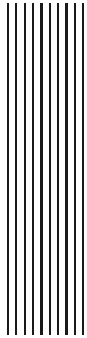
Luis Fernando Martínez Álvarez



Contents

List of Tables	3
List of Figures	3
Resumen	7
Abstract	8
Introduction	9
1 Preliminaries	12
1.1 Basic definitions	12
1.2 Important partial differential equations	14
1.3 Modified Klein-Gordon equations	17
1.4 Elementary solutions	20
1.5 Elements of numerical analysis	24
1.6 Finite differences	27
2 Numerical method for a nonlinear chain	33
2.1 Introduction	33
2.2 Analytical results	34
2.3 Numerical analysis	38
2.4 Numerical results	42
2.5 Application	47
3 Numerical method for a fractional medium	50
3.1 Introduction	50
3.2 Preliminaries	53
3.3 Numerical method	55
3.4 Energy invariants	57
3.5 Auxiliary lemmas	60
3.6 Numerical results	64

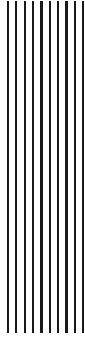




List of Tables

1.1 Different types of soliton solutions of the sine-Gordon equation. 23





List of Figures

1.1	Schematic representation of a small Josephson junction.	18
1.2	Schematic representation of a long Josephson junction.	19
1.3	Soliton solution (solid line) and anti-soliton solution (dotted line) of the sine-Gordon equation at time 0, with $v = 0.1$	22
1.4	Soliton solution (solid line) and anti-soliton solution (dotted line) of the Landau-Ginzburg equation at time 0, with $v = 0.1$	24
1.5	Computational grid and example of backward (red dashed line), forward (blue dashed line) and centered (magenta dashed line) linear interpolation to the function.	28
2.1	Approximate solution $u_{60}(t)$ of a sine-Gordon system in the first row and a Klein-Gordon system in the second, for a driving frequency of 0.9 and two different amplitude values A : (a) before and (b) after the bifurcation threshold.	35
2.2	Graphs of total energy transmitted into the massless sine-Gordon and Klein-Gordon systems vs. driving amplitude for a driving frequency of 0.9, with $\beta = 0$ and $\gamma = 0$ (solid), 0.01 (dashed), 0.02 (dash-dotted), 0.03 (dotted).	36
2.3	Total energy transmitted into the sine-Gordon system vs. driving amplitude for a driving frequency of 0.9, with $\beta = 0$, $\gamma = 0.01$, and pure-imaginary and real masses of magnitude 0 (solid), 0.05 (dashed), 0.075 (dash-dotted) and 0.1 (dotted).	37
2.4	Graphs of total energy transmitted into the massless sine-Gordon and Klein-Gordon systems vs. driving amplitude for a driving frequency of 0.9, with $\gamma = 0$ and $\beta = 0$ (solid), 0.1 (dashed), 0.2 (dash-dotted), 0.3 (dotted).	38
2.5	Total energy transmitted into the sine-Gordon system vs. driving amplitude for a driving frequency of 0.9, with $\beta = 0.2$, $\gamma = 0$, and pure-imaginary and real masses of magnitude 0 (solid), 0.05 (dashed), 0.075 (dash-dotted) and 0.1 (dotted).	40
2.6	Graphs of total energy vs. driving frequency and amplitude for massless and undamped sine-Gordon and Klein-Gordon chains of coupled oscillators.	42
2.7	Diagram of smallest driving amplitude value at which supratransmission begins vs. driving frequency for a massless system with $\beta = 0$ and values of γ equal to 0 (solid), 0.1 (dashed), 0.2 (dash-dotted) and 0.3 (dotted). The theoretical threshold A_s in the undamped is shown as a sequence of \times -marks.	43

2.8 Diagram of smallest driving amplitude value at which supratransmission begins vs. driving frequency for a massless system with $\gamma = 0$ and values of β equal to 0 (solid), 0.1 (dashed), 0.4 (dash-dotted) and 0.7 (dotted). The theoretical threshold A_s in the undamped case is shown as a sequence of \times -marks. 44

2.9 Diagram of smallest driving amplitude value at which supratransmission begins vs. driving frequency for an undamped sine-Gordon system with $\sqrt{m_\ell^2 + 1} = 1 + \frac{\ell}{40}$ for $\ell = -4, -2, -1, 0, 1, 2, 4$ 45

2.10 Time-dependent graphs of the position of the breathers generated in (2.3) by the binary signal ‘1111’. 46

2.11 Time-dependent graphs of the maximum energy of the breathers generated in (2.3) by the binary signal ‘1111’. 47

2.12 Local energy of the 100-th (left) and 300-th (right) sites in (2.3) vs. normalized time, as a response to the transmission of the binary signal ‘10111001011011101001’. 48

3.1 Forward-difference stencil for the approximation to the exact solution of the one dimensional form of (3.3) at the time t_n , using the finite-difference scheme (3.28). The black circles represent the known approximations at the times t_{n-1} , t_n and t_{n+1} , while the cross denotes the unknown approximation at the time t_{n+2} 56

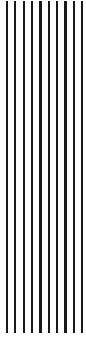
3.2 Graphs of the numerical solution (left column) and the associated energy density (right column) of the one-dimensional problem (3.3) with $G(u) = 1 - \cos u$ obtained using (3.28) and (3.46) on $\Omega = (-30, 30) \times (0, 100)$. The initial data were provided by (3.93) with $\omega = 0.9$, and the parameters employed were $\gamma = 0$, $h_1 = 0.5$ and $\tau = 0.05$. Various derivative orders were used, namely, $\alpha_1 = 2$ (top row), $\alpha_1 = 1.6$ (middle row) and $\alpha_1 = 1.2$ (bottom row). The insets of the graphs of the right column represent the discrete dynamics of the total energy (3.40) of the system. 67

3.3 Graphs of the numerical solution (left column) and the associated energy density (right column) of the one-dimensional problem (3.3) with $G(u) = 1 - \cos u$ obtained using (3.28) and (3.46) on $\Omega = (-30, 30) \times (0, 100)$. The initial data were provided by (3.93) with $\omega = 0.9$, and the parameters employed were $\gamma = 0.05$, $h_1 = 0.5$ and $\tau = 0.05$. Various derivative orders were used, namely, $\alpha_1 = 2$ (top row), $\alpha_1 = 1.6$ (middle row) and $\alpha_1 = 1.2$ (bottom row). The insets of the graphs of the right column represent the discrete dynamics of the total energy (3.40) of the system. 68

3.4 Graphs of the approximate solution of (3.3) in two spatial dimensions at the times (a) $t = 0.22$, (b) $t = 0.34$, (c) $t = 0.46$, (d) $t = 0.58$, (e) $t = 0.70$ and (f) $t = 0.82$. The model parameters employed were $\alpha_1 = 1.8$, $\alpha_2 = 1.6$, $\gamma = 0$, $G(u) = 1 - \cos u$, $B = (-5, 5) \times (-5, 5)$ and $T = 10$. Meanwhile, the initial conditions were provided by $\varphi(x^2 + y^2, t)$, where φ is given by (3.93) with $\omega = 0.8$. Numerically, we used the method (3.28) with $M_1 = M_2 = 100$ and $N = 500$ 69

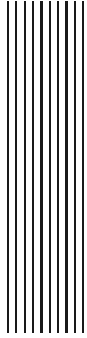
3.5 Graphs of the energy dynamics of the solution of (3.3) in two spatial dimensions using various sets of the parameters α_1 and α_2 , $G(u) = 1 - \cos u$, $B = (-5, 5) \times (-5, 5)$ and $T = 10$. The initial conditions were provided by $\varphi(x^2 + y^2, t)$, where φ is given by (3.93) with $\omega = 0.8$, and various damping coefficients were considered, namely, $\gamma = 0$ (solid), $\gamma = 0.01$ (dashed), $\gamma = 0.02$ (dashed-dotted) and $\gamma = 0.03$ (dotted). Numerically, we used the method (3.28) with $M_1 = M_2 = 100$ and $N = 500$ 70





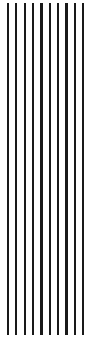
Resumen

En este capítulo investigamos numéricamente un modelo gobernado por una ecuación de onda no lineal multidimensional con amortiguamiento y difusión fraccionaria. La ecuación en cuestión es una ecuación diferencial parcial que considera la presencia de derivadas fraccionarias de Riesz de órdenes en $(1, 2]$, así como una condición de Dirichlet homogénea sobre un dominio espacial cerrado y acotado. El modelo de investigación posee una función de energía que se conserva en el régimen sin amortiguamiento. En el caso amortiguado, establecemos la propiedad de disipación de energía del modelo usando argumentos de análisis funcional. Motivados por estos resultados, proponemos una discretización explícita en diferencias finitas de nuestro modelo fraccionario, basado en el uso de diferencias centradas fraccionadas. Asociado a nuestro modelo discreto, también proponemos discretizaciones de las cantidades de energía. Más aún, establecemos el hecho que en el régimen sin amortiguamiento se conserva la energía discreta, y que se disipa en el escenario amortiguado. Entre las más importantes características numéricas de nuestro esquema, se muestra que el método tiene una consistencia de segundo orden, que es estable y que tiene un orden cuadrático de convergencia. En esta tesis se muestran algunas simulaciones de una y dos dimensiones para ilustrar el hecho de que la técnica es capaz de preservar la energía discreta en el régimen sin amortiguamiento.



Abstract

In this chapter, we investigate numerically a model governed by a multidimensional nonlinear wave equation with damping and fractional diffusion. The governing partial differential equation considers the presence of Riesz space-fractional derivatives of orders in $(1, 2]$, and homogeneous Dirichlet boundary data are imposed on a closed and bounded spatial domain. The model under investigation possesses an energy function which is preserved in the undamped regime. In the damped case, we establish the property of energy dissipation of the model using arguments from functional analysis. Motivated by these results, we propose an explicit finite-difference discretization of our fractional model based on the use of fractional centered differences. Associated to our discrete model, we also propose discretizations of the energy quantities. We establish that the discrete energy is conserved in the undamped regime, and that it dissipates in the damped scenario. Among the most important numerical features of our scheme, we show that the method has a consistency of second order, that it is stable and that it has a quadratic order of convergence. Some one- and two-dimensional simulations are shown in this chapter to illustrate the fact that the technique is capable of preserving the discrete energy in the undamped regime.



Introduction

Aims and scope

The design of numerical methods that preserve the discrete energy of conservative systems governed by partial differential equations has been an important area of research in computational physics [15, 107]. Many different approaches have been employed in order to provide numerical techniques that preserve the total energy of discrete models, including finite differences [117], mimetic finite differences [54], finite elements [33], Galerkin methods [24], symplectic techniques [115], G-symplectic schemes [23] and finite pointset methods [56] among other approaches. Historically, the development of numerical techniques that preserve physical properties of the solutions of systems of partial differential equations was popularized by D. Furihata and coworkers at the turn of the 21st century [30, 31]. Many reports on the design of numerical techniques that preserve physical or mathematical invariants of systems of partial differential equations were proposed afterwards [14], including manuscripts on methods that preserve the mass [42] and the momentum [98] of a system. Of course, many physical applications have been proposed using those techniques.

The design of techniques to approximate the solution of physical systems has been largely enriched with the study of partial differential equations of fractional orders. Indeed, fractional calculus has found interesting applications in many fields of the natural sciences and engineering, including the theory of viscoelasticity [48], the theory of thermoelasticity [82], financial problems under a continuous time frame [89], self-similar protein dynamics [37] and quantum mechanics [74]. Distributed-order fractional diffusion-wave equations are used in groundwater flow modelling to and from wells [96, 79]. A vast amount of nonequivalent approaches have been followed, and new criteria of fractional differentiation have been proposed constantly in the last decades. However, the problem in those cases is the common lack of a physically meaningful formulation of the Euler–Lagrange formality for fractional variational systems [2]. As expected, this has been a major problem in the design of energy-preserving method for fractional partial differential equations.

In spite of this shortcoming, many of the partial differential equations from mathematical physics have been extended to the fractional scenario. Physically, problems that only considered local contributions to the dynamics of discrete or continuous systems have been extended to account for global effects. In such way, various classical models that were traditionally described by partial differential equations have been formulated using derivatives of fractional order under different approaches

[88, 75, 102]. Among the models that have been extended to the fractional scenario are the classical nonlinear wave equations [84, 4]. Here, it is important to point out that the Riesz definition of spatial derivatives of fractional order has been extensively employed in order to account physically for anomalous diffusion [38], and to provide pertinent conservation laws and Hamiltonian-like equations [105]. In view of these remarks, a natural question that arises immediately is whether it is feasible to propose finite-difference discretizations of nonlinear hyperbolic equations with Riesz space-fractional derivatives, in such way that known conservation laws are likewise conserved in the discrete domain.

The purpose of this thesis is to provide a discretization of Riesz space-fractional models that generalizes the well-known wave equation with a general nonlinear potential. The continuous model is complemented by suitable initial and boundary constraints on a closed and bounded spatial interval. An energy-like functional that resembles the Hamiltonian of classical nonlinear wave equations is already available for our fractional model. Using these facts, we propose a numerical method based on fractional centered differences to approximate the solutions of our fractional system. The method is implicit and nonlinear, so its implementation requires Newton's method for the solution of systems of nonlinear equations. As we will see in this manuscript, the finite-difference method possesses a quantity that estimates the pseudo-energy of the system and, moreover, we will show that this quantity is conserved at each temporal step. This fact will be confirmed through some numerical experiments, and an application to a novel generalized nonlinear problem in physics will be proposed at the end of this thesis.

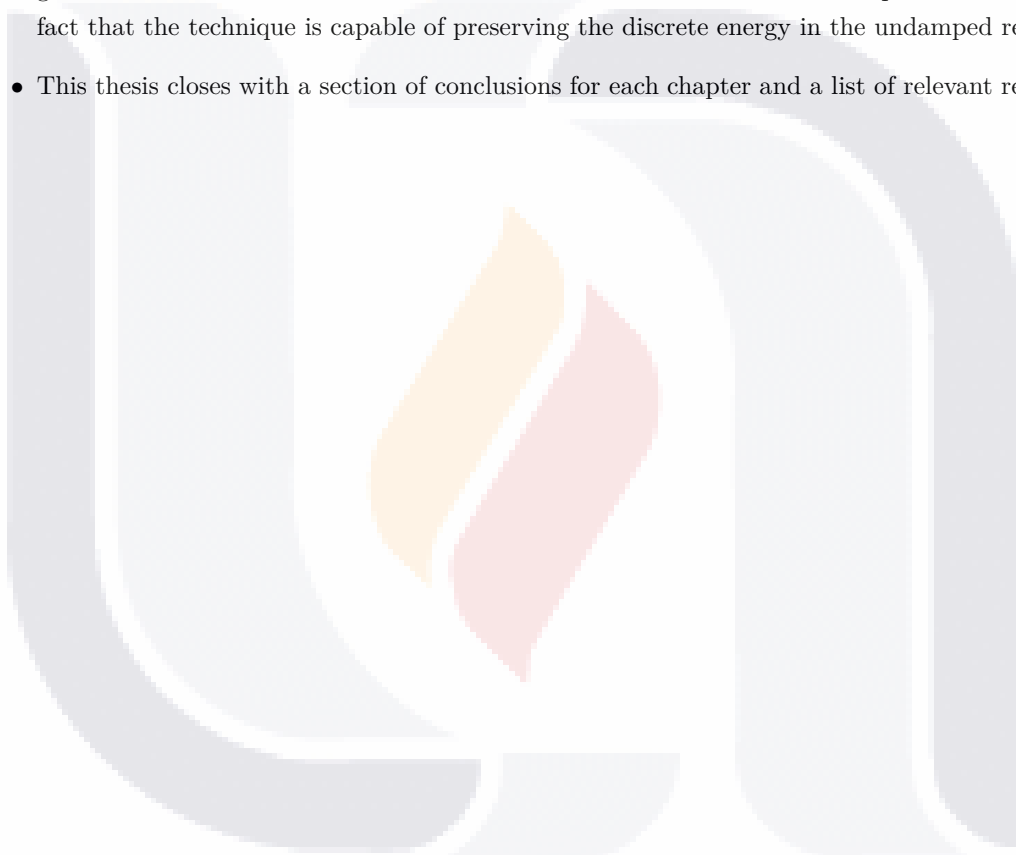
Summary

This thesis is sectioned as follows.

- Chapter 1 provides a list of important second-order partial differential equations that constitute particular cases of the equation under study. We state the general form of our problem, describe the most important applications that it models, and provide analytical methods to compute solution and, particularly, soliton-like solutions to several particular cases. We close this chapter stating some important definitions and results from numerical analysis that we use in this thesis without reference.
- Chapter 2 presents a discrete space, mixed-value problem version of the model introduced in the previous chapter. The model under study in this section describes the motion of a semi-infinite chain of coupled oscillators with damping, subject to harmonic driving at the free end. In this chapter, we derive a finite-difference scheme to approximate solutions to our new problem, and derive energy properties of the system. The study of the process of nonlinear supratransmission of the chain is carried out in detail, and we obtain bifurcation diagrams to predict the occurrence of nonlinear supratransmission under the presence of the parameters of the model. In that stage, we show how nonlinear supratransmission in nonlinear chains of coupled oscillators can be controlled in order to achieve a successful transmission of binary information.
- In Chapter 3, we investigate numerically a model governed by a multidimensional nonlinear wave equation with damping and fractional diffusion. The governing partial differential equation considers the presence of Riesz space-fractional derivatives of orders in $(1, 2]$, and homogeneous

Dirichlet boundary data are imposed on a closed and bounded spatial domain. The model under investigation possesses an energy function which is preserved in the undamped regime. In the damped case, we establish the property of energy dissipation of the model using arguments from functional analysis. Motivated by these results, we propose an explicit finite-difference discretization of our fractional model based on the use of fractional centered differences. Associated to our discrete model, we also propose discretizations of the energy quantities. We establish that the discrete energy is conserved in the undamped regime, and that it dissipates in the damped scenario. Among the most important numerical features of our scheme, we show that the method has a consistency of second order, that it is stable and that it has a quadratic order of convergence. Some one- and two-dimensional simulations are shown in this chapter to illustrate the fact that the technique is capable of preserving the discrete energy in the undamped regime.

- This thesis closes with a section of conclusions for each chapter and a list of relevant references.



1. Preliminaries

The nonlinear Klein-Gordon equation is one of the most important and simplest nonlinear differential equations that appear in relativistic quantum mechanics. As a second-order partial differential equation, the Klein-Gordon equation generalizes several other important problems in various branches of physics, chemistry and mathematical biology that range from the classical diffusion equation to the stochastic Fisher-KPP equation, from the classical wave equation to the Schrödinger and the telegrapher's equations. The present chapter is devoted to introduce and evidence the importance of the differential equation under study in this thesis. We also present some important definitions and results of numerical analysis that will be used without reference in further chapters.

1.1 Basic definitions

By a **domain** we understand a closed connected subset of \mathbb{R}^n . A function u defined in a domain D is said to be have **compact support** if it is zero outside a compact subset of D . A function u defined on a domain D is called **smooth** in D if it has continuous partial derivatives of all orders in D . The function u is called **small at infinity** if for every \bar{x}_0 in the boundary of D ,

$$\lim_{\substack{\bar{x} \rightarrow \bar{x}_0 \\ \bar{x} \in D}} u(\bar{x}) = 0.$$

Let a, b, c, d and e be real numbers with at least one of a, b or c not equal to zero. A second-order partial differential equation in the variables x and y with constant coefficients is an equation of the form

$$a \frac{\partial^2 u}{\partial x^2} + b \frac{\partial^2 u}{\partial x \partial y} + c \frac{\partial^2 u}{\partial y^2} + d \frac{\partial u}{\partial x} + e \frac{\partial u}{\partial y} = F(x, y), \quad (1.1)$$

where u is a function of (x, y) usually assumed to be defined and of compact support in some domain D , that has continuous partial derivatives up to the second order in D . The number $b^2 - 4ac$ is called the **discriminant** of Equation (1.1) and yields a criterion to classify second-order partial differential equations:

- If $b^2 - 4ac > 0$ then Equation (1.1) is called a **hyperbolic** equation. As an example of this type

of equation we have the classical one-dimensional **wave equation**

$$\frac{\partial^2 u}{\partial x^2} = \frac{1}{\nu^2} \frac{\partial^2 u}{\partial t^2}.$$

It describes the vertical disturbance of a wave with phase velocity ν as it travels on the horizontal direction. The wave equation applies to a stretched string or a plane electromagnetic wave. Given initial and boundary conditions the wave equation can be solved exactly by using a Fourier transform method or via separation of variables.

- If $b^2 - 4ac = 0$ then Equation (1.1) is called a **parabolic** equation. An example of parabolic equation is the one-dimensional **diffusion equation** (also called **heat equation**)

$$\frac{\partial u}{\partial t} = \kappa \frac{\partial^2 u}{\partial x^2}.$$

This equation commonly arises in problems of heat conductivity. In those situations κ represents thermal diffusivity and u represents temperature. If initial and boundary conditions are given, the diffusion equation can be solved analytically by separation of variables.

- If $b^2 - 4ac < 0$ then Equation (1.1) is called an **elliptic** equation. **Laplace's equation**

$$\frac{\partial^2 u}{\partial x^2} + \frac{\partial^2 u}{\partial y^2} = 0$$

is an example of an elliptic equation. It is satisfied by the potential of any distribution of matter which attracts according to the Newtonian Law. A solution to Laplace's equation is uniquely determined if the value of the function or the normal derivative of the function is specified on all boundaries.

We must remark that the wave equation, the heat equation and Laplace's equation have generalizations that model the corresponding physical phenomena in three dimensions. For example, the **wave equation** in three space variables reads

$$\nabla^2 u = \frac{1}{\nu^2} \frac{\partial^2 u}{\partial t^2},$$

where u is a scalar function that depends on the space coordinate (x, y, z) and time t . The symbol ∇^2 denotes the **Laplacian** differential operator, which is the divergence of the gradient of a scalar function. With this notation the three-dimensional **diffusion equation** is described by the equation

$$\frac{\partial u}{\partial t} = \frac{1}{\kappa} \nabla^2 u,$$

and the three-dimensional **Laplace's equation** by

$$\nabla^2 u = 0.$$

Let V and ρ be scalar functions depending only on space. An important variation of the three-dimensional Laplace's equation occurs in classical electromagnetic theory when relating the electric

potential V of a distribution and its charge density ρ . The relation between V and ρ is described by the equation $\epsilon_0 \nabla^2 V = \rho$, which is called **Poisson's equation**. More generally, every equation of the form

$$\nabla^2 u = F(x, y, z, t),$$

where u is a scalar function depending on x, y, z and t , is called a Poisson equation. Another useful classification of second-order partial differential equations with constant coefficients is in terms of a property called *linearity*. Differential equation (1.1) is called **linear** if for arbitrary real constants k_1, k_2 and solutions u_1, u_2 of (1.1), $k_1 u_1 + k_2 u_2$ is also a solution of (1.1).

Finally, if the variable time is one of the independent variables of the scalar function u then the term $k \partial u / \partial t$ in the differential equation modeling u is called the **external damping term** and the constant k is called the **external damping coefficient**. The differential equation is said to be **damped** if k is not equal to zero, otherwise it is called **undamped**.

1.2 Important partial differential equations

Many other three-dimensional generalizations of the wave equation, the diffusion equation and Laplace's equation happen to appear in mathematical physics and biology. For example, the manipulation of Maxwell's equations to obtain propagating waves gives rise to the so called **Helmholtz equation** [120], whose general form is

$$\nabla^2 u + k^2 u = 0,$$

where k is a real constant and u is a scalar function in the variables x, y, z, t . Obviously, Helmholtz equation is a linear second-order partial differential equation that generalizes the three-dimensional wave equation.

Another physical example appears in the field of non-relativistic quantum mechanics: Let \hbar denote Planck's original constant divided by 2π . The wave function associated to a particle of mass m with potential scalar function V is a scalar function u that depends on the position vector (x, y, z) of the particle and the time t , given by the differential equation

$$i\hbar \frac{\partial u}{\partial t} = -\frac{\hbar^2}{2m} \nabla^2 u + Vu.$$

This differential equation is called **Schrödinger's equation**. In this equation the scalar function u may be complex, but the square of its modulus is a real scalar function that represents the probability density function associated with the location of the particle at any time. It is worth noticing that Schrödinger's equation provides a mathematical generalization of the three-dimensional diffusion equation. Observe that because the scalar function V does not need to be constant, Schrödinger's equation is a linear partial differential equation with not necessarily constant coefficients.

The relativistic counterpart of Schrödinger's equation is the Klein-Gordon equation. By the **linear Klein-Gordon equation** we understand the linear second-order partial differential equation

$$\nabla^2 u = \frac{1}{c^2} \frac{\partial^2 u}{\partial t^2} + m^2 u,$$

where m is a real constant and u is a scalar function of position and time. This is the equation for

a relativistic quantum-mechanical scalar (spin-zero) particle of mass m . The exact solution of this equation in the form of a traveling wave is given in [81]. An important nonlinear variation of this equation that often appears in the study of the collisional properties of **solitons** [78, 97], that is solitary waves, and a number of other physical applications [5, 36, 9] is the **sine-Gordon equation**

$$\nabla^2 u = \frac{1}{c^2} \frac{\partial^2 u}{\partial t^2} + m^2 \sin u.$$

Several nonlinear variations of the Klein-Gordon equation appear in many branches of physics, chemistry and other sciences. The **Landau-Ginzburg equation** is one of those equations. Studied by Lev Landau and Vitaly Grinzburg in 1950 while studying the theory of superconductivity, this equation is used to study simple periodic oscillations and the change of their amplitude and frequency with respect to initial excitations in problems that arise in oscillating chemical reactions and atomic physics. In dimensionless form, the three-dimensional Landau-Grinzburg equation is given by

$$\frac{\partial^2 u}{\partial t^2} - \nabla^2 u - m^2 u + G'(u) = 0$$

In mathematical biology, consider a population distributed in a linear habitat with uniform density. If at any point of the habitat a mutation advantageous to survival occurs then the mutant gene increases at the expense of the allelomorphs previously occupying the same locus. Mathematically, let u be the frequency of the mutant gene and let m be a constant representing intensity of selection in favor of the mutant gene. Then u must satisfy **Fisher's equation** (also called the **Fisher-KPP equation**)

$$\frac{\partial u}{\partial t} = k \frac{\partial^2 u}{\partial x^2} + F(u),$$

where k is a diffusion coefficient and u depends on the position x in the linear habitat and time t given in generations. This parabolic equation was simultaneously and independently investigated by Fisher [27] and Kolmogoroff *et al.* [49], using $F(u) = mu(1 - u)$. It is used also in describing the process of epidermal wound healing [91]. Other applications appear in the theory of superconducting electrodynamics [114] and in the study of excitons [83]. Fisher's equation is a nonlinear equation that obviously generalizes the three-dimensional diffusion model if we rewrite Fisher's equation as

$$\frac{\partial u}{\partial t} = k \nabla^2 u + F(u).$$

The **stochastic Fisher-KPP equation** is the one-dimensional Fisher equation with $F(u) = mu(1 - u) + \gamma \sqrt{u(1 - u)} \eta(x, t)$, where $0 \leq u \leq 1$, γ is a real constant, and $\eta(x, t)$ is a *Gaussian white noise process* in space and time with mean equal to zero [21]. To fix ideas, we may think of a **noise** as a random signal of known statistical properties of amplitude, distribution, and spectral density. A noise is a **white noise** in space and time if it is uncorrelated in these two variables, and it is **Gaussian** if its probability density function over a given frequency band is normal. The stochastic Fisher-KPP equation is a stochastic partial differential equation that describes random walk processes that have applications in hydrodynamics and economics.

Second-order partial differential equations describing diffusion or conduction happen to appear in the area of thermodynamics [70]. Heat conduction is understood as the transfer of heat from warm

areas to cooler ones, and effectively occurs by diffusion. Under the assumption of a macroscopic continuum formulation, the **Fourier equation** [28] for the heat flux \bar{q} in a medium of density ρ , mass heat capacity C_P , and temperature function u , is

$$\bar{q} = -k\nabla u,$$

where both \bar{q} and u depend on the three spatial coordinates and time, $k = \rho\kappa C_P$ is the thermal conductivity of the medium, and κ is the thermal diffusivity term of the classical diffusion equation.

The previously mentioned Fourier heat conduction equation is diffusive and does not account for the temperature propagation speed in transient situations. Because of certain issues argued and identified earlier, attempts to account for a finite speed of heat propagation have evolved over the years. The **Maxwell-Cattaneo model** [12], which is based on the notion of relaxing the heat flux, is given as

$$\tau \frac{\partial \bar{q}}{\partial t} = -\bar{q} - k\nabla u,$$

where τ is the relaxation time. Assuming that there are no heat sources and that k is constant, the one-dimensional version of the Maxwell-Cattaneo equation together with the energy equation

$$\rho C_P \frac{\partial u}{\partial t} + \frac{\partial q}{\partial x} = 0,$$

yield the hyperbolic equation

$$\tau \rho C_P \frac{\partial^2 u}{\partial t^2} - k \frac{\partial^2 u}{\partial x^2} + \rho C_P \frac{\partial u}{\partial t} = 0.$$

Obviously, it can be generalized to the three-dimensional case as

$$\frac{\partial^2 u}{\partial t^2} - \frac{k}{\tau \rho C_P} \nabla^2 u + \frac{1}{\tau} \frac{\partial u}{\partial t} = 0.$$

The **telegraph equation** is a hyperbolic equation that describes heat or mass transport. It models phenomena that are mixtures between diffusion and wave propagation. In this model a small section of a telegraph wire is treated to study the pulse of voltage moving along the wire. It was studied in 1876 by Heaviside in his research on coaxial marine telegraph cables [53]. The telegraph equation is the linear second-order partial differential equation

$$\frac{\partial^2 u}{\partial x^2} - \frac{1}{\nu^2} \frac{\partial^2 u}{\partial t^2} - \gamma \frac{\partial u}{\partial t} - b^2 u = 0,$$

where ν is positive, and γ and b are nonnegative constants. The one-dimensional wave equation is just a particular case of the telegraph equation with γ and b both equal to zero. The generalization of the telegraph equation to three dimensions is

$$\nabla^2 u - \frac{1}{\nu^2} \frac{\partial^2 u}{\partial t^2} - \gamma \frac{\partial u}{\partial t} - b^2 u = 0.$$

1.3 Modified Klein-Gordon equations

The objective of this paper is to study a general form of the Klein-Gordon equation that embraces the partial differential equations described in the previous section and, at the same time, takes into account a third-order term proportional to the Laplacian of the partial derivative of u in time, which physically represents the **internal damping term**. More precisely, let u be a function of the spatial variables X, Y, Z , and the time variable T . The nonlinear partial differential equation with constant coefficients that we wish to study in this thesis is

$$a \frac{\partial^2 u}{\partial T^2} - b \nabla^2 u - c \frac{\partial}{\partial T} (\nabla^2 u) + d \frac{\partial u}{\partial T} + m^2 u + G'(u) = 0,$$

Let $x = X/\sqrt{b}$, $y = Y/\sqrt{b}$, $z = Z/\sqrt{b}$, and $t = T/\sqrt{a}$ for a and b positive numbers. Let $\beta = c/(b\sqrt{a})$ and $\gamma = d/\sqrt{a}$. Our problem can be stated in dimensionless form as

$$\frac{\partial^2 u}{\partial t^2} - \nabla^2 u - \beta \frac{\partial}{\partial t} (\nabla^2 u) + \gamma \frac{\partial u}{\partial t} + m^2 u + G'(u) = 0,$$

$$\text{subject to : } \begin{cases} u(\bar{x}, 0) = \phi(\bar{x}), & \bar{x} \in D, \\ \frac{\partial u}{\partial t}(\bar{x}, 0) = \psi(\bar{x}), & \bar{x} \in D. \end{cases} \quad (1.2)$$

This initial-value problem will be referred to as the **modified nonlinear Klein-Gordon equation** or the **dissipative nonlinear Klein-Gordon equation**, and its numerical study for the particular choice $G'(u) = u^p$, for $p > 1$ an odd number, is the topic of this paper. We identify the term containing the coefficient β as the internal damping term, while the term containing γ is easily identified as the external damping term. Needless to say that the differential equation in (1.2) generalizes the equations listed in Section 1.2 either by choosing suitable coefficients or by suppressing terms; the classical Klein-Gordon equation, for instance, can be obtained by setting β and γ both equal to zero and G' identically zero. It is worthwhile mentioning that the undamped nonlinear Klein-Gordon equation with $G'(u) = u^3$ is called the **quasilinear Klein-Gordon equation**, and it also has physical applications [76].

The following is the major theoretic result we will use in our investigation. It is valid only for certain classical one-dimensional nonlinear Klein-Gordon equations. Here $M(t)$ represents the amplitude of a solution of (1.2) at time t , that is

$$M(t) = \max_x |u(x, t)|.$$

Theorem 1.1. *Let β and γ be both equal to zero, and let $G'(u) = |u|^{p-1}u$. Suppose that ϕ and ψ are smooth and small at infinity. Then*

- (1) *If $p < 5$, a unique smooth solution of (1.2) exists with amplitude bounded at all time [43].*
- (2) *If $p \geq 5$, a weak solution exists for all time [90].*
- (3) *For $p > 8/3$ and for solutions of bounded amplitude, there is a scattering theory; in particular, they decay uniformly as fast as $M(t) \leq c(1 + |t|)^{-3/2}$ [73].* □

Josephson transmission lines

As we stated in the introductory chapter, initial-value problem (1.2) has applications in several physical problems. In the remainder of this section we will describe some of them.

A **Josephson junction** is a type of electronic circuit capable of switching at very high speeds when operated at temperatures approaching absolute zero. Named for the British physicist who designed it, a Josephson junction exploits the phenomenon of superconductivity, that is the ability of certain materials to conduct electric current with practically zero resistance. Josephson junctions are used in certain specialized instruments such as highly-sensitive microwave detectors, magnetometers, and quantum interference devices.

A Josephson junction is made up of two superconductors, separated by a nonsuperconducting layer so thin that electrons can cross through the insulating barrier. The flow of current between the superconductors in the absence of an applied voltage is called a **Josephson current**, and the movement of electrons across the barrier is known as **Josephson tunneling**. Two or more junctions joined by superconducting paths form what is called a **Josephson interferometer**.

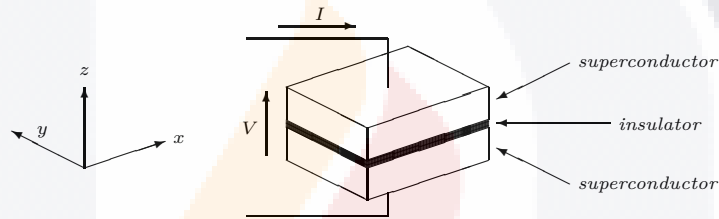


Figure 1.1: Schematic representation of a small Josephson junction.

While researching superconductivity, Josephson studied the properties of a junction between two superconductors [44]. Following up on earlier works by Leo Esaki and Ivar Giaever, he demonstrated that in a situation when there is electron flow between two superconductors through an insulating layer (in the absence of an applied voltage), and a voltage is applied, the current stops flowing and oscillates at a high frequency. This phenomenon is called the **Josephson effect**, and it is influenced by magnetic fields in the vicinity, a capacity that enables the Josephson junction to be used in devices that measure extremely weak magnetic fields, such as superconducting quantum interference devices. For their efforts, Josephson, Esaki, and Giaever shared the Nobel Prize for Physics in 1973.

It is worthwhile mentioning that the theory of low temperature conductivity tells us that a superconductor is a system where a fraction of the conduction electrons form pairs called **Cooper pairs**. In these pairs the two electrons have opposite momentum and spin. These pairs are able to condense in the same quantum state so that the superconductor can be described by a single macroscopic wave function

$$\Psi = \sqrt{\rho}e^{i\phi}.$$

Here ρ represents the pair density and ϕ is the quantum phase common to all pairs. A **small Josephson junction** consists of two small layers of superconducting metal separated by a thin dielectric barrier layer, which is small enough to permit tunneling of Cooper pairs (equivalently, coupling of the wave functions of the two superconductors).

A **long Josephson junction** consists of two identical superconducting long strips separated by

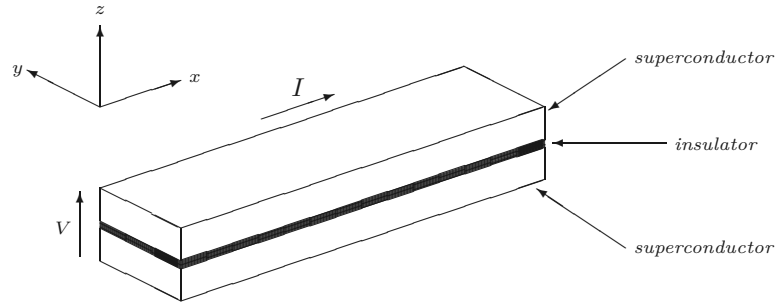


Figure 1.2: Schematic representation of a long Josephson junction.

a thin dielectric layer. This long tunneling junction can be regarded as a transmission line as far its electromagnetic behavior is concerned [5]. However, in dealing with real transmission lines for the long Josephson junction one must take into account losses, bias, and junction irregularities which influence motion [85]. When we account for all of these effects, we obtain the third-order partial differential equation

$$\frac{\partial^2 \phi}{\partial x^2} - \frac{\partial^2 \phi}{\partial t^2} - \alpha \frac{\partial \phi}{\partial t} + \beta \frac{\partial^3 \phi}{\partial x^2 \partial t} = \sin \phi - \gamma,$$

where α , β and γ are constants.

The statistical mechanics of kinks

The statistical mechanics of **kinks** (that is, exact solitary waves) of nonlinear coherent structures has been studied by two approaches. In the first approach one assumes that the kinks may be treated as weakly interacting elementary excitations. Provided the kink density is low, the canonical partition function can be found by standard methods [67, 50, 19]. Alternatively, it is possible to calculate the partition function to exploit a transfer operator technique. This method was used by Krumhansl and Schrieffer in [50], and it showed that in the low temperature limit the partition function naturally factorizes into two contributions: A tunneling term which they were able to identify with the kink contribution, and the remainder which they identified as linearized phonons (by a **phonon** we mean a quantized mode of vibration occurring in a rigid crystal lattice, such as the atomic lattice of a solid).

The ideas of Krumhansl and Schrieffer were further refined and extended to a wider class of systems [19]. In particular, interactions of kinks with linearized phonons were considered, leading to substantial corrections of results. Computer simulations based on standard methods [3] made possible to verify results on the equilibrium statistical mechanics of kinks using a dimensionless **Langevin equation** describing the (1 + 1)-dimensional theory:

$$\frac{\partial^2 \phi}{\partial t^2} = \frac{\partial^2 \phi}{\partial x^2} - \gamma \frac{\partial \phi}{\partial t} - \phi(1 - \phi^2) + F(x, t).$$

The wave equation revisited

Initial-value problem (1.2) also describes the mechanical motion of strings for certain physical situations. Consider the one-dimensional motion of a string immersed in a non-Hookean medium. We represent the vertical motion of the string as a function $u(r, t)$ of horizontal position and time, and

the nonlinear force of the medium by $G'(u)$. The string is assumed to possess internal damping due to its inner stiffness, which is proportional to u_{rrt} . Finally, we assume that there exists friction between the string and the medium that derives in a force which opposes the motion of the string and is proportional to the vertical velocity of the string. In these circumstances, the motion of our string will be described by (1.2).

1.4 Elementary solutions

In our study we will be often interested in studying soliton solutions. As mentioned before, solitons are solitary waves found in many nonlinear physical phenomena. They were first named by Zabusky and Kruskal in 1965 [118], and first appeared in the solution of the **Korteweg-de Vries equation**

$$\frac{\partial u}{\partial t} + \frac{\partial^3 u}{\partial x^3} - 6u \frac{\partial u}{\partial x} = 0.$$

Later on it was proved that equations such as the nonlinear Schrödinger equation, the nonlinear Klein-Gordon equation and the sine-Gordon equation also possess soliton solutions. Mathematically, **solitons** have been defined [22] as solutions of nonlinear partial differential equations which

- (i) represent waves of permanent form and velocity,
- (ii) decay or approach a constant at infinity, and
- (iii) can interact strongly with other solitons and retain their identity.

Given a differential equation in the variables x and t , an **elementary soliton solution** is a solution of the differential equation u of the form $u(x, t) = \phi(x - vt)$ with the property that the infinite limits $\lim_{x \rightarrow -\infty} u(x, t)$ and $\lim_{x \rightarrow +\infty} u(x, t)$ are constant with respect to time. In this section we derive the solution of the linear Klein-Gordon equation using Fourier transforms and some elementary soliton solutions for some important nonlinear partial differential equations. Throughout ξ will denote the quantity $x - vt$.

The linear Klein-Gordon equation

First we wish to use Fourier transform to solve an arbitrary initial value-problem involving the linear Klein-Gordon equation and provide a solution in terms of the source function. After that, we will find the traveling wave solutions of this differential equation. Thus, let m be a real constant and the consider the $(1 + 1)$ -dimensional initial-value problem

$$\frac{\partial^2 u}{\partial t^2} - \nabla^2 u + m^2 u = 0,$$

$$\text{subject to : } \begin{cases} u(x, 0) = \phi(x), & \bar{x} \in \mathbb{R}, \\ \frac{\partial u}{\partial t}(x, 0) = \psi(x), & x \in \mathbb{R}. \end{cases}$$

Using Fourier transform, this problem in terms of the source function $S(x, t)$ can be expressed as the initial-value problem

$$\frac{\partial^2 \hat{S}}{\partial t^2} + k^2 \hat{S} + m^2 \hat{S} = 0,$$

$$\text{subject to : } \begin{cases} \hat{S}(k, 0) = 0, & -\pi < k < \pi, \\ \frac{\partial \hat{S}}{\partial t}(k, 0) = 1, & -\pi < k < \pi. \end{cases}$$

For a fixed value of k , the differential equation in the initial-value problem above is ordinary, and its solution is a linear combination of sines and cosines. It can be seen then that the particular solution to this problem is of the form $\hat{S}(k, t) = \sin(\omega t)/\omega$, where $\omega = \sqrt{k^2 + m^2}$. After applying inverse Fourier transform to \hat{S} and simplifying, it is easy to obtain that

$$S(x, t) = \begin{cases} \frac{1}{2} J_0 \left(m \sqrt{t^2 - x^2} \right), & \text{for } |x| < t, \\ 0, & \text{for } |x| \geq t, \end{cases}$$

Where J_0 is the Bessel function of the first kind of order 0 whose general definition may be found in [41]. Needless to say that the source function S of the linear Klein-Gordon equation converges to the source function corresponding to the classical wave equation when m tends to 0.

We are interested now in computing radially symmetric solutions of the three-dimensional linear Klein-Gordon equation using Fourier transforms. It is easy to verify that the expression $\hat{S}(\vec{k}, t)$ of the Fourier transform of the source function in this case will be the same as that of the (1+1)-dimensional one. Letting r represent the Euclidean norm of \vec{x} in \mathbb{R}^3 and computing the inverse Fourier transform of \hat{S} we get

$$\begin{aligned} S(r, t) &= \frac{1}{8\pi^3} \int_0^{2\pi} \int_0^\pi \int_0^\infty \frac{\sin(\omega t)}{\omega} k^2 \sin \theta e^{ikr \cos \theta} dk d\theta d\phi \\ &= \frac{1}{2\pi r^2} \int_0^\infty \frac{\sin(t\sqrt{k^2 + m^2})}{\sqrt{k^2 + m^2}} k \sin kr dk \\ &= -\frac{1}{4\pi r} \frac{\delta}{\delta r} \int_{-\infty}^\infty \frac{\sin(t\sqrt{k^2 + m^2})}{\sqrt{k^2 + m^2}} e^{ikr} dk. \end{aligned}$$

Let H represent the Heaviside function. Computing the above derivative with respect to r and using the identities $J_0 = -J_1$ and $J_0(0) = 1$, we obtain that

$$S(r, t) = \frac{1}{2\pi} \delta(t^2 - r^2) - m H(t^2 - r^2) \frac{J_1(m\sqrt{t^2 - r^2})}{4\pi\sqrt{t^2 - r^2}}.$$

The sine-Gordon equation

The sine-Gordon equation has been used as a mathematical model in many different applications, including the propagation of ultra-short optical pulses in resonant laser media [51], a universal theory of elementary particles [92, 93, 25], and the propagation of magnetic flux in Josephson junctions [45]. Here we consider the classical (1+1)-dimensional sine-Gordon equation presented in Section 1.2, with parameters $m^2 = c = 1$, and assume that $u(x, t) = \phi(x - vt) = u(\xi)$ is an elementary soliton solution. Then ϕ satisfies the ordinary differential equation $(1 - v^2)\phi_{\xi\xi} - \sin \phi = 0$. Multiplying then by ϕ_x ,

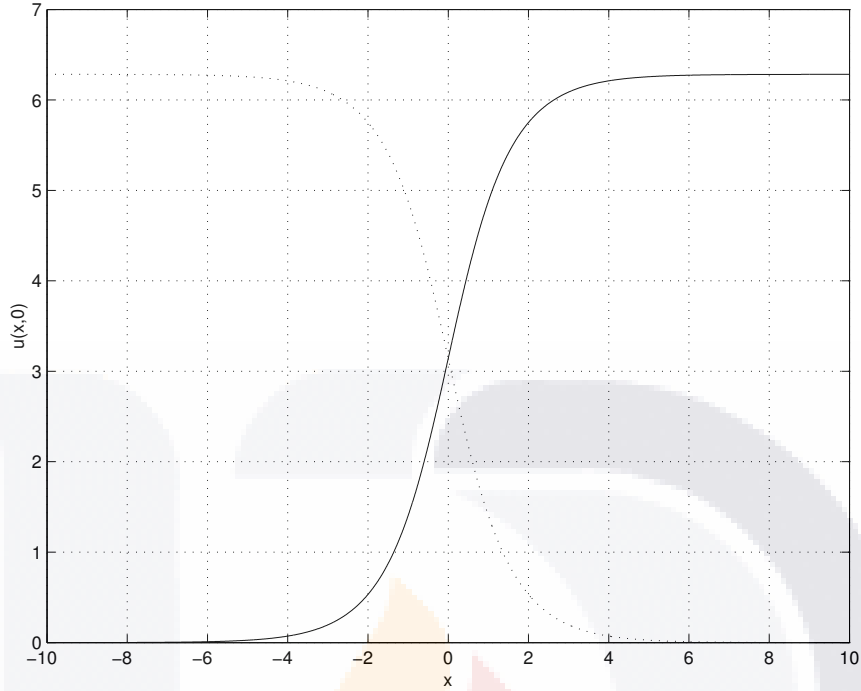


Figure 1.3: Soliton solution (solid line) and anti-soliton solution (dotted line) of the sine-Gordon equation at time 0, with $v = 0.1$.

integrating with respect to ξ and solving for ϕ_ξ , we obtain that

$$\frac{d\phi}{d\xi} = \left(2A - \frac{2 \cos \phi}{1 - v^2} \right)^{1/2},$$

where A is the constant of integration. Now we use separation of variables and the substitution $A(1 - v^2) = 1$. Integrating both sides and noting that $1 - \cos \phi = 2 \sin^2(\frac{1}{2}\phi)$ and noting that the derivative with respect to ϕ of $\ln \tan(\frac{1}{4}\phi)$ equals $\frac{1}{2} \csc(\frac{1}{2}\phi)$, we get

$$\sqrt{2} \ln \left[\frac{\tan(\frac{1}{4}\phi)}{\tan(\frac{1}{4}\phi_0)} \right] = \left[\frac{2}{1 - v^2} \right]^{1/2} (\xi - \xi_0).$$

Finally, solving for ϕ and expressing the result in terms of x and t , it is possible to write the elementary soliton solution as

$$u(x, t) = 4 \arctan \left[\exp \left(\frac{x - vt}{\sqrt{1 - v^2}} \right) \right].$$

This solution is sometimes called a **kink**; its profile is shown in Figure 1.3. The other soliton solution that can be obtained from the sine-Gordon equation, called the **anti-kink** or **anti-soliton**, is shown in the same figure. Its analytical expression is given by

$$u(x, t) = 4 \operatorname{arccot} \left[\exp \left(\frac{x - vt}{\sqrt{1 - v^2}} \right) \right].$$

We must mention here that the sine-Gordon equation possesses solutions built up from the superposition of solitons and/or anti-solitons. Those solutions and the elementary soliton solutions obtained above are listed in the following table for the sake of future reference (see [113]).

Type of solution	Analytical expression
single soliton	$u(x, t) = 4 \arctan \left[\exp \left(\frac{x - vt}{\sqrt{1 - v^2}} \right) \right]$
single anti-soliton	$u(x, t) = u(x, t) = 4 \operatorname{arccot} \left[\exp \left(\frac{x - vt}{\sqrt{1 - v^2}} \right) \right]$
two solitons	$u(x, t) = 4 \arctan \left[\frac{v \sinh(x/\sqrt{1 - v^2})}{\cosh(vt/\sqrt{1 - v^2})} \right]$
soliton and anti-soliton	$4 \arctan \left[\frac{\sinh(vt/\sqrt{1 - v^2})}{v \cosh(x/\sqrt{1 - v^2})} \right]$
"breather"	$u(x, t) = 4 \arctan \left[\frac{\sqrt{1 - v^2}}{v} \frac{\sin(vt)}{\cosh(x\sqrt{1 - v^2})} \right]$

Table 1.1: Different types of soliton solutions of the sine-Gordon equation.

The Landau-Ginzburg equation

The (1 + 1)-dimensional Landau-Ginzburg equation is another important nonlinear partial differential equation arising in physics that possesses soliton solutions. From the mathematical point of view, the Landau-Ginzburg equation can be seen as a quasilinear Klein-Gordon equation with purely imaginary mass and nonlinear term proportional to u^3 . More concretely, the Landau-Ginzburg equation with real parameters m and λ under study in this section can be written as

$$\frac{\partial^2 u}{\partial t^2} - \frac{\partial^2 u}{\partial x^2} - m^2 u + \lambda u^3 = 0.$$

Using the same technique to find elementary, solitary wave solutions, we suppose that $u(x, t) = \phi(\xi)$, where $\xi = x - vt$ for some $v \in \mathbb{R}$. Then ϕ satisfies the ordinary differential equation

$$(1 - v^2) \frac{d^2 \phi}{d\xi^2} = -m^2 \phi + \lambda \phi^3.$$

Solving and then multiplying by $2\phi'(\xi)$, we obtain that

$$\frac{d}{d\xi} \left[\left(\frac{d\phi}{d\xi} \right)^2 \right] = \frac{1}{2(1 - v^2)} \frac{d}{d\xi} (\lambda \phi^4 - 2m^2 \phi^2).$$

We integrate now with respect to ξ both sides of the equation. An integration constant will appear in the right-hand side of the resulting equality. By choosing this constant of integration equal to $m^2/(2\lambda(1 - v^2))$, taking the negative square root on both sides of the equation, separating variables, and completing the square in the radical that contains ϕ , we obtain that

$$-\frac{1}{\sqrt{\lambda}} \int_{\phi_0}^{\phi} \frac{d\phi}{\phi^2 - m^2/\lambda} = \int_{\xi_0}^{\xi} \frac{d\xi}{\sqrt{2(1 - v^2)}}.$$

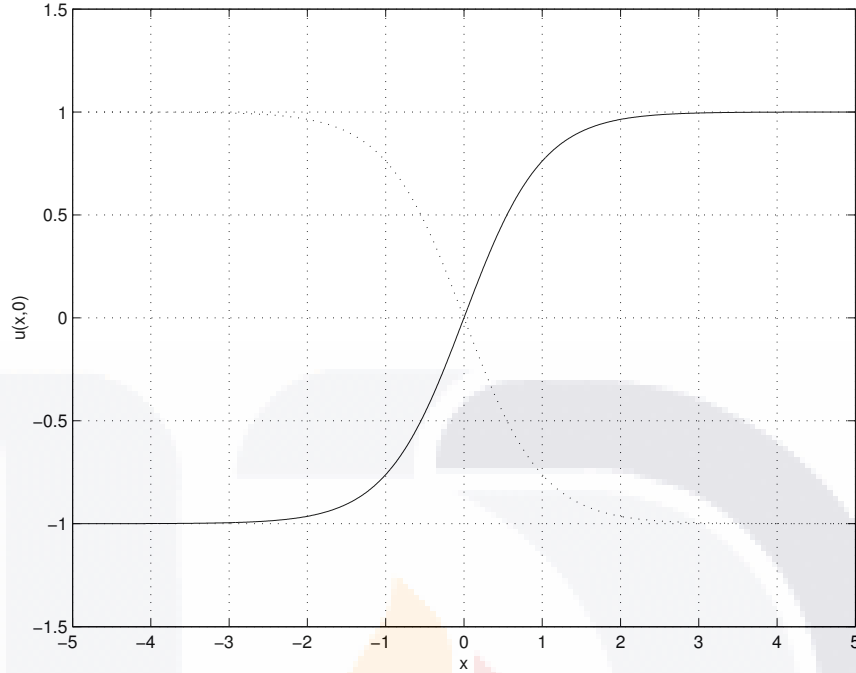


Figure 1.4: Soliton solution (solid line) and anti-soliton solution (dotted line) of the Landau-Ginzburg equation at time 0, with $v = 0.1$.

Let ξ_0 and ϕ_0 be both equal to zero. Expressing the integrand in the left-hand side of the preceding equality, integrating, and then evaluating from ϕ_0 to ϕ , we get

$$\frac{1}{2m} \ln \left| \frac{(\phi + m/\sqrt{\lambda})(\phi_0 - m/\sqrt{\lambda})}{(\phi - m/\sqrt{\lambda})(\phi_0 + m/\sqrt{\lambda})} \right| = \frac{\xi - \xi_0}{\sqrt{2(1 - v^2)}}$$

We choose ϕ_0 and ξ_0 to be equal to zero. Solving then for ϕ we obtain the following soliton (kink) solution for the Landau-Ginzburg equation

$$u(x, t) = \frac{m}{\sqrt{\lambda}} = \tanh \left[\frac{m(x - vt)}{\sqrt{2(1 - v^2)}} \right]$$

The corresponding anti-soliton (anti-kink) solution to the Landau-Ginzburg equation is obtained by evaluating the soliton solution at $(-x, t)$. A graph showing the kink and anti-kink of the Landau-Ginzburg equation is shown in Figure 1.4.

1.5 Elements of numerical analysis

In our investigation, we are interested in developing finite-difference schemes to approximate radially symmetric solutions of modified nonlinear Klein-Gordon equations. In order to determine how accurate our approximations are, we need to introduce the notions of convergence, consistency and stability. To understand these concepts we must first clarify some ideas from mathematical analysis. Here we

follow [86] and [106]. Throughout K denotes the fields \mathbb{R} and \mathbb{C} .

Normed linear spaces

A **norm** on a vector space V over a scalar field K is a function $\|\cdot\|$ that associates every element of V with a real number, such that for any vectors \bar{u} and \bar{v} , and any scalar a , the following properties are satisfied:

- (i) $\|\bar{v}\| \geq 0$, and $\|\bar{v}\| = 0$ iff $\bar{v} = 0$,
- (ii) $\|a\bar{v}\| = |a| \|\bar{v}\|$, and
- (iii) $\|\bar{u} + \bar{v}\| \leq \|\bar{u}\| + \|\bar{v}\|$.

It is worthwhile mentioning that a vector space with a norm associated with it is called a **normed linear space** or simply **normed space**. The following are examples of normed linear spaces with the given norms.

Example 1.2. Denote by $|\cdot|$ the standard norm in K . The linear space K^n can be given the **p -norm** ($p \geq 1$)

$$\|\bar{x}\|_p = \left(\sum_{i=1}^n |x_i|^p \right)^{1/p}.$$

The 1-norm and the 2-norm in K^n are called the **taxicab norm** and the **Euclidean norm**, respectively. K^n can also be normed by the so called **infinity norm** $\|\bar{x}\|_\infty = \max\{|x_1|, \dots, |x_n|\}$. \square

Example 1.3. Let Δx and p be positive numbers with $p > 1$. The space $\ell_{p,\Delta x}$ is the normed linear space of all infinite sequences $\mathbf{u} = (\dots, u_{-1}, u_0, u_1, \dots)$ of elements in K with vector addition and scalar multiplication given componentwise, such that $\sum_{-\infty < j < \infty} |u_j|^p < \infty$. The norm is given by

$$\|\mathbf{u}\|_{p,\Delta x} = \left(\sum_{k=-\infty}^{\infty} |u_k|^p \Delta x \right)^{1/p}.$$

The space ℓ_p is the space $\ell_{p,1}$. If p is equal to 2 then $\ell_{p,\Delta x}$ is called the **energy space**. \square

Example 1.4. Let λ represent the Lebesgue measure on $X \subseteq \mathbb{R}$. The space $L_p(X)$ for $p > 1$ is the normed linear space of all equivalence classes of functions $f: X \rightarrow \mathbb{R}$ under the relation of equivalence almost everywhere, together with addition and scalar multiplication defined in representatives, such that $\int_X f^p d\lambda < \infty$. Its norm is given by

$$\|f\|_p = \left(\int_X f^p d\lambda \right)^{1/p}. \quad \square$$

Example 1.5. Let $\|\cdot\|$ be any norm in K^n . The space of all $n \times n$ -matrices with coefficients in K is a normed linear space with the usual operations of addition of matrices and scalar multiplication, with **matrix norm** defined by

$$\|Q\| = \sup_{\|\bar{u}\| \leq 1} \|Q\bar{u}\|. \quad \square$$

Convergence

A difference scheme $L_k^n u_k^n = G_k^n$ approximating the partial differential equation $\mathcal{L}v = F$ is a **convergent** scheme at time t in the norm $\|\cdot\|$ of $\ell_{p,\Delta x}$ if, as $(n+1)\Delta t \rightarrow t$,

$$\|\mathbf{u}^{n+1} - \mathbf{v}^{n+1}\| \rightarrow 0$$

as $\Delta x, \Delta t \rightarrow 0$. Here $\mathbf{u}^n = (\dots, u_{-1}^n, u_0^n, u_1^n, \dots)$ and $\mathbf{v}^n = (\dots, v_{-1}^n, v_0^n, v_1^n, \dots)$ are the sequences representing the vector of approximations to the solution of the partial differential equation and the vector of exact solutions whose k -th component is $v(k\Delta x, n\Delta t)$, respectively.

Consistency

The difference scheme $\mathbf{u}^{n+1} = Q\mathbf{u}^n + \Delta t\mathbf{G}^n$ is **consistent** with the partial differential equation $\mathcal{L}v = F$ in the norm $\|\cdot\|$ if the solution v of the differential equation satisfies

$$\mathbf{v}^{n+1} = Q\mathbf{v}^n + \Delta t\mathbf{g}^n + \Delta t\boldsymbol{\tau}^n,$$

and $\|\boldsymbol{\tau}^n\| \rightarrow 0$ as $\Delta x, \Delta t \rightarrow 0$. Moreover, the scheme is said to be accurate with order $\mathcal{O}(\Delta x^p) + \mathcal{O}(\Delta t^q)$ if

$$\|\boldsymbol{\tau}^n\| = \mathcal{O}(\Delta x^p) + \mathcal{O}(\Delta t^q).$$

Stability

One interpretation of stability of a finite-difference scheme is that, for a stable scheme, small errors in the initial conditions cause small errors in the solution. As we will see, the definition does allow the errors to grow but limits them to grow no faster than exponential. More precisely, the finite-difference scheme $\mathbf{u}^{n+1} = Q\mathbf{u}^n$ is said to be **stable** with respect to the norm $\|\cdot\|$ if there exist positive constants Δx_0 and Δt_0 , and nonnegative constants K and β so that

$$\|\mathbf{u}^{n+1}\| \leq K e^{\beta t} \|\mathbf{u}^0\|,$$

for $0 \leq t = (n+1)\Delta t$, $0 < \Delta x \leq \Delta x_0$ and $0 < \Delta t \leq \Delta t_0$. If further restrictions on the relationship between Δt and Δx are needed in order to guarantee stability of the finite-difference scheme, we say that the scheme is **conditionally stable**.

One characterization of stability that is often useful comes from the inequality in the definition above. We state this in the following result.

Theorem 1.6. *The scheme $\mathbf{u}^{n+1} = Q\mathbf{u}^n$ is stable with respect to the norm $\|\cdot\|$ if and only if there exist positive constants Δx_0 and Δt_0 , and nonnegative constants K and β so that*

$$\|Q^{n+1}\| \leq K e^{\beta t},$$

for $0 \leq t = (n+1)\Delta t$, $0 < \Delta x \leq \Delta x_0$ and $0 < \Delta t \leq \Delta t_0$. □

The scheme $\mathbf{u}^{n+1} = Q\mathbf{u}^n$ is said to be **stable order n** with respect to the norm $\|\cdot\|$ if there exist

positive constants Δx_0 and Δt_0 , and nonnegative constants K_1 , K_2 and β such that

$$\|\mathbf{u}^{n+1}\| \leq (K_1 + nK_2)e^{\beta t}\|\mathbf{u}^0\|,$$

for $0 \leq t = (n + 1)\Delta t$, $0 < \Delta x \leq \Delta x_0$ and $0 < \Delta t \leq \Delta t_0$. Obviously, if a finite-difference scheme is stable then it will be stable order n . We also realize that the above definition is equivalent to requiring that Q satisfy $\|Q^n\| \leq (K_1 + nK_2)e^{\beta t}$.

The use of the discrete Fourier transform is a useful tool in the analysis of stability of finite-difference schemes for initial-value problems. We define the **discrete Fourier transform** of $\mathbf{u} \in \ell_2$ as the function $\hat{u} \in L_2([-\pi, \pi])$ given by

$$\hat{u}(\xi) = \frac{1}{\sqrt{2\pi}} \sum_{m=-\infty}^{\infty} e^{-im\xi} u_m,$$

for $\xi \in [-\pi, \pi]$. The ℓ_2 vectors that we will be using later will be the $\ell_{2,\Delta x}$ vectors that are the solutions to our finite-difference schemes at time step n .

Example 1.7. The **central second-order difference** is the linear operator δ^2 that associates with each infinite sequence $\mathbf{u} = (\dots, u_{-1}, u_0, u_1, \dots)$ of real numbers the infinite sequence $\delta^2\mathbf{u}$ whose m -th component is given by $u_{m+1} - 2u_m + u_{m-1}$. It is easy to check that the Fourier transform of $\delta^2\mathbf{u}$ is given by $-4\sin^2 \frac{\xi}{2}\hat{u}$. □

It is important to remark that if $\mathbf{u} \in \ell_2$ has discrete Fourier transform \hat{u} then $\|\hat{u}\|_2 = \|\mathbf{u}\|_2$, where the first norm is the L_2 -norm on $[-\pi, \pi]$ and the second norm is the ℓ_2 -norm. This fact constitutes a bridge between the spaces ℓ_2 and $L_2([-\pi, \pi])$ that provides us with the following important result for stability.

Theorem 1.8. *The sequence $\{\mathbf{u}^n\}$ is stable in $\ell_{2,\Delta x}$ if and only if $\{\hat{u}^n\}$ is stable in $L_2([-\pi, \pi])$.* □

Let $\mathbf{u}^{n+1} = Q\mathbf{u}^n$ be a finite difference scheme. Taking discrete Fourier transform in both sides we obtain an equation of the form $\hat{u}^{n+1} = A(\xi)\hat{u}^n$. The matrix $A(\xi)$ is called the **amplification matrix** of the difference scheme. By virtue of Theorem 1.8, the stability of the scheme depends on the growth of the amplification matrix raised to the n -th power.

Theorem 1.9 (Lax Theorem). *If a two-level difference scheme $\mathbf{u}^{n+1} = Q\mathbf{u}^n + \Delta t\mathbf{G}^n$ is consistent in the norm $\|\cdot\|$ to an initial-value problem and is stable with respect to $\|\cdot\|$, then it is convergent with respect to $\|\cdot\|$.* □

1.6 Finite differences

We could begin by recalling the standard definition of derivative which we have learned in elementary calculus.

Definition 1.10. The *derivative* of the function $u(x)$ is defined by the equation

$$u'(x) = \lim_{\Delta x \rightarrow 0} \frac{u(x + \Delta x) - u(x)}{\Delta x}. \tag{1.3}$$

provided the limit exists. The number $u'(x)$ is also called the rate of change of u at x .

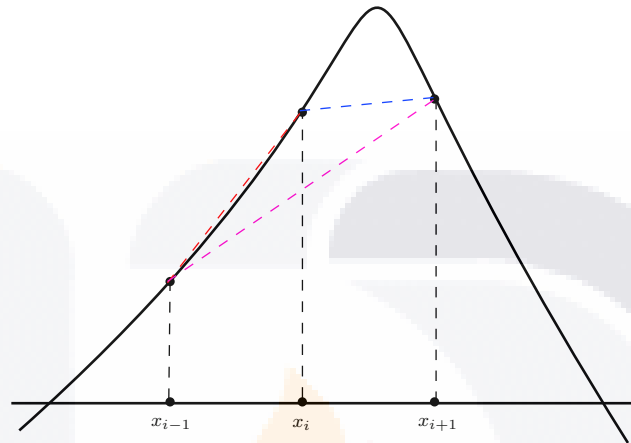


Figure 1.5: Computational grid and example of backward (red dashed line), forward (blue dashed line) and centered (magenta dashed line) linear interpolation to the function.

However, the computers can not handle the previous limit, namely, when $\Delta x \rightarrow 0$, and hence a *discrete* analogue of the continuous scenario need to be considered. In the discretization, we can regard that the set of points on which the function is defined is finite, and the function value is available on a discret set of points. The approximations to the derivative of the function will must to come from these finite sets of points.

Figure 1.5 shows us the discrete set of points x_i where the function is known. We use the notation $u_i = u(x_i)$ to denote the value of the function at the i -th node of the computational grid. We divide the axis into a set of intervals of width $\Delta x_i = x_{i+1} - x_i$. We can fix the grid spacing, it means that all intervals are of equal size, so we will refer to the grid spacing as Δx . If we make the last, we will obtain several advantages when we develop the method as we will see afterward.

Finite difference approximation

We employ the definition of derivative in the continuous case to approximate the derivative in the discrete case:

$$u'(x_i) \approx \frac{u(x_i + \Delta x_i) - u(x_i)}{\Delta x} = \frac{u_{i+1} - u_i}{\Delta x}, \tag{1.4}$$

where now Δx is a finite and small but not necessarily infinitesimally small quantity. In the literature, this is known as a *forward Euler* approximation since it uses forward differencing.

Intuitively, we hope that the approximation improves, it means, the error will decrease, as Δx is made smaller. The above is not the only way to approximate the derivative. We provide two other

equally valid approximations:

$$u'(x_i) \approx \frac{u(x_i) - u(x_i - \Delta x)}{\Delta x} = \frac{u_i - u_{i-1}}{\Delta x}, \tag{1.5}$$

and

$$u'(x_i) \approx \frac{u(x_i + \Delta x) - u(x_i - \Delta x)}{2\Delta x} = \frac{u_{i+1} - u_{i-1}}{2\Delta x}. \tag{1.6}$$

Equation (1.5) is known as *backward Euler's* approximation whereas Equation (1.6) represents the *centered difference* approximation. All these definitions are equally equivalent in the continuous case but yield to different approximations in the discrete case. The question becomes which one is better, and is there a way to quantify the error committed. The answer lies in the application of Taylor series analysis.

Taylor series

Let's start with the identity

$$u(x) = u(x_i) + \int_{x_i}^x u'(s) ds. \tag{1.7}$$

Since $u(x)$ is arbitrary, the formula should hold with $u(x)$ replaced by $u'(x)$, it means,

$$u'(x) = u'(x_i) + \int_{x_i}^x u''(s) ds. \tag{1.8}$$

Replacing this expression in the original formula and carrying out the integration (since $u(x_i)$ is constant) we get

$$u(x) = u(x_i) + (x - x_i)u'(x_i) + \int_{x_i}^x \int_{x_i}^s u''(s) ds ds. \tag{1.9}$$

The process can be repeated with

$$u''(x) = u''(x_i) + \int_{x_i}^x u'''(s) ds, \tag{1.10}$$

to get

$$u(x) = u(x_i) + (x - x_i)u'(x_i) + \frac{(x - x_i)^2}{2!}u''(x_i) + \int_{x_i}^x \int_{x_i}^s \int_{x_i}^t u'''(s) ds ds ds. \tag{1.11}$$

We can repeat this process under the assumption that $u(x)$ is sufficiently differentiable, and we find

$$u(x) = u(x_i) + (x - x_i)u'(x_i) + \frac{(x - x_i)^2}{2!}u''(x_i) + \dots + \frac{(x - x_i)^n}{n!}u^{(n)}(x_i) + R_{n+1}, \tag{1.12}$$

where the remainder is given by

$$R_{n+1} = \int_{x_i}^x \dots \int_{x_i}^x u^{(n+1)}(s) (ds)^{n+1}. \tag{1.13}$$

Equation (1.12) is known as the Taylor series of the function $u(x)$ about the point x_i . Notice that the series is a polynomial in $(x - x_i)$ and the coefficients are the (scaled) derivatives of the function

evaluated at x_i .

If the $(n + 1)$ -th derivative of the function u has minimum m and maximum M over the interval $[x_i, x]$ then we can write

$$\int_{x_i}^x \cdots \int_{x_i}^x m(ds)^{n+1} \leq R_{n+1} \leq \int_{x_i}^x \cdots \int_{x_i}^x M(ds)^{n+1}, \quad (1.14)$$

$$m \frac{(x - x_i)^{n+1}}{(n + 1)!} \leq R_{n+1} \leq M \frac{(x - x_i)^{n+1}}{(n + 1)!}, \quad (1.15)$$

which shows that the remainder is bounded by the values of the derivative and the distance of the point x to the expansion point x_i raised to the power $n + 1$. If we further assume that $u^{(n+1)}$ is continuous then it must take all values between m and M , that is

$$R_{n+1} = u^{(n+1)}(\xi) \frac{(x - x_i)^{n+1}}{(n + 1)!}, \quad (1.16)$$

for some $\xi \in [x_i, x]$.

Taylor series and finite differences

The behaviour of numerical approximation to differential equations can be studied using Taylor series. First, we consider the forward Euler with Taylor series. For this, we need to expand the function u at x_{i+1} about the point x_i :

$$u(x_i + \Delta x_i) = u(x_i) + \Delta x_i \left. \frac{\partial u}{\partial x} \right|_{x_i} + \frac{\Delta x_i^2}{2!} \left. \frac{\partial^2 u}{\partial x^2} \right|_{x_i} + \frac{\Delta x_i^3}{3!} \left. \frac{\partial^3 u}{\partial x^3} \right|_{x_i} + \dots \quad (1.17)$$

We can rearranged the Taylor series to get the following

$$\frac{u(x_i + \Delta x_i) - u(x_i)}{\Delta x_i} - \left. \frac{\partial u}{\partial x} \right|_{x_i} = \underbrace{\frac{\Delta x_i^2}{2!} \left. \frac{\partial^2 u}{\partial x^2} \right|_{x_i} + \frac{\Delta x_i^3}{3!} \left. \frac{\partial^3 u}{\partial x^3} \right|_{x_i} + \dots}_{\text{Truncation Error}} \quad (1.18)$$

where it is now clear that the forward Euler formula (1.4) corresponds to truncating the Taylor series after the second term. We can see that the right-hand side of Equation (1.18) coincides with the error committed when we terminate the series and is referred to as the *truncation error*. The truncation error could be defined as the difference between the partial derivative and its finite difference representation. For sufficiently smooth functions and adequately small Δx_i , the first term in the series is usually used to establish the order of magnitude of the error. The first term in the truncation error is the product of the second derivative evaluated at x_i and the grid spacing Δx_i : the former is a property of the function itself while the latter is a numerical parameter which we can change. Thereby, for finite $\frac{\partial^2 u}{\partial x^2}$, the numerical approximation depends linearly on the parameter Δx_i . If we were to half Δx_i , we would expect a linear decrease in the error, if we make Δx_i sufficiently small. We know that there is a notation to refer this behaviour, that is truncation error $\sim \mathcal{O}(\Delta x_i)$. In general, if Δx_i is not constant we choose a representative value of the grid spacing. Note that in general, we can not calculate the exact truncation error; all we can do is characterize the behaviour of this error as $\Delta x \rightarrow 0$. Thus, we

can rewrite Equation (1.18) as

$$\left. \frac{\partial u}{\partial x} \right|_{x_i} = \frac{u_{i+1} - u_i}{\Delta x_i} + \mathcal{O}(\Delta x) \quad (1.19)$$

Now, we can use the Taylor series expansion to obtain an expression for the truncation error when we consider the backward difference formula

$$u(x_i - \Delta x_{i-1}) = u(x_i) - \Delta x_{i-1} \left. \frac{\partial u}{\partial x} \right|_{x_i} + \frac{\Delta x_{i-1}^2}{2!} \left. \frac{\partial^2 u}{\partial x^2} \right|_{x_i} - \frac{\Delta x_{i-1}^3}{3!} \left. \frac{\partial^3 u}{\partial x^3} \right|_{x_i} + \dots \quad (1.20)$$

where $\Delta x_{i-1} = x_i - x_{i-1}$. We proceed to get an expression for the error corresponding to backward difference approximation of the first derivative

$$\frac{u(x_i) - u(x_i - \Delta x_{i-1})}{\Delta x_{i-1}} - \left. \frac{\partial u}{\partial x} \right|_{x_i} = \underbrace{-\frac{\Delta x_{i-1}^2}{2!} \left. \frac{\partial^2 u}{\partial x^2} \right|_{x_i} + \frac{\Delta x_{i-1}^3}{3!} \left. \frac{\partial^3 u}{\partial x^3} \right|_{x_i} + \dots}_{\text{Truncation Error}} \quad (1.21)$$

We realize that the truncation error of the backward difference is not the same as the forward difference; it behave similarly in terms of order of magnitude analysis, and is linear in Δx , that is

$$\left. \frac{\partial u}{\partial x} \right|_{x_i} = \frac{u_i - u_{i-1}}{\Delta x_{i-1}} + \mathcal{O}(\Delta x) \quad (1.22)$$

Observe that in both cases we used the information provided at just two points to obtain the approximation, and the error performs linearly in both instances.

We can obtain a higher order approximation of the first derivative by combining the two Taylor series Equation (1.17) and (1.20). Notice first that the high order derivatives of the function u are all evaluated at the same point x_i and are the same in both expansions. Now, if we form a linear combination of the equations, the prime error will vanish. Observe Equations (1.18) and (1.21). Multiplying the first by Δx_{i-1} and the second by Δx_i and adding both equations we get:

$$\frac{1}{\Delta x_i + \Delta x_{i-1}} \left[\Delta x_{i-1} \frac{u_{i+1} - u_i}{\Delta x_i} + \Delta x_i \frac{u_i - u_{i-1}}{\Delta x_{i-1}} \right] - \left. \frac{\partial u}{\partial x} \right|_{x_i} = \frac{\Delta x_{i-1} \Delta x_i}{3!} \left. \frac{\partial^3 u}{\partial x^3} \right|_{x_i} + \dots \quad (1.23)$$

The approximation uses information about the function u at three points: x_{i-1} , x_i and x_{i+1} . Thus, the truncation error $\sim \mathcal{O}(\Delta x_{i-1} \Delta x_i)$ and is second order. We can observe that on the important case where the grid spacing is constant, the expression simplifies to

$$\frac{u_{i+1} - u_{i-1}}{2\Delta x} - \left. \frac{\partial u}{\partial x} \right|_{x_i} = \frac{\Delta x^2}{3!} \left. \frac{\partial^3 u}{\partial x^3} \right|_{x_i} + \dots \quad (1.24)$$

Hence, for an equally spaced grid, the centered difference approximation converges quadratically as $\Delta x \rightarrow 0$:

$$\left. \frac{\partial u}{\partial x} \right|_{x_i} = \frac{u_{i+1} - u_{i-1}}{2\Delta x} + \mathcal{O}(\Delta x^2) \quad (1.25)$$

Higher order approximation

The Taylor expansion provides a suitable tool to derive a higher order approximation to derivatives of any order. In most of the following we will consider the grid spacing to be constant as is usually the case in most applications. In fact, we will assume constant spacing grid in this thesis.

Equation (1.24) yields the simplest way to derive a fourth order approximation. As an important property of this centered formula is that its truncation error contains only odd derivative terms:

$$\frac{u_{i+1} - u_{i-1}}{2\Delta x} = \frac{\partial u}{\partial x} + \frac{\Delta x^2}{3!} \frac{\partial^3 u}{\partial x^3} + \frac{\Delta x^4}{5!} \frac{\partial^5 u}{\partial x^5} + \frac{\Delta x^6}{7!} \frac{\partial^7 u}{\partial x^7} + \dots + \frac{\Delta x^{2m}}{(2m+1)!} \frac{\partial^{2m+1} u}{\partial x^{2m+1}} + \dots \quad (1.26)$$

The above formula can be applied with Δx replace by $2\Delta x$, and $3\Delta x$ respectively, to get:

$$\frac{u_{i+2} - u_{i-2}}{4\Delta x} = \frac{\partial u}{\partial x} + \frac{(2\Delta x)^2}{3!} \frac{\partial^3 u}{\partial x^3} + \frac{(2\Delta x)^4}{5!} \frac{\partial^5 u}{\partial x^5} + \frac{(2\Delta x)^6}{7!} \frac{\partial^7 u}{\partial x^7} + O(\Delta x^8), \quad (1.27)$$

$$\frac{u_{i+3} - u_{i-3}}{6\Delta x} = \frac{\partial u}{\partial x} + \frac{(3\Delta x)^2}{3!} \frac{\partial^3 u}{\partial x^3} + \frac{(3\Delta x)^4}{5!} \frac{\partial^5 u}{\partial x^5} + \frac{(3\Delta x)^6}{7!} \frac{\partial^7 u}{\partial x^7} + O(\Delta x^8). \quad (1.28)$$

Multiplying Equation (1.26) by 2^2 and subtracting it from Equation (1.27), we cancel the second order error term to get:

$$\frac{8(u_{i+1} - u_{i-1}) - (u_{i+2} - u_{i-2})}{12\Delta x} = \frac{\partial u}{\partial x} - \frac{4\Delta x^4}{5!} \frac{\partial^5 u}{\partial x^5} - \frac{20\Delta x^6}{7!} \frac{\partial^7 u}{\partial x^7} + O(\Delta x^8). \quad (1.29)$$

Repeating this process for Equation (1.27) but using the factor 3^2 and subtracting it from Equation (1.28), we get

$$\frac{27(u_{i+1} - u_{i-1}) - (u_{i+3} - u_{i-3})}{48\Delta x} = \frac{\partial u}{\partial x} - \frac{9\Delta x^4}{5!} \frac{\partial^5 u}{\partial x^5} - \frac{90\Delta x^6}{7!} \frac{\partial^7 u}{\partial x^7} + O(\Delta x^8). \quad (1.30)$$

Even though both Equation (1.29) and (1.30) are meaningful, the latter is not used in the practice since it does not sense to ignore neighboring points while using more distant ones. Nevertheless, this expression is appropriate to derive a sixth approximation to the first derivative: multiply equation (1.30) by 9 and the same equation by 4 and subtract to get:

$$\frac{45(u_{i-1} - u_{i-1}) - 9(u_{i+2} - u_{i-2}) + (u_{i+3} - u_{i-3})}{60\Delta x} = \frac{\partial u}{\partial x} + \frac{36\Delta x^6}{7!} \frac{\partial^7 u}{\partial x^7} + O(\Delta x^8). \quad (1.31)$$

The process can be repeated to derive higher order approximations.

2. Numerical method for a nonlinear chain

In this chapter we study the phenomenon of nonlinear supratransmission in a semi-infinite discrete chain of coupled oscillators described by modified sine-Gordon equations with constant external and internal damping, and subject to harmonic external driving at the end. We develop a consistent and conditionally stable finite-difference scheme in order to analyze the effect of damping in the amount of energy injected in the chain of oscillators; numerical bifurcation analyses to determine the dependence of the amplitude at which supratransmission first occurs with respect to the frequency of the driving oscillator are carried out in order to show the consequences of damping on harmonic phonon quenching and the delay of appearance of critical amplitude.

2.1 Introduction

The study of nonlinear continuous media described by modified Klein-Gordon equations subject to initial conditions is a topic of interest in several branches of the physical sciences [85, 55, 66, 5]. Here the analytical study on features of solutions of Klein-Gordon-like equations as well as the development of new and more powerful computational techniques to approximate them have been the most transited highways in the mathematical research of the area. The behavior of nonlinear continuous media described by modified Klein-Gordon equations subject to boundary conditions is also an interesting topic of study in mathematical physics. This type of mathematical models have proved to be useful when applied, for instance, to the description of the project of data transmission in optical fibers in nonlinear Kerr regimes [39, 72] or in the study of the property of self-induced transparency of a two-level system submitted to a high-energy incident (resonant) laser pulse [69, 1]. More concretely, the behavior of a continuous medium submitted to a continuous wave radiation constitutes a fundamental problem that has not been studied in-depth, yet it has shown to have potential applications as a model in the study of Josephson transmission lines [108, 109, 110]. Numerical studies on discrete versions of these models [34] followed by experimental results [35] have shown that there exists a bifurcation of wave transmission within a forbidden band gap in certain semi-infinite undamped Klein-Gordon-like chains of coupled oscillators which are periodically forced at the end. This bifurcation is a consequence of the generation of nonlinear modes by the periodic forcing at the end of the chain, and allows energy to flow into the medium via a nonlinear process called *nonlinear supratransmission*, which has been proved numerically not to depend on integrability as long as the model possesses a natural forbidden

band gap.

The process of nonlinear supratransmission has been studied numerically by means of computational algorithms already built in standard mathematical packages. Most particularly, the numerical results obtained in [34], for instance, rely on the use of a Runge-Kutta method of high order, which has the advantage of possessing high accuracy and efficiency in the computations, but lacks the consistency in the numerical estimation of the energy flowing into the medium which is desired in the study of supratransmission. With this shortcoming in mind, we present in this chapter an alternate numerical formulation to study the process of supratransmission in a nonlinear system of differential equations, that has the advantage of being consistent in the approximation of the solutions to the problem and in the estimation of the continuous energy. More concretely, in the present chapter we study the process of nonlinear supratransmission in a semi-infinite nonlinear discrete system of coupled oscillators governed by modified sine-Gordon and Klein-Gordon equations with constant internal and external damping. We exploiting some numerical results for dissipative nonlinear modified Klein-Gordon equations that generalize a method proposed by Stauss and Vázquez [94], and validate our conclusions against [34]. Our study — rigorous in numerical nature — will soon be succeeded by future applications in forthcoming papers.

In Section II of this chapter we introduce the mathematical problem under study and derive the expression of the instantaneous rate of change of the energy transmitted to the system through the boundary. Section III is devoted to introducing the finite-difference scheme; here we present the discrete energy analysis associated with the problem under study and establish in detail the numerical properties of our method. Numerical results are presented in the next section, followed by a brief discussion.

2.2 Analytical results

Mathematical model

In this article we study the effects of the nonnegative constant parameters β and γ , and the real constant m^2 on the behavior of solutions to the mixed-value problem with mass m ,

$$\frac{d^2 u_n}{dt^2} - \left(c^2 + \beta \frac{d}{dt} \right) \Delta_x^2 u_n + \gamma \frac{du_n}{dt} + m^2 u_n + V'(u_n) = 0,$$

$$\text{subject to : } \begin{cases} u_n(0) = \phi(n), & n \in \mathbb{Z}^+, \\ \frac{du_n}{dt}(0) = \varphi(n), & n \in \mathbb{Z}^+, \\ u_0(t) = \psi(t), & t \geq 0, \end{cases} \quad (2.1)$$

which describes a system of coupled oscillators with coupling coefficient $c \gg 1$, and where β and γ clearly play the roles of internal and external damping coefficients, respectively. The number $\Delta_x^2 u_n$ is used to represent the spatial second-difference $u_{n+1} - 2u_n + u_{n-1}$ for every $n \in \mathbb{Z}^+$, and the boundary-driving function ψ is assumed continuously differentiable on $(0, +\infty)$. In our study, we will let $V(u) = 1 - \cos u$ for a chain of coupled *sine-Gordon* equations, and $V(u_n) = \frac{1}{2!}u_n^2 - \frac{1}{4!}u_n^4 + \frac{1}{6!}u_n^6$ for zero mass in the case of a *Klein-Gordon* chain.

It is worth recalling that the differential equation under study has multiple applications in the continuous limit. For instance, a similar equation appears in the study of Josephson junctions between

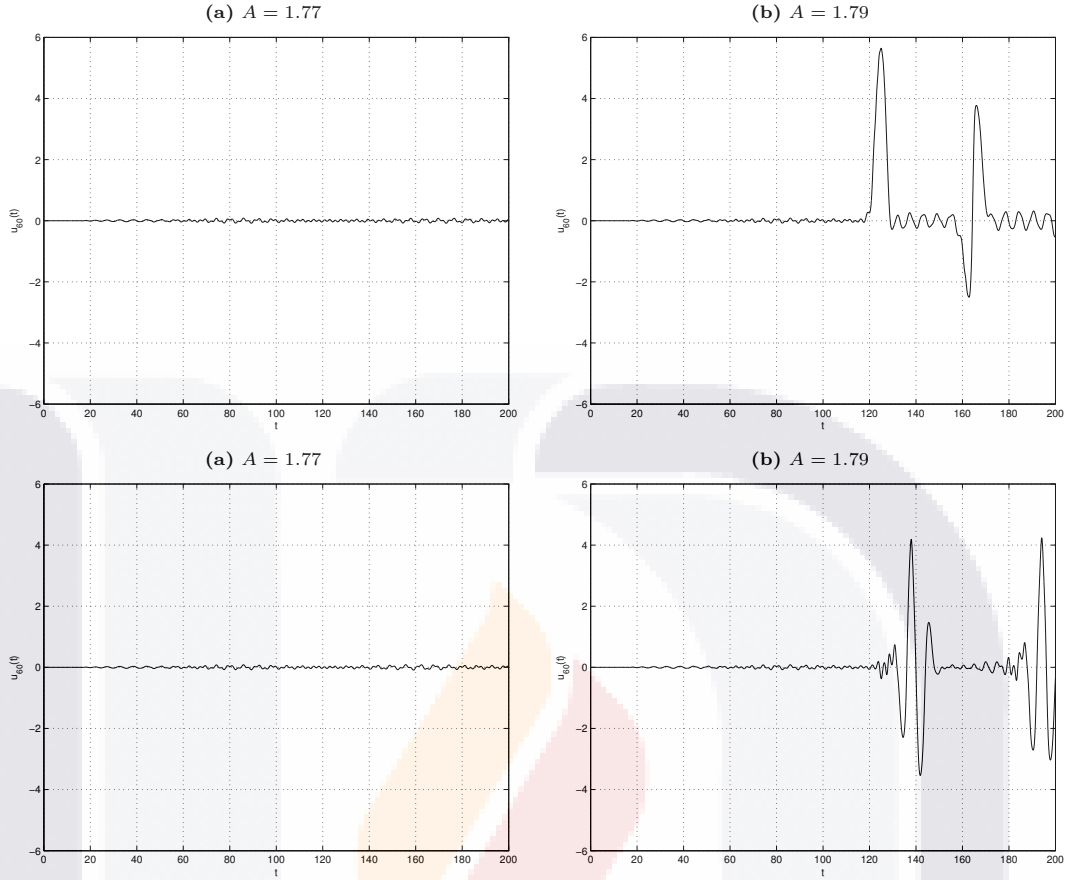


Figure 2.1: Approximate solution $u_{60}(t)$ of a sine-Gordon system in the first row and a Klein-Gordon system in the second, for a driving frequency of 0.9 and two different amplitude values A : (a) before and (b) after the bifurcation threshold.

superconductors when dissipative effects are taken into account [85]. A modification of this equation is used in the study of fluxons in Josephson transmission lines [55], and a version in the form of a modified Klein-Gordon equation appears in the statistical mechanics of nonlinear coherent structures such as solitary waves (see [66] pp. 298–309) when no internal damping is present. Besides, our equation clearly describes the motion of a damped string in a non-Hookean medium.

For purposes of this chapter, we will consider a system of coupled oscillators initially at rest at the origin of the system of reference, subject to an external harmonic forcing described by $\psi(t) = A \sin \Omega t$, and pure-imaginary or real mass satisfying $|m| \ll 1$. Analysis of the undamped linearized system of differential equations in (2.1) shows that the linear dispersion relation reads $\omega^2(k) = m^2 + 1 + 2c^2(1 - \cos k)$, in any case. The driving frequency will take on values in the forbidden band gap region $\Omega < \sqrt{m^2 + 1}$, in which case the linear analysis yields the exact solutions $u_n(t) = A \sin(\Omega t)e^{-\lambda n}$, where

$$\lambda = \operatorname{arccosh} \left(1 + \frac{m^2 + 1 - \Omega^2}{2c^2} \right).$$

Meanwhile, the massless undamped nonlinear case possesses an exact solution in the continuous

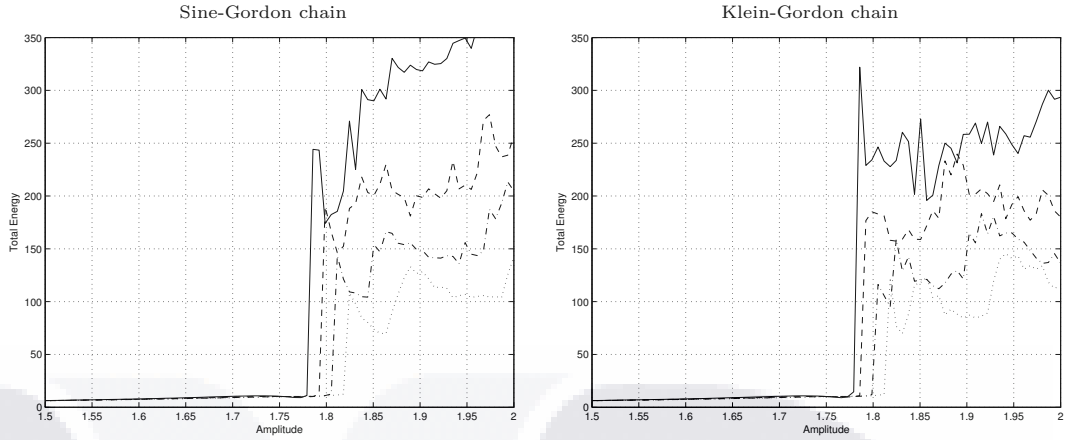


Figure 2.2: Graphs of total energy transmitted into the massless sine-Gordon and Klein-Gordon systems vs. driving amplitude for a driving frequency of 0.9, with $\beta = 0$ and $\gamma = 0$ (solid), 0.01 (dashed), 0.02 (dash-dotted), 0.03 (dotted).

limit which happens to work well for high values of the coupling coefficient. It has been shown numerically that, for each frequency Ω in the forbidden band gap, the massless medium starts to transmit energy by means of nonlinear mode generation for amplitudes greater than the threshold value $A_s = 4 \arctan(\lambda c/\Omega)$.

Energy analysis

In this section we derive the expression of the instantaneous rate of change of total energy in system (2.1). Here, by a *square-summable* sequence we understand a real sequence $(a_n)_{n=0}^\infty$ for which $\sum a_n^2$ is convergent.

Lemma 2.1 (Discrete Green’s First Identity). *If $(a_n)_{n=0}^\infty$ is a square-summable sequence then*

$$\sum_{n=1}^{\infty} (a_{n+1} - 2a_n + a_{n-1})a_n = a_0(a_0 - a_1) - \sum_{n=1}^{\infty} (a_n - a_{n-1})^2.$$

Proof. Hölder’s inequality implies that both series in the formula of the lemma converge. Moreover, the sequence defined by $t_n = a_n a_{n-1} - (a_{n-1})^2$ for every positive integer n converges to zero and the result follows now from the identities

$$\begin{aligned} \sum_{n=1}^{\infty} (a_{n+1} - 2a_n + a_{n-1})a_n &= \sum_{n=1}^{\infty} (t_{n+1} - t_n) - \sum_{n=1}^{\infty} (a_n - a_{n-1})^2 \\ &= -t_1 - \sum_{n=1}^{\infty} (a_n - a_{n-1})^2. \end{aligned}$$

□

Proposition 2.2. *Let $(u_n(t))_{n=0}^\infty$ be solutions to (2.1) such that $(\dot{u}_n(t))_{n=0}^\infty$ is square-summable at any*

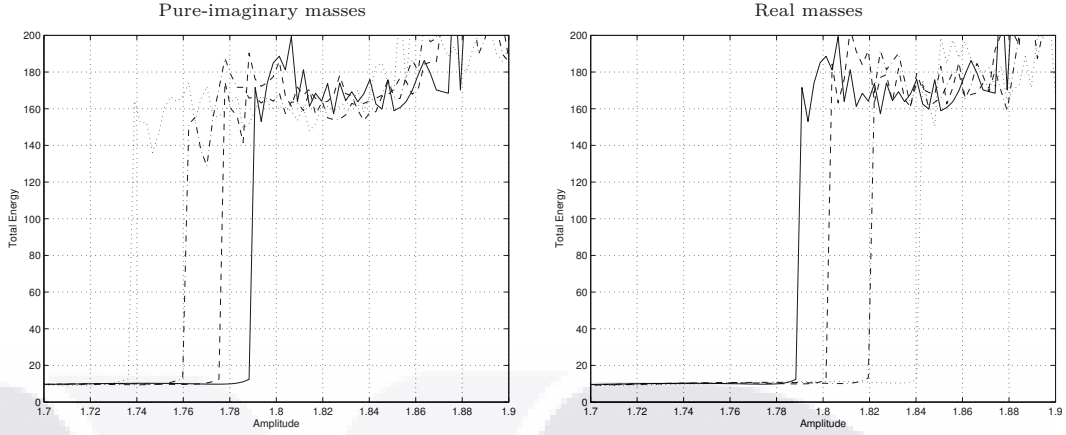


Figure 2.3: Total energy transmitted into the sine-Gordon system vs. driving amplitude for a driving frequency of 0.9, with $\beta = 0$, $\gamma = 0.01$, and pure-imaginary and real masses of magnitude 0 (solid), 0.05 (dashed), 0.075 (dash-dotted) and 0.1 (dotted).

fixed time t . The instantaneous rate of change of the total energy in the system is given by

$$\frac{dE}{dt} = c^2(u_0 - u_1)\dot{u}_0 - \gamma \sum_{n=1}^{\infty} (\dot{u}_n)^2 - \beta \left[\sum_{n=1}^{\infty} (\dot{u}_n - \dot{u}_{n-1})^2 + (\dot{u}_1 - \dot{u}_0)\dot{u}_0 \right].$$

Proof. The energy density of the undamped system of coupled equations with a potential energy $V(u_n)$ in the n -th oscillator is given by $H_n = \frac{1}{2}[\dot{u}_n^2 + c^2(u_{n+1} - u_n)^2 + m^2 u_n^2] + V(u_n)$. After including the potential energy from the coupling between the first two oscillators, the total energy of the system at any time becomes ”

$$E = \sum_{n=1}^{\infty} H_n + \frac{c^2}{2}(u_1 - u_0)^2,$$

and the fact that u_n tends to 0 as n increases implies that the sequence $J_n = -c^2\dot{u}_n(u_n - u_{n-1})$ converges to zero pointwisely at any fixed time. Simplifying and rearranging terms of the derivative of the Hamiltonian H_n yields the expression

$$\frac{dH_n}{dt} = (J_n - J_{n+1}) + \beta(\dot{u}_{n+1} - 2\dot{u}_n + \dot{u}_{n-1})\dot{u}_n - \gamma(\dot{u}_n)^2.$$

The result follows now from this identity after computing the derivative of the total energy of the system, using the formula for telescoping series and applying our discrete version of Green’s First Identity. \square

Observe from the proposition that the expression of the rate of change of energy associated with damped system (2.1) is in agreement with the undamped formula derived in [34]. Moreover, it is clear that the external damping coefficient contributes decreasing the total amount of energy in the chain system for β equal to zero.

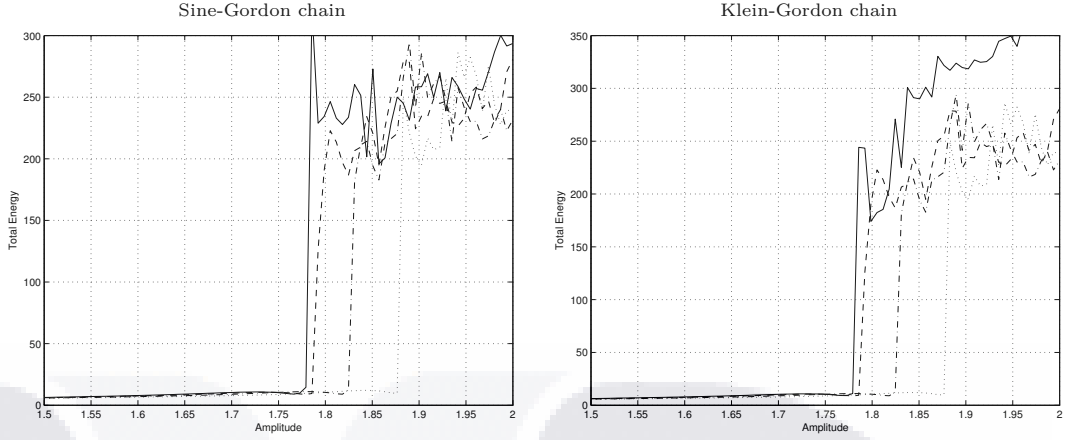


Figure 2.4: Graphs of total energy transmitted into the massless sine-Gordon and Klein-Gordon systems vs. driving amplitude for a driving frequency of 0.9, with $\gamma = 0$ and $\beta = 0$ (solid), 0.1 (dashed), 0.2 (dash-dotted), 0.3 (dotted).

2.3 Numerical analysis

Finite-difference scheme

From a practical point of view, we will restrict our study to a system consisting of a finite number N of coupled oscillators with constant internal and external damping coefficients, described by the system of ordinary differential equations

$$\frac{d^2 u_n}{dt^2} - \left(c^2 + \beta \frac{d}{dt} \right) \Delta_x^2 u_n + \alpha \frac{du_n}{dt} + m^2 u_n + V'(u_n) = 0$$

for $1 \leq n \leq N$, where α includes both the effect of external damping and a simulation of an absorbing boundary slowly increasing in magnitude on the last $N - N_0$ oscillators. More concretely, we let $u_{N+1}(t)$ be equal to zero at all time t , and let α be the sum of external damping and the function

$$\gamma'(n) = \begin{cases} \kappa \left[1 + \tanh \left(\frac{2n - N_0 + N}{2\sigma} \right) \right], & N_0 < n \leq N, \\ 0, & \text{otherwise.} \end{cases}$$

In practice, we will let $\kappa = 0.5$, $\sigma = 3$, $N_0 = 150$ and $N = 200$.

We proceed now to discretize problem (2.1) using a finite system of N differential equations and a regular partition $0 = t_0 < t_1 < \dots < t_M = T$ of the time interval $[0, T]$ with time step equal to Δt . For each $k = 0, 1, \dots, M$, let us represent the approximate solution to our problem on the n -th oscillator at time t_k by u_n^k . If we convey that $\delta_t u_n^k = u_n^{k+1} - u_n^{k-1}$, that $\delta_t^2 u_n^k = u_n^{k+1} - 2u_n^k + u_n^{k-1}$ and that

$\delta_x^2 u_n^k = u_{n+1}^k - 2u_n^k + u_{n-1}^k$, our problem takes then the discrete form

$$\frac{\delta_t^2 u_n^k}{(\Delta t)^2} - \left(c^2 + \frac{\beta}{2\Delta t} \delta_t \right) \delta_x^2 u_n^k + \frac{\alpha}{2\Delta t} \delta_t u_n^k + \frac{m^2}{2} [u_n^{k+1} + u_n^{k-1}] + \frac{V(u_n^{k+1}) - V(u_n^{k-1})}{u_n^{k+1} - u_n^{k-1}} = 0, \quad (2.2)$$

subject to :

$$\begin{cases} u_n^0 = \phi(n), & 1 \leq n \leq N, \\ u_n^1 = \phi(n) + \Delta t \varphi(n), & 1 \leq n \leq N, \\ u_0^k = \psi(k\Delta t), & 1 \leq k \leq M, \\ u_{N+1}^k = 0, & 1 \leq k \leq M. \end{cases}$$

Observe that the proposed numerical method is nonlinear and requires an application of Newton's method for systems of equations in order to be implemented. Notice also that if $V'(u_n)$ at the k -th time step is approximated by $V'(u_n^k)$ then the finite-difference scheme becomes linear and an application of Crout's reduction technique for tridiagonal systems suffices to approximate solutions of (2.1). In such case, it is readily seen that the vector equation

$$A\mathbf{u}^{k+1} = B\mathbf{u}^k + C\mathbf{u}^{k-1} - V'(\mathbf{u}^k) + \mathbf{v}^k$$

must be satisfied for every $k \geq 2$, for the three N -dimensional tridiagonal matrices and the N -dimensional vector

$$A = \begin{pmatrix} b & a & \cdots & 0 \\ a & b & \cdots & 0 \\ \vdots & \vdots & \ddots & \vdots \\ 0 & 0 & \cdots & b \end{pmatrix}, \quad B = \begin{pmatrix} d & c^2 & \cdots & 0 \\ c^2 & d & \cdots & 0 \\ \vdots & \vdots & \ddots & \vdots \\ 0 & 0 & \cdots & d \end{pmatrix},$$

and

$$C = \begin{pmatrix} e & a & \cdots & 0 \\ a & e & \cdots & 0 \\ \vdots & \vdots & \ddots & \vdots \\ 0 & 0 & \cdots & e \end{pmatrix}, \quad \mathbf{v}^k = \begin{pmatrix} c^2 u_0^k - a \delta_t u_0^k \\ 0 \\ 0 \\ \vdots \\ 0 \end{pmatrix},$$

respectively, and constants

$$a = -\frac{\beta}{2\Delta t}, \quad b = \frac{\alpha + 2\beta}{2\Delta t} + \frac{m^2}{2} + \frac{1}{(\Delta t)^2},$$

$$d = \frac{2}{(\Delta t)^2} - 2c^2 \quad \text{and} \quad e = \frac{\alpha + 2\beta}{2\Delta t} - \frac{m^2}{2} - \frac{1}{(\Delta t)^2}.$$

Here $\mathbf{u}^k = (u_1^k, \dots, u_n^k)^t$ for every $k \in \{0, 1, \dots, M\}$, and $V(\mathbf{u}^k)$ is the n -th dimensional vector whose i -th component is equal to $V(u_i^k)$. This latter formulation of our problem will be used for validation purposes only, since we will prefer the nonlinear formulation due to the quadratic order of convergence of Newton's method and other reasons that will be presented in the next section.

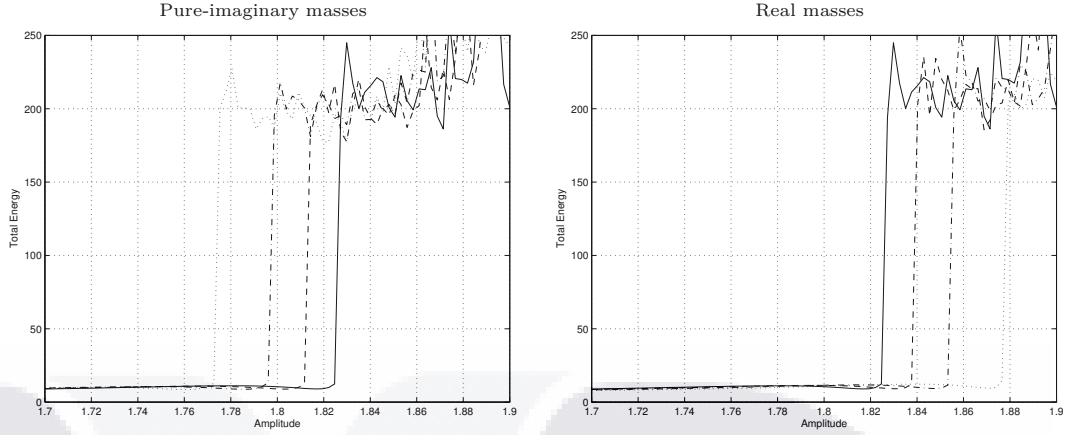


Figure 2.5: Total energy transmitted into the sine-Gordon system vs. driving amplitude for a driving frequency of 0.9, with $\beta = 0.2$, $\gamma = 0$, and pure-imaginary and real masses of magnitude 0 (solid), 0.05 (dashed), 0.075 (dash-dotted) and 0.1 (dotted).

Discrete energy

The total energy in the system at the k -th time step will be approximated numerically via

$$\begin{aligned}
 E_k = & \frac{1}{2} \sum_{n=1}^M \left(\frac{u_n^{k+1} - u_n^k}{\Delta t} \right)^2 + \frac{c^2}{2} \sum_{n=1}^M (u_{n+1}^{k+1} - u_n^{k+1})(u_{n+1}^k - u_n^k) \\
 & + \frac{m^2}{2} \sum_{n=1}^M \frac{(u_n^{k+1})^2 + (u_n^k)^2}{2} + \sum_{n=1}^M \frac{V(u_n^{k+1}) + V(u_n^k)}{2} \\
 & + \frac{c^2}{2} (u_1^{k+1} - u_0^{k+1})(u_1^k - u_0^k).
 \end{aligned}$$

Proposition 2.3. *The following identity holds for every sequence (u_n^k) satisfying (2.2) and every positive index k :*

$$\begin{aligned}
 \frac{E_k - E_{k-1}}{\Delta t} = & c^2(u_0^k - u_1^k) \frac{\delta_t u_0^k}{2\Delta t} - \gamma \sum_{n=1}^N \left(\frac{\delta_t u_n^k}{2\Delta t} \right)^2 \\
 & - \beta \left[\sum_{n=1}^{\infty} \left(\frac{\delta_t u_n^k - \delta_t u_{n-1}^k}{2\Delta t} \right)^2 + \left(\frac{\delta_t u_1^k - \delta_t u_0^k}{2\Delta t} \right) \frac{\delta_t u_0^k}{2\Delta t} \right].
 \end{aligned}$$

Proof. The proof of this result is merely an algebraic task. We need only say that an application of the discrete Green's First Identity with $a_n = (u_n^{k+1} - 2u_n^k + u_n^{k-1})/2\Delta t$ is indispensable in order to reach the correct expression of the term with coefficient β . \square

We conclude that the discrete energy associated with scheme (2.2) is a consistent approximation of order $\mathcal{O}(\Delta t)$ of the total energy of system (2.1), whereas the discrete rate of change of energy is consistent order $\mathcal{O}(\Delta t)^2$ with the instantaneous rate of change.

Stability analysis

The following result summarizes the numerical properties of our method.

Proposition 2.4. *Scheme (2.2) is consistent order $\mathcal{O}(\Delta t)^2$ with the linear contribution of (2.1) for a potential equal to zero. Moreover, a necessary condition for the scheme to be stable order n is that*

$$\left(c^2 - \frac{m^2}{4}\right) (\Delta t)^2 < 1 + \left(\frac{\alpha}{4} + \beta\right) \Delta t.$$

Proof. Following the notation in [106], let $U_{1n}^{k+1} = u_n^{k+1}$ and $U_{2n}^{k+1} = u_n^k$ for each $n = 0, 1, \dots, M$ and $k = 0, 1, \dots, N - 1$. For every $n = 0, 1, \dots, M$ and $k = 1, 2, \dots, N$ let \bar{U}_n^k be the column vector whose components are U_{1n}^k and U_{2n}^k . Our problem can be written then in matrix form as

$$\begin{pmatrix} g & 0 \\ 0 & 1 \end{pmatrix} \bar{U}_n^{k+1} = \begin{pmatrix} 2 + c^2(\Delta t)^2 \delta_x^2 & -h \\ 1 & 0 \end{pmatrix} \bar{U}_n^k,$$

where

$$\begin{aligned} g &= 1 + \alpha \frac{\Delta t}{2} - \beta \frac{\Delta t}{2} \delta_x^2 + m^2 \frac{(\Delta t)^2}{2} & \text{and} \\ h &= 1 - \alpha \frac{\Delta t}{2} + \beta \frac{\Delta t}{2} \delta_x^2 + m^2 \frac{(\Delta t)^2}{2}. \end{aligned}$$

Applying Fourier transform to the vector equation we obtain

$$\hat{U}_n^{k+1} = \begin{pmatrix} \frac{2}{\hat{g}(\xi)} \left(1 - 2c^2(\Delta t)^2 \sin^2 \frac{\xi}{2}\right) & -\frac{\hat{h}(\xi)}{\hat{g}(\xi)} \\ 1 & 0 \end{pmatrix} \hat{U}_n^k.$$

The matrix $A(\xi)$ multiplying \hat{U}_n^k in this equation is the amplification matrix of the problem. It is easy to check that the eigenvalues of A for $\xi = \pi$ are given by

$$\lambda_{\pm} = \frac{1 - 2c^2(\Delta t)^2 \pm \sqrt{(1 - 2c^2(\Delta t)^2)^2 - \hat{h}(\pi)\hat{g}(\pi)}}{\hat{g}(\pi)}.$$

Suppose for a moment that $1 - 2c^2(\Delta t)^2 < -\hat{g}(\pi)$. If the radical in the expression for the eigenvalues of $A(\pi)$ is a pure real number then $|\lambda_-| > 1$. So for every $n \in \mathbb{N}$, $\|A^n\| \geq |\lambda_-|^n$ grows faster than $K_1 + nK_2$ for any constants K_1 and K_2 . A similar situation happens when the radical is a pure imaginary number, except that in this case $|\cdot|$ represents the usual Euclidean norm in the field of complex numbers. Therefore in order for our numeric method to be stable order n it is necessary that $1 - 2c^2(\Delta t)^2 > -\hat{g}(\pi)$, which is what we wished to establish. \square

It is worth mentioning that our stability region is in agreement with the stability condition proposed in [58] when $c = 1$ for a similar nonlinear continuous problem.

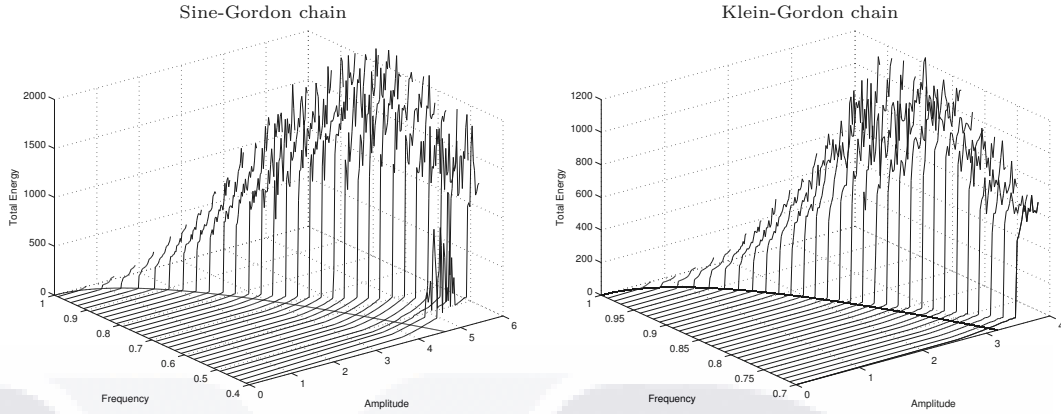


Figure 2.6: Graphs of total energy vs. driving frequency and amplitude for massless and undamped sine-Gordon and Klein-Gordon chains of coupled oscillators.

2.4 Numerical results

In this section we study the effects of the internal and external damping coefficients on the behavior of solutions to mixed-value problem (2.1). Particularly, we wish to establish the effect of weak damping on the minimum amplitude value necessary for the phenomenon of supratransmission to take place at a fixed driving frequency. Throughout we validate our code against [34] and against an implementation of our finite-difference scheme using the Runge-Kutta method of order four.

External Damping

For the remainder of this chapter we consider a semi-infinite coupled chain of oscillators initially at rest in their equilibrium positions, subject to harmonic forcing at the end described by $\psi(t) = A \sin(\Omega t)$ at any time t . The functions ϕ and φ are both identically equal to zero and, in order to avoid the shock wave produced by the vanishing initial velocity in the boundary, we let the driving amplitude linearly increase from 0 to A in a finite period of time before we start to compute the total energy. In the present section we will let β be equal to zero and consider a discrete system of 200 coupled oscillators described by (2.1) over a typical time period of 200, with a time step of 0.05 and a coupling coefficient equal to 4.

Let us first examine the massless case when no damping is present at all and $\Omega = 0.9$. In order to verify that our mixed-value problem produces a bifurcation it is necessary to study the qualitative behavior of solutions near the predicted threshold value A_s which, in this case, reads approximately 1.80. The first row of Figure 2.1 shows the function $u_{60}(t)$ in the solution of a sine-Gordon system for two different values of the amplitude of the driving end, while the second row presents the corresponding graphs in the solution of a Klein-Gordon chain. The graphs evidence the presence of a bifurcation in the behavior of solutions around the amplitude value 1.79 for both chains.

Naturally, the next step in our investigation will be to determine the behavior of the total energy flow injected by the periodic forcing at the end of the undamped discrete chain of oscillators as a function of the amplitude. The solid lines of Figure 2.2 represent the graphs of total energy transmitted into the system vs. amplitude for a forcing frequency of 0.9 and external damping coefficient equal

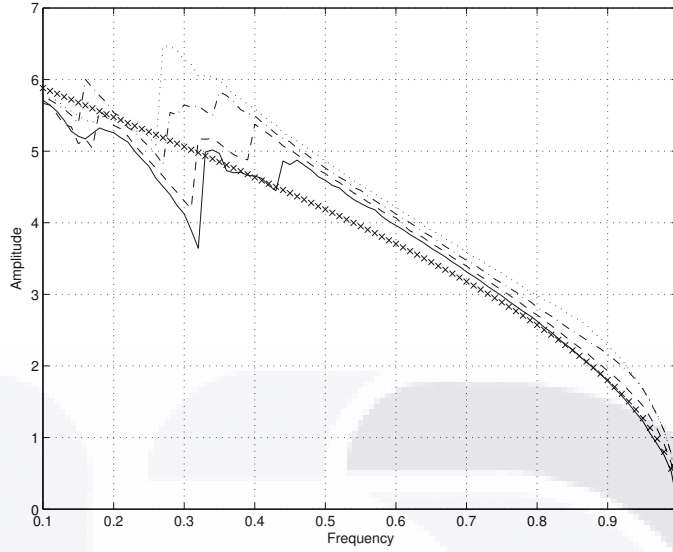


Figure 2.7: Diagram of smallest driving amplitude value at which supratransmission begins vs. driving frequency for a massless system with $\beta = 0$ and values of γ equal to 0 (solid), 0.1 (dashed), 0.2 (dash-dotted) and 0.3 (dotted). The theoretical threshold A_s in the undamped is shown as a sequence of \times -marks.

to zero, for a sine-Gordon system in the first column and a Klein-Gordon system in the second. It is worthwhile noticing the abrupt increase in the total energy administered to the system for some amplitude value between 1.77 and 1.79. This feature of the graphs evidences the existence of a bifurcation value around the predicted amplitude A_s , after which the phenomenon of nonlinear supratransmission takes place.

Figure 2.2 also presents graphs of total energy vs. forcing amplitude for weak constant damping coefficients $\gamma = 0.01, 0.02$ and 0.03 in a sine-Gordon system of oscillators. The graphs show a tendency of the bifurcation value to increase linearly as the external damping coefficient is increased. Another interesting feature of this figure is the decrease of total energy for increasing values of γ , at least for fixed amplitudes greater than the undamped bifurcation threshold. Needless to point out that similar conclusions are obtained for Klein-Gordon chains of oscillators.

The qualitative effect of m in a sine-Gordon system is also of interest in the analysis of solutions of this chain and is numerically carried out in Figure 2.3 for a chain with external damping equal to 0.01 and pure-imaginary and real masses, using graphs of total energy administered into the system through the boundary vs. driving amplitude. A horizontal shift in the occurrence of the bifurcation value is readily noticed in these graphs. Indeed, the displacement of the bifurcation amplitude for the system (2.1) of mass m with respect to the bifurcation amplitude of the massless system is a monotone increasing function of m^2 . Analogous computational results (not included here) were obtained for a similar Klein-Gordon chain.

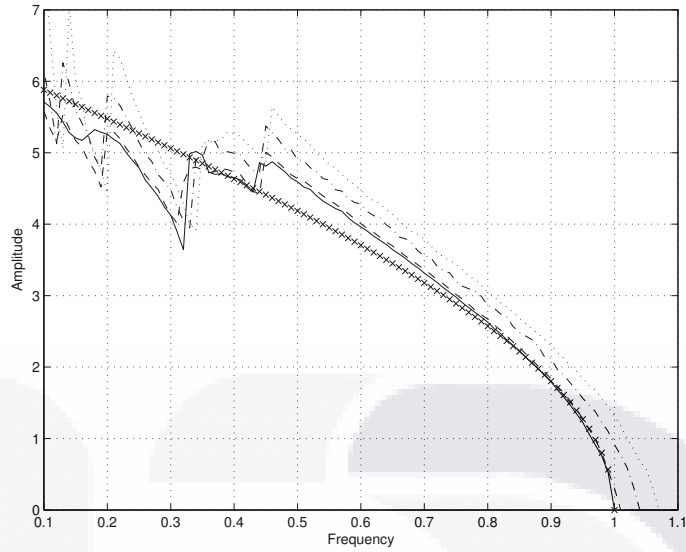


Figure 2.8: Diagram of smallest driving amplitude value at which supratransmission begins vs. driving frequency for a massless system with $\gamma = 0$ and values of β equal to 0 (solid), 0.1 (dashed), 0.4 (dash-dotted) and 0.7 (dotted). The theoretical threshold A_s in the undamped case is shown as a sequence of \times -marks.

Internal damping

Consider again a system of 200 oscillators ruled by mixed-value problem (2.1) over a time period of 200, with time step 0.05, coupling coefficient equal to 4 and constant external damping equal to zero. In this context, Figure 2.4 shows graphs of total energy vs. forcing amplitude for internal damping coefficients $\beta = 0, 0.1, 0.2$ and 0.3 , for sine-Gordon and Klein-Gordon systems. As in the case of external damping, we observe that the threshold value at which supratransmission starts tends to increase as the value of β is increased. Opposite to the case of external damping, though, the minimum value for which supratransmission starts varies with β in a nonlinear way.

Next we verify our conclusions on the effect of the mass m on the qualitative behavior of solutions of the sine-Gordon system. Figure 2.5 shows graphs of total energy vs. driving amplitude for a system with no external damping, $\beta = 0.2$ and driving frequency of 0.9, for different pure-imaginary and real masses. As observed before, the graphs evidence a shift on the bifurcation amplitude with respect to the massless bifurcation value which is an increasing function of m^2 .

Bifurcation analysis

Both the chain of coupled sine-Gordon equations and the chain of Klein-Gordon equations have numerically proved to undergo nonlinear supratransmission for a driving frequency equal to 0.9 and different values of the external and internal damping coefficients, thus establishing that the results obtained in this chapter do not depend on integrability. Naturally we are interested in determining that the process of nonlinear supratransmission happens for any frequency value in the forbidden band gap. With that purpose in mind, we obtained graphs of total energy vs. driving frequency and various amplitude values for undamped discrete systems of 200 coupled oscillators with coupling coefficient

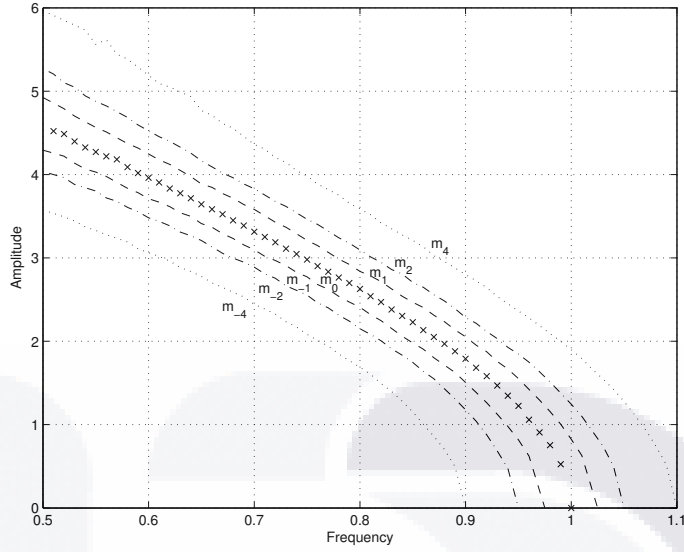


Figure 2.9: Diagram of smallest driving amplitude value at which supratransmission begins vs. driving frequency for an undamped sine-Gordon system with $\sqrt{m_\ell^2 + 1} = 1 + \frac{\ell}{40}$ for $\ell = -4, -2, -1, 0, 1, 2, 4$.

4, time period of 200 and time step 0.05. The 3-dimensional results for both chains of oscillators are shown in Figure 2.6 together with a graph of the continuous-limit threshold amplitude A_s vs. driving frequency on the amplitude-frequency plane for comparison purposes.

Several observations may be immediately drawn from Figure 2.6. First of all, the predicted bifurcation values A_s display an excellent concordance to the corresponding values obtained using the finite difference-schemes associated with the sine-Gordon and the Klein-Gordon chains. Second, the process of supratransmission ceases to appear in the Klein-Gordon case for driving frequencies below 0.7. Third, for driving frequencies close to the band gap limit, the bifurcation threshold is not clearly determined from the energy vs. driving amplitude graph of the sine-Gordon chain, as prescribed by [34]. For those frequencies, it is indispensable to increase the time period of approximation at least up to 500. Fourth, strong numerical proof of the existence of the occurrence of the supratransmission process is at hand and we have now reasons to believe that there exists a bifurcation function $A(\Omega; \beta, \gamma, m^2)$ for driving amplitude associated with (2.1).

We proceed then to obtain graphs of amplitude values for which nonlinear supratransmission starts vs. driving frequency for a massless sine-Gordon chain of coupled oscillators with internal damping coefficient equal to zero and different values of γ . The numerical results are summarized in Figure 2.7 together with the plot of the prescribed continuous-limit bifurcation amplitudes A_s . It is worth noticing that the bifurcation threshold increases with γ for fixed frequencies above 0.35, as previously evidenced for a frequency equal to 0.9. We must notice also that the discrepancies that appear for frequencies below 0.35 when $\gamma = 0$, also appear for greater values of γ , each time bounded in smaller intervals. In fact, we have checked that the discrepancy region — an effect of the phenomenon of harmonic phonon quenching — tends to vanish for higher values of external damping (results not included). In this state of matters, we wish to point out that better numerical approximations to the bifurcation threshold are obtained for larger systems of oscillators at the expense of superior needs in

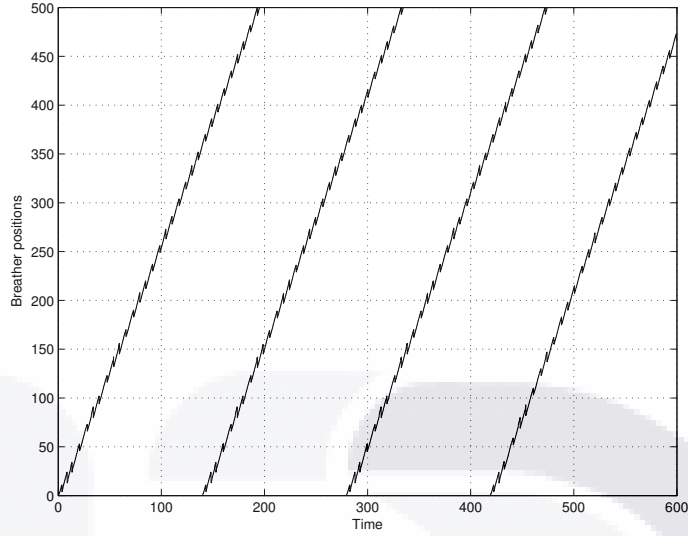


Figure 2.10: Time-dependent graphs of the position of the breathers generated in (2.3) by the binary signal ‘1111’.

terms of computational time. Likewise, we have confirmed that larger values of the coupling coefficient lead to better approximations to the bifurcation threshold, as prescribed by [34].

Figure 2.8 shows bifurcation diagrams for a massless sine-Gordon system of oscillators with no external damping and different constant internal damping coefficients. As expected, the bifurcation threshold tends to increase with β for a fixed driving frequency. The effects of harmonic phonon quenching are present again in all the bifurcation diagrams, but contrary to the case of external damping, in the case of internal damping the range over which discrepancies occur slightly widens as β increases. Also, it is worth observing that the length of the forbidden band gap increases with the parameter β apparently in a linear fashion. Moreover, the graphs of bifurcation diagrams for nonzero values of β are approximately obtained by shifting horizontally the corresponding graph of the undamped diagram a number of β units to the right. More concretely, $A(\Omega; 0, 0, 0)$ is a good approximation for $A(\Omega - \beta; \beta, 0, 0)$.

Finally, we compute bifurcation diagrams for an undamped sine-Gordon system with different real and pure-imaginary masses in order to establish the effect of m on the occurrence of the bifurcation threshold. The numerical results are summarized in Figure 2.9 for some real and pure-imaginary masses, and driving frequencies starting at 0.5. Our results lead us to conclude that the bifurcation diagram of the sine-Gordon system of oscillators with mass m is approximately equal to the graph of the corresponding massless graph shifted $\sqrt{1 + m^2} - 1$ horizontal units, for $|m| \ll 1$. In order to test our claim numerically, we obtained graphs of absolute differences between the massless undamped bifurcation diagram, and shifted undamped bifurcation diagrams for several mass values (results not included). We observed that the differences tend to attenuate for high frequency values and that smaller differences are obtained for smaller values of m in magnitude.

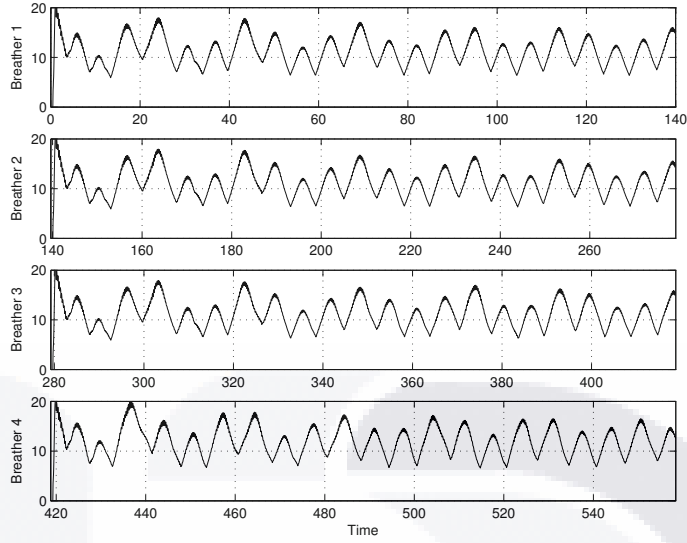


Figure 2.11: Time-dependent graphs of the maximum energy of the breathers generated in (2.3) by the binary signal ‘1111’.

2.5 Application

Throughout this section, we assume that α , β and γ are nonnegative real numbers, and that $c \gg 1$ (see [34]). Likewise, we consider a system $(u_n)_{n=1}^\infty$ of oscillators satisfying the mixed-value problem studied in [59], namely,

$$\frac{d^2 u_n}{dt^2} - \left(c^2 + \alpha \frac{d}{dt} \right) \Delta_x^2 u_n + \beta \frac{du_n}{dt} + V'(u_n) = 0,$$

subject to :

$$\begin{cases} u_n(0) = 0, & n \in \mathbb{Z}^+, \\ \frac{du_n}{dt}(0) = 0, & n \in \mathbb{Z}^+, \\ u_0(t) = \psi(t), & t \geq 0, \end{cases} \quad (2.3)$$

where c is the coupling coefficient, and α and β evidently play the roles of internal and external damping coefficients, respectively. Here, $\Delta_x^2 u_n$ is used to denote the spatial second-difference $u_{n+1} - 2u_n + u_{n-1}$ for every $n \in \mathbb{Z}^+$, the boundary-driving function is given by $\psi(t) = A(t) \sin(\Omega t)$ for every $t \in (0, +\infty)$, and $V(u_n) = 1 - \cos(u_n) - \gamma u_n$ where, due to the analogy with the Josephson model [111], γ will be called here the *normalized current*. Notice that the Hamiltonian of the n -th lattice site is given by

$$H_n = \frac{1}{2} [\dot{u}_n^2 + c^2(u_{n+1} - u_n)^2] + V(u_n),$$

for any differentiable function V . After including the potential energy from the coupling between the first two oscillators, the total energy of the system becomes

$$E = \sum_{n=1}^{\infty} H_n + \frac{c^2}{2}(u_1 - u_0)^2.$$

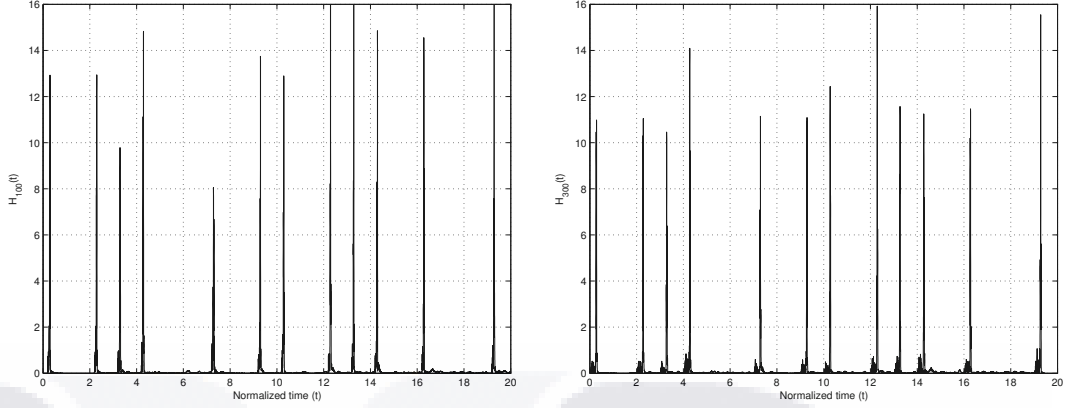


Figure 2.12: Local energy of the 100-th (left) and 300-th (right) sites in (2.3) vs. normalized time, as a response to the transmission of the binary signal ‘10111001011101101001’.

Bifurcation analysis

The existence of a bifurcation threshold of the energy administered into a semi-infinite chain of damped coupled oscillators described by (2.3) has been established and numerically predicted in [59] for a potential $V(u) = 1 - \cos u$. Numerical experiments on undamped mechanical chains with nonzero normalized bias currents have shown that the process of nonlinear supratransmission is likewise present in these models. In fact, in the previous sections we provided bifurcation diagrams of driving amplitude at which supratransmission first occurs vs. driving frequency Ω for a system of 200 undamped oscillators with coupling coefficient equal to 4 and several values of γ , over a time interval $[0, T(\Omega)]$ where $T(\Omega)$ is equal to 200 for all frequencies except for those satisfying $\Omega > 0.95$, in which case $T(\Omega)$ had to be increased up to 500.

Moving breather solutions

For the sake of simplification, let $\gamma = 0$ and consider a discrete system described by (2.3), harmonically driven at the boundary by a frequency Ω . A binary bit b will be transmitted into the medium during a fixed and sufficiently long period of signal generation P equal to an integer multiple of the driving period, by defining

$$A(t) = \frac{8}{5}bCA_s \left(e^{-\Omega t/4.5} - e^{-\Omega t/0.45} \right)$$

for every $t \in [0, P]$, where A_s represents the critical amplitude at which nonlinear supratransmission starts and $C > 0$ is an *adjusting constant*.

In the previous sections, we provided numerical evidence that shows the time evolution of the local energies H_n corresponding to solutions of the undamped problem (2.3) with coupling coefficient equal to 4, driving frequency 0.9 (in which case A_s is approximately equal to 1.79) and $C = A_s$. The period of signal generation is equal to 20 driving periods, and the binary code transmitted at the boundary is ‘1111’. The results show that a single moving breather is generated per period, and that the phase velocity v_p through the medium is approximately constant. To verify this claim, we include in Fig. 2.10 the graphs of the positions of the four breathers generated by the binary signal vs. time. The fact that the breathers are transmitted at a constant velocity is now obvious, the common phase velocity

being approximately 2.549.

In order to determine the strength of the emitted signals at sites located far away from the source, it is important to determine the time behavior of the maximum local energy attained by a discrete breather. Fig. 2.11 presents this behavior for the breather solutions obtained under the conditions above. Notice that the maximum local energy is well above a cutoff limit of 2.

Signal propagation

The discrete medium described by (2.3) with $\alpha = \beta = \gamma = 1 \times 10^{-3}$, and the rest of the parameters as in the previous section, will be our object of study in this section. Local energy-based reception devices will be placed on the 100-th and 300-th lattice sites, and the signal to be transmitted through the chain system is ‘10111001011011101001’. Our system will consist of 600 sites, and a time step of 0.05 will be employed.

Assuming the general convention that site $n_0 \geq 100$ will start signal reception at time $t = (n_0 - 100)/v_p$, Fig. 2.12 shows the evolution of the local energy in the 100-th and 300-th sites in terms of the time normalized with respect to the period of signal generation. In either case, it is clear that the transmission of a bit equal to 1 in the n -th period is completely characterized in the graph by peak(s) of height greater than the cutoff limit 2 on the interval $[n - 1, n]$.

TESIS TESIS TESIS TESIS TESIS



3. Numerical method for a fractional medium

In this chapter, we investigate numerically a model governed by a multidimensional nonlinear wave equation with damping and fractional diffusion. The governing partial differential equation considers the presence of Riesz space-fractional derivatives of orders in $(1, 2]$, and homogeneous Dirichlet boundary data are imposed on a closed and bounded spatial domain. The model under investigation possesses an energy function which is preserved in the undamped regime. In the damped case, we establish the property of energy dissipation of the model using arguments from functional analysis. Motivated by these results, we propose an explicit finite-difference discretization of our fractional model based on the use of fractional centered differences. Associated to our discrete model, we also propose discretizations of the energy quantities. We establish that the discrete energy is conserved in the undamped regime, and that it dissipates in the damped scenario. Among the most important numerical features of our scheme, we show that the method has a consistency of second order, that it is stable and that it has a quadratic order of convergence. Some one- and two-dimensional simulations are shown in this chapter to illustrate the fact that the technique is capable of preserving the discrete energy in the undamped regime.

3.1 Introduction

In the last decades, the investigation of physical media described by systems with long-range interactions has been a fruitful avenue of research. In particular, a wide variety of physical phenomena described by linear systems with long-range interactions have been reported in the literature. One of the typical examples in classical physics is the linear interaction of particles in a three-dimensional gravitational system [7]. Other examples are the interactions of vortices in two dimensions, engineering problems on elasticity arising from the study of planar stress, systems of electric charges and systems that consider dipolar forces [11]. Moreover, there are several well-characterized cases of long-range interactions involved in the activation and the repression of transcription in chromosomal and gene regulation [71], and many other applications have been proposed to polymer science (including some applications to microscopic models of polymer dynamics and rheological constitutive equations), to regular variations in thermodynamics and to Hamiltonian chaotic systems [40]. It is worth pointing out that various works have been devoted to the physical and mathematical investigation of generalized forms of these models [104, 103], including systems which exhibit the presence of the phenomenon of

TESIS TESIS TESIS TESIS TESIS

nonlinear supratransmission of energy in fractional sine-Gordon-type equations [62], models of Josephson transmission lines [63] and extensions of the Fermi–Pasta–Ulam chains [64]. Additionally, some models of oscillators with long-range interactions possess conservation laws that resemble those quantities preserved by classical systems [100, 105].

It is important to recall that certain long-range interactions (namely, the so-called α -interactions) yield fractional derivatives in some continuous-limit process. This process involves the Fourier series transform, the inverse Fourier transform and the limiting process when the distance between consecutive particles tends to zero [101]. In such way, fractional models in the form of ordinary or partial differential equations are obtained from discrete physical systems. In fact, there are various types of long-range interactions which lead to systems that include fractional derivatives of the Riesz type. From this perspective, the use of the Riesz differential operator is physically justified, at least as the continuous limit of physically meaningful discrete systems appearing in various branches of sciences. Obviously, this fact has encouraged the mathematical modeling using fractional differential equations, as well as the analytical and the physical investigation of these models. Needless to mention that the specialized literature has benefited from the investigation of fractional equations. Indeed various interesting reports have been published on the existence and the uniqueness of solutions of fractional forms of parabolic models, like the porous media equation [20], the nonlinear diffusion equation in multiple dimensions [112] and nonlinear degenerate diffusion equations in bounded domains [10].

On the other hand, the recent advances of fractional calculus have led to the development of numerical techniques to approximate the solution of fractional partial differential equations. As examples, numerical models have been proposed to solve a time-space fractional Fokker–Planck equation with variable force field and diffusion [80] and nonlinear fractional-order Volterra integro-differential equations [119]. Some fractional models that extend well-known equations from mathematical physics have been the motivation to develop suitable numerical schemes. For instance, some highly accurate numerical schemes have been proposed for variable-order fractional Schrödinger equations [8], a new technique based on Legendre polynomials has been reported to solve the fractional two-dimensional heat equation [46], some improvements of the sub-equation method have been designed to solve a $(3 + 1)$ -dimensional generalization of the Korteweg–de Vries–Zakharov–Kuznetsov equation [87] and some novel methods have been constructed to approximate the solutions of a two-dimensional variable-order fractional percolation equation in non-homogeneous porous media [16]. Like these reports, the literature shows that the numerical investigation of fractional partial differential equations has been a fruitful avenue of current research in numerical analysis [57]. However, it is important to point out that the design of structure-preserving methods to solve such models is still a direction of research which has not been sufficiently exploited.

In this context, the notion of structure-preserving method refers to those numerical techniques which are capable of preserving physical features of the solutions of interest. As opposed to numerical efficiency which is typically associated to the computational properties inherent to those techniques (consistency, stability and convergence), the properties of preservation of the structure of solutions depend on each physical problem itself. As examples of those properties, we can quote the conservation of physical quantities like energy, momentum or mass [31]. Mathematical characteristics such as positivity, boundedness, monotonicity and convexity are also considered in this chapter as structural properties [65]. Some structure-preserving methods have been designed for the numerical solution of

partial differential equations of fractional order. For instance, some energy-preserving schemes have been proposed for the nonlinear fractional Schrödinger equation [116], and some finite-difference scheme based on fractional centered differences has been used to approximate positive and bounded solutions of a fractional population model [61]. However, it is important to note that there are very few reports in the literature on energy-conserving methods for fractional partial differential equations which are consistent, stable and convergent. In particular, fractional extensions of hyperbolic models like the sine-Gordon and the Klein-Gordon equations have been practically left without investigation. This is a topic that merits deeper investigation in view of all the potential applications of those equations to the continuous mathematical modeling of nonlinear systems with long-range interactions [101, 18, 17].

The purpose of the present chapter is to study numerically a multidimensional Riesz space-fractional generalization of the nonlinear and damped wave equation that extends various models from mathematical physics, including the sine-Gordon and the Klein-Gordon equations. It is well known that these two models possess an energy functional that dissipates or is conserved, depending on suitable analytical and parameter conditions. Thus the design of dissipation and conserving schemes to approximate its solution is pragmatically justified. The method reported in this chapter has some associated energy density functionals along with a function of total energy which is capable of resembling this property of the continuous model. Moreover, we will show that our methodology is an explicit technique which is second-order consistent, stable and quadratically convergent. Some simulations will be provided to illustrate the capability of the scheme to preserve the energy when the damping coefficient is equal to zero. Evidently, the explicit nature of our approach makes the technique an ideal tool in the investigation of multidimensional systems governed by Riesz space-fractional nonlinear wave equations.

This chapter is sectioned as follows. The multidimensional nonlinear dissipative wave equation with Riesz space-fractional derivatives is presented in Section 3.2, together with the definition of the fractional differential operator and a dimensional extension of an energy functional proposed in the literature [4]. We show in that section that the initial-boundary-value problem under investigation is a dissipative system, and that it is conservative when the damping coefficient is equal to zero. Section 3.3 introduces the discrete nomenclature and the explicit method to solve numerically the problem under investigation. The concept of fractional centered differences will be recalled therein and some useful lemmas will be proved in the way. The most important physical properties of the method will be established in Section 3.4. Concretely, we will establish the capability of the finite-difference scheme to preserve the dissipation or the conservation of energy of the discrete system. The most important numerical properties of our technique will be proved in Section 3.6. In that stage we will show that our method is a consistent technique, and we will establish the stability and the convergence properties. The proofs will make use of various technical lemmas established in Section 3.5. Additionally, Section 3.6 offers some qualitative simulations that illustrate the capability of our scheme to preserve the energy or the dissipation of energy in Riesz space-fractional wave equations. This chapter closes with a section of concluding remarks.

3.2 Preliminaries

In this chapter we let $p \in \mathbb{N}$, $T \in \mathbb{R}^+$ and $\gamma \in \mathbb{R}^+ \cup \{0\}$. Let us define the set $I_n = \{1, \dots, n\}$ for each natural number n , and let $\bar{I}_n = I_n \cup \{0\}$. Suppose that $a_i, b_i \in \mathbb{R}$ satisfy $a_i < b_i$ for each $i \in I_p$. Throughout we will assume that $1 < \alpha_i \leq 2$ for each $i \in I_p$, and we let

$$B = \prod_{i=1}^p (a_i, b_i) \subseteq \mathbb{R}^p, \quad (3.1)$$

$$\Omega = B \times (0, T) \subseteq \mathbb{R}^{p+1}. \quad (3.2)$$

We introduce the symbols \bar{B} and $\bar{\Omega}$ to denote the closures of B and Ω in \mathbb{R}^{p+1} under the standard topology, respectively, and let ∂B represent the boundary of B . Assume that $G : \mathbb{R} \rightarrow \mathbb{R}$ and that $\phi, \psi : B \rightarrow \mathbb{R}$ are sufficiently smooth functions that satisfy $\phi(x) = \psi(x) = 0$ for each $x \in \partial B$. Additionally, we will suppose that G is nonnegative and that $u : \bar{\Omega} \rightarrow \mathbb{R}$ is a sufficiently smooth function that satisfies the initial-boundary-value problem

$$\begin{aligned} \frac{\partial^2 u}{\partial t^2}(x, t) - \sum_{i=1}^p \frac{\partial^{\alpha_i} u}{\partial |x_i|^{\alpha_i}}(x, t) + \gamma \frac{\partial u}{\partial t}(x, t) + G'(u(x, t)) = 0, \quad \forall (x, t) \in \Omega, \\ \text{such that } \begin{cases} u(x, 0) = \phi(x), & \forall x \in B, \\ \frac{\partial u}{\partial t}(x, 0) = \psi(x), & \forall x \in B, \\ u(x, t) = 0, & \forall (x, t) \in \partial B \times (0, T). \end{cases} \end{aligned} \quad (3.3)$$

Here we assume that $x = (x_1, x_2, \dots, x_p) \in \mathbb{R}^p$, and the Riesz differential operators are defined for each $i \in I_p$ by

$$\frac{\partial^{\alpha_i} u}{\partial |x_i|^{\alpha_i}}(x, t) = \frac{-1}{2 \cos(\frac{\pi \alpha_i}{2}) \Gamma(2 - \alpha_i)} \frac{\partial^2}{\partial x_i^2} \int_{a_i}^{b_i} \frac{u(x_1, \dots, x_{i-1}, \xi, x_{i+1}, \dots, x_p, t)}{|x_i - \xi|^{\alpha_i - 1}} d\xi, \quad \forall (x, t) \in \Omega. \quad (3.4)$$

Let $L_{x,2}(\bar{\Omega})$ denote the set of all functions $f : \bar{\Omega} \rightarrow \mathbb{R}$ such that $f(\cdot, t) \in L_2(\bar{B})$ for each $t \in [0, T]$. For each pair $f, g \in L_{x,2}(\bar{\Omega})$, the inner product of f and g is the function of t defined by

$$\langle f, g \rangle_x = \int_{\bar{B}} f(x, t) g(x, t) dx, \quad \forall t \in [0, T]. \quad (3.5)$$

In turn, the Euclidean norm of $f \in L_{x,2}(\bar{\Omega})$ is the function of t defined by $\|f\|_{x,2} = \sqrt{\langle f, f \rangle}$. The set of all functions $f : \bar{\Omega} \rightarrow \mathbb{R}$ such that $f(\cdot, t) \in L_1(\bar{B})$ for each $t \in [0, T]$ will be denoted by $L_{x,1}(\bar{\Omega})$, and for each such f we define its norm as the function of t given by

$$\|f\|_{x,1} = \int_{\bar{B}} |f(x, t)| dx, \quad \forall t \in [0, T]. \quad (3.6)$$

The literature on mathematical physics has proposed various functionals to calculate the energy of one-dimensional systems governed by (3.3) when $\gamma = 0$ (see [105], for instance). For purposes of this

chapter, we will use the following dimensional extension of the energy integral employed in [4]:

$$\mathcal{E}(t) = \frac{1}{2} \left\| \frac{\partial u}{\partial t} \right\|_{x,2}^2 + \frac{1}{2} \sum_{i=1}^p \left\langle u, -\frac{\partial^{\alpha_i} u}{\partial |x_i|^{\alpha_i}} \right\rangle_x + \|G(u)\|_{x,1}, \quad \forall t \in [0, T]. \quad (3.7)$$

It is important to note here that the Riesz fractional derivative of order α_i in the i th component is a self-adjoint and negative operator [52] for each $i \in I_p$. This fact implies that the additive inverse of the Riesz fractional derivative has a unique square root operator [29] which will be denoted by $\Xi_{x_i}^{\alpha_i}$. Moreover, the following holds for any two functions u and v :

$$\left\langle -\frac{\partial^{\alpha_i} u}{\partial |x_i|^{\alpha_i}}, v \right\rangle_x = \langle \Xi_{x_i}^{\alpha_i} u, \Xi_{x_i}^{\alpha_i} v \rangle_x. \quad (3.8)$$

The next result is now easy to verify.

Lemma 3.1. *The energy function (3.7) may be rewritten alternatively as*

$$\mathcal{E}(t) = \frac{1}{2} \left\| \frac{\partial u}{\partial t} \right\|_{x,2}^2 + \frac{1}{2} \sum_{i=1}^p \|\Xi_{x_i}^{\alpha_i} u\|_{x,2}^2 + \|G(u)\|_{x,1}, \quad (3.9)$$

for each $t \in (0, T)$. □

Obviously, the associated energy density is defined for each $(x, t) \in \Omega$ by

$$\begin{aligned} \mathcal{H}(x, t) &= \frac{1}{2} \left[\frac{\partial u}{\partial t}(x, t) \right]^2 - \frac{1}{2} \sum_{i=1}^p u(x, t) \frac{\partial^{\alpha_i} u}{\partial |x_i|^{\alpha_i}}(x, t) + G(u(x, t)) \\ &= \frac{1}{2} \left[\frac{\partial u}{\partial t}(x, t) \right]^2 + \frac{1}{2} \sum_{i=1}^p [\Xi_{x_i}^{\alpha_i} u(x, t)]^2 + G(u(x, t)). \end{aligned} \quad (3.10)$$

The following result is the cornerstone of our investigation. It is a generalization of Theorem 1.1 of [60], which is a result valid for fractional wave equations in one spatial variable. A proof is provided here for completeness.

Theorem 3.2 (Macías-Díaz [60]). *If u is a solution of (3.3) then*

$$\mathcal{E}'(t) = -\gamma \left\| \frac{\partial u}{\partial t} \right\|_{x,2}^2, \quad \forall t \in (0, T). \quad (3.11)$$

Proof. Note that the following hold for each $i \in I_p$:

$$\frac{1}{2} \frac{d}{dt} \left\| \frac{\partial u}{\partial t} \right\|_{x,2}^2 = \frac{1}{2} \int_B \frac{\partial}{\partial t} \left(\frac{\partial u}{\partial t}(\xi, t) \right)^2 d\xi = \left\langle \frac{\partial u}{\partial t}, \frac{\partial^2 u}{\partial t^2} \right\rangle, \quad (3.12)$$

$$\frac{1}{2} \frac{d}{dt} \|\Xi_{x_i}^{\alpha_i} u\|_{x,2}^2 = \left\langle \frac{\partial}{\partial t} (\Xi_{x_i}^{\alpha_i} u), \Xi_{x_i}^{\alpha_i} u \right\rangle_x = \left\langle \Xi_{x_i}^{\alpha_i} \left(\frac{\partial u}{\partial t} \right), \Xi_{x_i}^{\alpha_i} u \right\rangle_x = \left\langle \frac{\partial u}{\partial t}, -\frac{\partial^{\alpha_i} u}{\partial |x_i|^{\alpha_i}} \right\rangle, \quad (3.13)$$

$$\frac{d}{dt} \|G(u)\|_{x,1} = \int_a^b \frac{\partial}{\partial t} G(u(\xi, t)) d\xi = \left\langle \frac{\partial u}{\partial t}, G'(u) \right\rangle. \quad (3.14)$$

Taking derivative with respect to t on both sides of (3.9), using the identities above and the partial

differential equation of (3.3), and simplifying algebraically we obtain

$$\mathcal{E}'(t) = \int_{\mathcal{B}} \frac{\partial u}{\partial t}(\xi, t) \left[\frac{\partial^2 u}{\partial t^2}(\xi, t) - \sum_{i=1}^p \frac{\partial^{\alpha_i} u}{\partial |x_i|^{\alpha_i}}(\xi, t) + G'(u(\xi, t)) \right] d\xi = -\gamma \int_{\mathcal{B}} \left[\frac{\partial u}{\partial t}(\xi, t) \right]^2 d\xi, \quad (3.15)$$

whence the result readily follows. \square

Corollary 3.3. *If u is a solution of (3.3) then*

$$\mathcal{E}(t) = \mathcal{E}(0) - \gamma \int_0^t \left\| \frac{\partial u}{\partial t} \right\|_{x,2}^2 dt, \quad \forall t \in [0, T]. \quad (3.16)$$

In particular, if $\gamma = 0$ then the system (3.3) is conservative. \square

In the following section, we will propose an explicit numerical method to approximate the solutions of (3.3) and the energy function (3.7). Our numerical technique will satisfy discrete versions of Theorem 3.2 and Corollary 3.3, along with the numerical properties of consistency, stability and convergence.

3.3 Numerical method

For the remainder of this chapter we let h_i and τ be positive step-sizes for each $i \in I_p$, and assume that $N = T/\tau$ and $M_i = (b_i - a_i)/h_i$ are positive integers for each $i \in I_p$. Consider uniform partitions of $[a_i, b_i]$ and $[0, T]$ given by

$$x_{i,j_i} = a_i + j_i h_i, \quad \forall i \in I_p, \forall j_i \in \bar{I}_{M_i}, \quad (3.17)$$

$$t_n = n\tau, \quad \forall n \in \bar{I}_N. \quad (3.18)$$

Let $J = \prod_{i=1}^p I_{M_i-1}$ and $\bar{J} = \prod_{i=1}^p \bar{I}_{M_i}$, and let ∂J represent the boundary of the mesh \bar{J} . Define $x_j = (x_{1,j_1}, \dots, x_{p,j_p})$ for each multi-index $j = (j_1, \dots, j_p) \in \bar{J}$. In this chapter, the symbol v_j^n will represent a numerical approximation to the exact value of $u_j^n = u(x_j, t_n)$ for each $j \in \bar{J}$ and each $n \in \bar{I}_N$. Define the discrete linear operators

$$\mu_t u_j^n = \frac{u_j^{n+1} + u_j^n}{2}, \quad (3.19)$$

$$\delta_t^{(1)} u_j^n = \frac{u_j^{n+1} - u_j^n}{\tau}, \quad (3.20)$$

$$\delta_t^{(2)} u_j^n = \frac{u_j^{n+1} - 2u_j^n + u_j^{n-1}}{\tau^2}, \quad (3.21)$$

$$\delta_{u,t}^{(1)} G(u_j^n) = \begin{cases} \frac{G(u_j^{n+1}) - G(u_j^n)}{u_j^{n+1} - u_j^n}, & \text{if } u_j^{n+1} \neq u_j^n, \\ G'(u_j^n), & \text{if } u_j^{n+1} = u_j^n, \end{cases} \quad (3.22)$$

for each $j \in J$ and $n \in I_{N-1}$.

Definition 3.4. For any function $f : \mathbb{R} \rightarrow \mathbb{R}$, any $h > 0$ and any $\alpha > -1$ we define the *fractional*

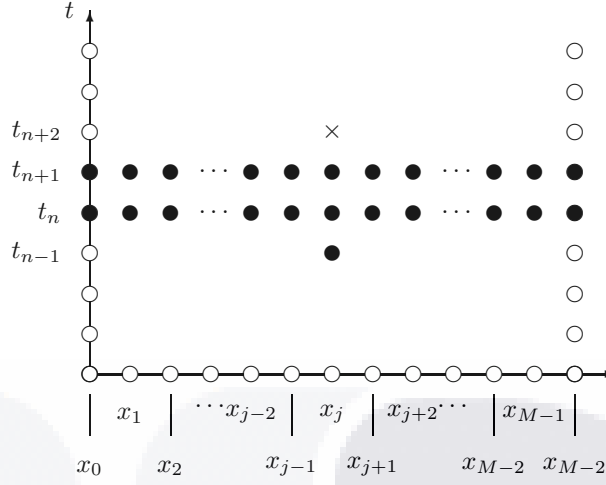


Figure 3.1: Forward-difference stencil for the approximation to the exact solution of the one dimensional form of (3.3) at the time t_n , using the finite-difference scheme (3.28). The black circles represent the known approximations at the times t_{n-1} , t_n and t_{n+1} , while the cross denotes the unknown approximation at the time t_{n+2} .

centered difference of order α of f at the point x as

$$\Delta_h^\alpha f(x) = \sum_{k=-\infty}^{\infty} g_k^{(\alpha)} f(x - kh), \quad \forall x \in \mathbb{R}, \quad (3.23)$$

where

$$g_k^{(\alpha)} = \frac{(-1)^k \Gamma(\alpha + 1)}{\Gamma(\frac{\alpha}{2} - k + 1) \Gamma(\frac{\alpha}{2} + k + 1)}, \quad \forall k \in \mathbb{N} \cup \{0\}. \quad (3.24)$$

Lemma 3.5 (Çelik and Duman [13]). *If $1 < \alpha \leq 2$ then*

- (i) $g_0^{(\alpha)} \geq 0$,
- (ii) $g_k^{(\alpha)} = g_{-k}^{(\alpha)} < 0$ for all $k \geq 1$, and
- (iii) $\sum_{k=-\infty}^{\infty} g_k^{(\alpha)} = 0$. □

As a consequence, the series on the right-hand side of (3.23) converges absolutely for any $f \in L_1(\mathbb{R}) \cap L_\infty(\mathbb{R})$. It is easy to see that any $f \in C^5(\mathbb{R})$ for which all of its derivatives up to order five belong to $L_1(\mathbb{R})$, satisfies

$$-\frac{1}{h^\alpha} \Delta_h^\alpha f(x) = \frac{\partial^\alpha f(x)}{\partial |x|^\alpha} + \mathcal{O}(h^2), \quad \forall x \in \mathbb{R}, \quad (3.25)$$

whenever $1 < \alpha \leq 2$ (see [13]). Moreover, if $u \in C^5(\bar{B})$ then

$$\frac{\partial^{\alpha_i} u}{\partial |x_i|^{\alpha_i}}(x_j, t_n) = \delta_{x_i}^{(\alpha_i)} u_j^n + \mathcal{O}(h^2), \quad \forall i \in I_p, \forall (j, n) \in J \times \bar{I}_N, \quad (3.26)$$

where

$$\delta_{x_i}^{(\alpha_i)} u_j^n = -\frac{1}{h_i^{\alpha_i}} \sum_{k=0}^{M_i} g_{j_i-k}^{(\alpha_i)} u(x_{1,j_1}, \dots, x_{i-1,j_{i-1}}, x_{i,k}, x_{i+1,j_{i+1}}, \dots, x_{p,j_p}, t_n). \quad (3.27)$$

With this nomenclature, the finite-difference method to approximate the solution of (3.3) on Ω is given by

$$\begin{aligned} \mu_t \delta_t^{(2)} v_j^n - \sum_{i=1}^p \mu_t \delta_{x_i}^{(\alpha_i)} v_j^n + \gamma \delta_t^{(1)} v_j^n + \delta_{v,t}^{(1)} G(v_j^n) &= 0, \quad \forall (j, n) \in J \times I_{N-2}, \\ \text{such that } \begin{cases} v_j^0 = \phi(x_j), & \forall j \in \bar{J}, \\ \delta_t v_j^0 = \psi(x_j), & \forall j \in \bar{J}, \\ v_j^n = 0, & \forall (j, n) \in \partial J \times \bar{I}_N. \end{cases} \end{aligned} \quad (3.28)$$

For illustration purposes, Figure 3.1 shows the forward-difference stencil in the case that $p = 1$ using the conventions $M = M_1$ and $x_j = x_{1,j}$. Note in general that this scheme is an explicit four-step method, and that the numerical approximation to the solution at the node x_j and time t_{n+2} is given by the formula

$$v_j^{n+2} = v_j^{n+1} + v_j^n - v_j^{n-1} + 2\tau \left[\sum_{i=1}^p \mu_t \delta_{x_i}^{(\alpha_i)} v_j^n - \gamma \delta_t^{(1)} v_j^n - \delta_{v,t}^{(1)} G(v_j^n) \right], \quad \forall (j, n) \in J \times I_{N-2}. \quad (3.29)$$

3.4 Energy invariants

In this section we show that the finite-difference method (3.28) satisfies physical properties similar to those satisfied by (3.3). More precisely, we will propose a numerical energy functional associated to the scheme (3.28) that is preserved under suitable parameter conditions. For the remainder of this chapter we will let

$$h = (h_1, \dots, h_p), \quad (3.30)$$

$$h_* = \prod_{i=1}^p h_i, \quad (3.31)$$

and employ the spatial mesh $R_h = \{x_j\}_{j \in J} \subseteq \mathbb{R}^p$. Let \mathcal{V}_h be the real vector space of all real grid functions on R_h . For any $u \in \mathcal{V}_h$ and $j \in I$ convey that $u_j = u(x_j)$. Moreover, define respectively the inner product $\langle \cdot, \cdot \rangle : \mathcal{V}_h \times \mathcal{V}_h \rightarrow \mathbb{R}$ and the norm $\| \cdot \|_1 : \mathcal{V}_h \rightarrow \mathbb{R}$ by

$$\langle u, v \rangle = h_* \sum_{j \in I} u_j v_j, \quad (3.32)$$

$$\|u\|_1 = h_* \sum_{j \in I} |u_j|, \quad (3.33)$$

for any $u, v \in \mathcal{V}_h$. The Euclidean norm induced by $\langle \cdot, \cdot \rangle$ will be denoted by $\| \cdot \|_2$. In the following, we will represent the solutions of the finite-difference method (3.28) by $(v^n)_{n=0}^N$, where we convey that $v^n = (v_j^n)_{j \in J}$ for each $n \in \bar{I}_N$.

Lemma 3.6 (Macías-Díaz [60]). *If $i \in I_p$ then the following are satisfied for the matrix*

$$A_{x_i}^{(\alpha_i)} = \begin{pmatrix} g_0^{(\alpha_i)} & g_{-1}^{(\alpha_i)} & \cdots & g_{2-M_i}^{(\alpha_i)} \\ g_1^{(\alpha_i)} & g_0^{(\alpha_i)} & \cdots & g_{3-M_i}^{(\alpha_i)} \\ \vdots & \vdots & \ddots & \vdots \\ g_{M_i-2}^{(\alpha_i)} & g_{M_i-3}^{(\alpha_i)} & \cdots & g_0^{(\alpha_i)} \end{pmatrix}. \quad (3.34)$$

- (a) $A_{x_i}^{(\alpha_i)}$ is Hermitian.
- (b) $A_{x_i}^{(\alpha_i)}$ is strictly diagonally dominant.
- (c) All the eigenvalues of $A_{x_i}^{(\alpha_i)}$ are positive real numbers bounded from above by $2g_0^{(\alpha_i)}$.
- (d) $A_{x_i}^{(\alpha_i)}$ is positive-definite. □

Before we state our next result, we require some additional notation. Let v be a grid function, let $j \in J$ and $i \in I_p$. If $k \in I_{M_i-1}$ then we define respectively the real constant and the $(M_i - 1)$ -dimensional real vector

$$v_{j|j_i=k} = v(x_{1,j_1}, \dots, x_{i-1,j_{i-1}}, x_{i,k}, x_{i+1,j_{i+1}}, \dots, x_{p,j_p}), \quad (3.35)$$

$$v_{j|j_i} = (v_{j|j_i=1}, v_{j|j_i=2}, \dots, v_{j|j_i=M_i-1})^\top. \quad (3.36)$$

These conventions will be required in the next lemma, whose proof will require a well-known result on the existence and the uniqueness of square-root operators from functional analysis [29].

Lemma 3.7. *For each $i \in I_p$ there exists a unique positive linear operator $\Lambda_{x_i}^{(\alpha_i)} : \mathcal{V}_h \rightarrow \mathcal{V}_h$ such that*

$$\langle -\delta_{x_i}^{(\alpha_i)} u, v \rangle = \langle \Lambda_{x_i}^{(\alpha_i)} u, \Lambda_{x_i}^{(\alpha_i)} v \rangle, \quad (3.37)$$

for each $u, v \in \mathcal{V}_h$.

Proof. Note firstly that if $u, v \in \mathcal{V}_h$ and if $i \in I_p$ then

$$\begin{aligned} \langle u, -\delta_{x_i}^{(\alpha_i)} v \rangle &= -h_* \sum_{j \in J} u_j \delta_{x_i}^{(\alpha_i)} v_j = \frac{h_*}{h^{\alpha_i}} \sum_{j \in J} \sum_{k=1}^{M_i-1} u_j g_{j_i-k}^{(\alpha_i)} v_{j|j_i=k} \\ &= \frac{h_*}{h^{\alpha_i}} \sum_{j_1=1}^{M_1-1} \cdots \sum_{j_{i-1}=1}^{M_{i-1}-1} \sum_{j_{i+1}=1}^{M_{i+1}-1} \cdots \sum_{j_p=1}^{M_p-1} \sum_{j_i=1}^{M_i-1} \sum_{k=1}^{M_i-1} u_j g_{j_i-k}^{(\alpha_i)} v_{j|j_i=k} \\ &= \frac{h_*}{h^{\alpha_i}} \sum_{j_1=1}^{M_1-1} \cdots \sum_{j_{i-1}=1}^{M_{i-1}-1} \sum_{j_{i+1}=1}^{M_{i+1}-1} \cdots \sum_{j_p=1}^{M_p-1} u_{j|j_i}^\top A_{x_i}^{(\alpha_i)} v_{j|j_i}. \end{aligned} \quad (3.38)$$

Using the symmetry of the matrix $A_{x_i}^{(\alpha_i)}$ we observe that

$$\langle u, -\delta_{x_i}^{(\alpha_i)} v \rangle = \langle u, -\delta_{x_i}^{(\alpha_i)} v \rangle^\top = \frac{h_*}{h^{\alpha_i}} \sum_{j_1=1}^{M_1-1} \cdots \sum_{j_{i-1}=1}^{M_{i-1}-1} \sum_{j_{i+1}=1}^{M_{i+1}-1} \cdots \sum_{j_p=1}^{M_p-1} v_{j|j_i}^\top A_{x_i}^{(\alpha_i)} u_{j|j_i} = \langle -\delta_{x_i}^{(\alpha_i)} u, v \rangle \quad (3.39)$$

holds for each $u, v \in \mathcal{V}_h$, which means that $-\delta_{x_i}^{(\alpha_i)}$ is a self-adjoint operator for each $i \in I_p$. On the other hand, the fact that the matrix $A_{x_i}^{(\alpha_i)}$ is positive definite implies that $u_{j|j_i}^\top A_{x_i}^{(\alpha_i)} u_{j|j_i} \geq 0$ for each $u \in \mathbb{R}^{M_i-1}$ and $i \in I_p$. As a consequence we note that $\langle u, -\delta_{x_i}^{(\alpha_i)} u \rangle \geq 0$ for each $u \in \mathcal{V}_h$, which means that $-\delta_{x_i}^{(\alpha_i)}$ is positive. We conclude that there exists a unique positive linear square-root operator $\Lambda_{x_i}^{(\alpha_i)}$ for $-\delta_{x_i}^{(\alpha_i)}$ which satisfies the conclusion of the theorem. \square

The next theorem establishes the existence of invariants for the discrete system (3.28).

Theorem 3.8 (Dissipation of energy). *Let $(v^n)_{n=0}^N$ be a solution of (3.28), and define*

$$E^n = \frac{1}{2} \langle \delta_t^{(1)} v^n, \delta_t^{(1)} v^{n-1} \rangle + \frac{1}{2} \sum_{i=1}^p \|\Lambda_{x_i}^{(\alpha_i)} v^n\|_2^2 + \|G(v^n)\|_1, \quad \forall n \in I_{N-1}. \quad (3.40)$$

Then $\delta_t E^n = -\gamma \|\delta_t^{(1)} v^n\|_2^2$ for each $n \in I_{N-2}$.

Proof. Recall that G is a nonnegative function and note that the following hold for each $n \in I_{N-2}$:

$$\langle \mu_t \delta_t^{(2)} v^n, \delta_t^{(1)} v^n \rangle = \frac{1}{2\tau} \left[\langle \delta_t^{(1)} v^{n+1}, \delta_t^{(1)} v^n \rangle - \langle \delta_t^{(1)} v^n, \delta_t^{(1)} v^{n-1} \rangle \right], \quad (3.41)$$

$$\langle -\mu_t \delta_{x_i}^{(\alpha_i)} v^n, \delta_t^{(1)} v^n \rangle = \frac{1}{2\tau} \left[\|\Lambda_{x_i}^{(\alpha_i)} v^{n+1}\|_2^2 - \|\Lambda_{x_i}^{(\alpha_i)} v^n\|_2^2 \right], \quad \forall i \in I_p, \quad (3.42)$$

$$\langle \delta_{v,t}^{(1)} G(v^n), \delta_t^{(1)} v^n \rangle = \frac{1}{\tau} \left[\|G(v^{n+1})\|_1 - \|G(v^n)\|_1 \right]. \quad (3.43)$$

Let Θ_j^n represent the left-hand side of the difference equations in (3.28) for each $j \in J$ and each $n \in I_{N-2}$, and let $\Theta^n = (\Theta_j^n)_{j \in J}$. Suppose that $(v^n)_{n=0}^N$ is a solution of (3.28). Calculating the inner product of Θ^n with $\delta_t^{(1)} v^n$, using the identities above and collecting terms, we note that

$$\begin{aligned} 0 = \langle \Theta^n, \delta_t^{(1)} v^n \rangle &= \frac{1}{2\tau} \left[\langle \delta_t^{(1)} v^{n+1}, \delta_t^{(1)} v^n \rangle - \langle \delta_t^{(1)} v^n, \delta_t^{(1)} v^{n-1} \rangle \right] \\ &\quad + \frac{1}{2\tau} \sum_{i=1}^p \left[\|\Lambda_{x_i}^{(\alpha_i)} v^{n+1}\|_2^2 - \|\Lambda_{x_i}^{(\alpha_i)} v^n\|_2^2 \right] \\ &\quad + \frac{1}{\tau} \left[\|G(v^{n+1})\|_1 - \|G(v^n)\|_1 \right] + \gamma \|\delta_t^{(1)} v^n\|_2^2 \\ &= \delta_t E^n + \gamma \|\delta_t^{(1)} v^n\|_2^2, \quad \forall n \in I_{N-2}, \end{aligned} \quad (3.44)$$

whence the conclusion of this result is obtained. \square

Corollary 3.9. *If $(v^n)_{n=0}^N$ is a solution of (3.28) then*

$$E^n = E^1 - \gamma\tau \sum_{k=1}^{n-1} \|\delta_t^{(1)} v^k\|_2^2, \quad \forall n \in I_{N-2}. \quad (3.45)$$

In particular, the quantities E^n are invariants of (3.28) when $\gamma = 0$.

Proof. It readily follows from Theorem 3.8. \square

Theorem 3.8 and Corollary 3.9 are clearly the discrete counterparts of Theorem 3.2 and Corollary 3.3, respectively, and they indicate that our method is a dissipation-preserving technique. Moreover,

it is important to point out that the energy quantity E^n defined in Theorem 3.8 has associated the following discrete energy density functions:

$$\begin{aligned} H_j^n &= \frac{1}{2} \left(\delta_t^{(1)} v_j^n \right) \left(\delta_t^{(1)} v_j^{n-1} \right) - \frac{1}{2} v_j^n \sum_{i=1}^p \delta_{x_i}^{(\alpha_i)} v_j^n + G(v_j^n) \\ &= \frac{1}{2} \left(\delta_t^{(1)} v_j^n \right) \left(\delta_t^{(1)} v_j^{n-1} \right) + \frac{1}{2} \sum_{i=1}^p \left| \Lambda_{x_i}^{(\alpha_i)} v_j^n \right|^2 + G(v_j^n), \quad \forall (j, n) \in J \times I_{N-2}. \end{aligned} \quad (3.46)$$

Theorem 3.10. *The discrete quantities (3.40) may be rewritten alternatively as*

$$E^n = \frac{1}{2} \mu_t \|\delta_t^{(1)} v^{n-1}\|_2^2 - \frac{\tau^2}{4} \|\delta_t^{(2)} v^n\|_2^2 + \frac{1}{2} \sum_{i=1}^p \|\Lambda_{x_i}^{(\alpha_i)} v^n\|_2^2 + \|G(v^n)\|_1, \quad \forall n \in I_{N-2}. \quad (3.47)$$

Proof. Note that

$$\begin{aligned} \langle \delta_t v^n, \delta_t v^{n-1} \rangle &= \|\delta_t^{(1)} v^n\|_2^2 - \frac{1}{\tau^2} \langle v^{n+1} - v^n, v^{n+1} - 2v^n + v^{n-1} \rangle \\ &= \|\delta_t^{(1)} v^n\|_2^2 - \tau^2 \|\delta_t^{(2)} v^n\|_2^2 - \frac{1}{\tau^2} \langle v^n - v^{n-1}, v^{n+1} - 2v^n + v^{n-1} \rangle \\ &= \|\delta_t^{(1)} v^n\|_2^2 + \|\delta_t^{(1)} v^{n-1}\|_2^2 - \tau^2 \|\delta_t^{(2)} v^n\|_2^2 - \langle \delta_t v^n, \delta_t v^{n-1} \rangle \end{aligned} \quad (3.48)$$

holds for each $n \in I_{N-1}$. It follows that

$$\langle \delta_t v^n, \delta_t v^{n-1} \rangle = \mu_t \|\delta_t^{(1)} v^{n-1}\|_2^2 - \frac{\tau^2}{2} \|\delta_t^{(2)} v^n\|_2^2, \quad \forall n \in I_{N-1}, \quad (3.49)$$

whence the conclusion of the theorem is reached. \square

3.5 Auxiliary lemmas

In this section, we prove some propositions needed to establish the properties of numerical efficiency of the finite-difference method (3.28). To start with, we will require the following elementary facts which will be employed in the sequel without an explicit reference:

- (A) If v and w are real vectors of the same dimension then $|2\langle v, w \rangle| \leq \|v\|_2^2 + \|w\|_2^2$.
- (B) As a consequence, $\|v + w\|_2^2 \leq 2\|v\|_2^2 + 2\|w\|_2^2$ for any two real vectors v and w of the same dimension.
- (C) More generally, if $k \in \mathbb{N}$ and v_1, \dots, v_k are real vectors of the same dimension then

$$\left\| \sum_{n=1}^k v_n \right\|_2^2 \leq k \sum_{n=1}^k \|v_n\|_2^2. \quad (3.50)$$

(D) If $(v^n)_{n=0}^N$ is a finite sequence in \mathcal{V}_h and $n \in I_N$ then $v^n = v^0 + \tau \sum_{k=0}^{n-1} \delta_t^{(1)} v^k$. It follows that

$$\|v^n\|_2^2 \leq 2\|v^0\|_2^2 + 2T\tau \sum_{k=0}^{n-1} \|\delta_t^{(1)} v^k\|_2^2, \quad \forall n \in I_N. \quad (3.51)$$

The following lemma summarizes some important properties of the operators $\delta_{x_i}^{(\alpha)}$ introduced in Section 3.3 along with their respective square roots.

Lemma 3.11. *Let $v \in \mathcal{V}_h$ and $i \in I_p$.*

- (a) $\|\Lambda_{x_i}^{(\alpha_i)} v\|_2^2 \leq 2g_0^{(\alpha_i)} h_* h^{-\alpha_i} \|v\|_2^2$.
- (b) $\|\delta_{x_i}^{(\alpha_i)} v\|_2^2 = \|\Lambda_{x_i}^{(\alpha_i)} \Lambda_{x_i}^{(\alpha_i)} v\|_2^2$.
- (c) $\|\delta_{x_i}^{(\alpha_i)} v\|_2^2 \leq 2g_0^{(\alpha_i)} h_* h^{-\alpha_i} \|\Lambda_{x_i}^{(\alpha_i)} v\|_2^2 \leq 4 \left(g_0^{(\alpha_i)} h_* h^{-\alpha_i}\right)^2 \|v\|_2^2$. It follows then that

$$\sum_{i=1}^p \|\delta_{x_i}^{(\alpha_i)} v\|_2^2 \leq 2h_* \sum_{i=1}^p g_0^{(\alpha_i)} h^{-\alpha_i} \|\Lambda_{x_i}^{(\alpha_i)} v\|_2^2 \leq 4h_*^2 \|v\|_2^2 \sum_{i=1}^p (g_0^{(\alpha_i)} h^{-\alpha_i})^2. \quad (3.52)$$

Proof.

- (a) The properties of the matrix $A_{x_i}^{(\alpha)}$ in Lemma 3.6 guarantee that $v_{j|j_i}^\top A_{x_i}^{(\alpha_i)} v_{j|j_i} \leq 2g_0^{(\alpha_i)} \|v_{j|j_i}\|_2^2$ holds for each $j \in J$. Moreover, Lemma 3.7 yields

$$\begin{aligned} \|\Lambda_{x_i}^{(\alpha_i)} v\|_2^2 &= \langle \Lambda_{x_i}^{(\alpha_i)} v, \Lambda_{x_i}^{(\alpha_i)} v \rangle = \langle v, -\delta_{x_i}^{(\alpha_i)} v \rangle \\ &= \frac{h_*}{h^{\alpha_i}} \sum_{j_1=1}^{M_1-1} \cdots \sum_{j_{i-1}=1}^{M_{i-1}-1} \sum_{j_{i+1}=1}^{M_{i+1}-1} \cdots \sum_{j_p=1}^{M_p-1} v_{j|j_i}^\top A_{x_i}^{(\alpha_i)} v_{j|j_i} \\ &\leq 2g_0^{(\alpha_i)} \frac{h_*}{h^{\alpha_i}} \sum_{j_1=1}^{M_1-1} \cdots \sum_{j_{i-1}=1}^{M_{i-1}-1} \sum_{j_{i+1}=1}^{M_{i+1}-1} \cdots \sum_{j_p=1}^{M_p-1} \|v_{j|j_i}\|_2^2 \\ &= 2g_0^{(\alpha_i)} h_* h^{-\alpha_i} \|v\|_2^2. \end{aligned} \quad (3.53)$$

- (b) Using Lemma 3.7 we readily check that

$$\begin{aligned} \|\delta_{x_i}^{(\alpha_i)} v\|_2^2 &= \langle -\delta_{x_i}^{(\alpha_i)} v, -\delta_{x_i}^{(\alpha_i)} v \rangle = \langle \Lambda_{x_i}^{(\alpha_i)} v, -\delta_{x_i}^{(\alpha_i)} \Lambda_{x_i}^{(\alpha_i)} v \rangle \\ &= \langle \Lambda_{x_i}^{(\alpha_i)} \Lambda_{x_i}^{(\alpha_i)} v, \Lambda_{x_i}^{(\alpha_i)} \Lambda_{x_i}^{(\alpha_i)} v \rangle = \|\Lambda_{x_i}^{(\alpha_i)} \Lambda_{x_i}^{(\alpha_i)} v\|_2^2. \end{aligned} \quad (3.54)$$

- (c) This property is a consequence of (a) and (b). Its proof is straightforward. \square

For the remainder of this chapter, we let $\alpha = (\alpha_1, \dots, \alpha_p)$, and define $g_h^{(\alpha)} = 2h_* \max\{g_0^{(\alpha_i)} h^{-\alpha_i} : i \in I_p\}$. In light of the last lemma, it is clear that $g_h^{(\alpha)}$ is a positive number such that

$$\sum_{i=1}^p \|\delta_{x_i}^{(\alpha_i)} v\|_2^2 \leq g_h^{(\alpha)} \sum_{i=1}^p \|\Lambda_{x_i}^{(\alpha_i)} v\|_2^2 \leq \left(g_h^{(\alpha)} \|v\|_2\right)^2. \quad (3.55)$$

Lemma 3.12. *Let $G \in C^2(\mathbb{R})$ and $G'' \in L^\infty(\mathbb{R})$, and suppose that $(u^n)_{n=0}^N$, $(v^n)_{n=0}^N$ and $(R^n)_{n=0}^N$ are sequences in \mathcal{V}_h . Let $\varepsilon^n = v^n - u^n$ and $\tilde{G}^n = \delta_{v,t}G(v^n) - \delta_{w,t}G(w^n)$ for each $n \in \bar{I}_{N-1}$. Then the following are satisfied.*

(a) *There exists a constant $C_0 \in \mathbb{R}^+$ that depends only on G such that*

$$\|\tilde{G}^n\|_2^2 \leq C_0(\|\varepsilon^{n+1}\|_2^2 + \|\varepsilon^n\|_2^2), \quad \forall n \in \bar{I}_{N-1}. \quad (3.56)$$

(b) *There exists $C_1 \in \mathbb{R}^+$ depending only on G such that*

$$2|\langle R^n - \tilde{G}^n, \delta_t^{(1)}\varepsilon^n \rangle| \leq 2\|R^n\|_2^2 + C_1\left(\|\varepsilon^{n+1}\|_2^2 + \|\varepsilon^n\|_2^2 + \|\delta_t^{(1)}\varepsilon^n\|_2^2\right), \quad \forall n \in \bar{I}_{N-1}. \quad (3.57)$$

(c) *There exist $C_2, C_3 \in \mathbb{R}^+$ that depend only on G such that for each $k \in I_{N-1}$,*

$$2\tau \sum_{n=1}^k \left| \langle R^n - \tilde{G}^n, \delta_t^{(1)}\varepsilon^n \rangle \right| \leq 2\tau \sum_{n=0}^k \|R^n\|_2^2 + C_2\|\varepsilon^0\|_2^2 + C_3\tau \sum_{n=0}^k \|\delta_t^{(1)}\varepsilon^n\|_2^2. \quad (3.58)$$

(d) *For each $k \in I_{N-1}$,*

$$k\tau^2 \sum_{n=1}^k \|\tilde{G}^n\|_2^2 \leq 4C_0T^2\|\varepsilon^0\|_2^2 + 4C_0T^3\tau \sum_{n=0}^k \|\delta_t^{(1)}\varepsilon^n\|_2^2. \quad (3.59)$$

Proof. Let $C'_0 = \sup\{|G''(u)| : u \in \mathbb{R}\}$.

(a) As a consequence of the Mean Value Theorem and a direct integration we obtain that $|\tilde{G}_j^n| \leq C'_0(|\varepsilon_j^{n+1}| + |\varepsilon_j^n|)$ for each $j \in J$ and each $n \in \bar{I}_{N-1}$. Raising both sides of this inequality to the second power and using the inequalities at the beginning of this section we readily reach (3.56) with $C_0 = 2C'_0$.

(b) Note that for each $n \in \bar{I}_{N-1}$,

$$\begin{aligned} 2|\langle R^n - \tilde{G}^n, \delta_t^{(1)}\varepsilon^n \rangle| &\leq 2\|R^n\|_2^2 + 2\|\tilde{G}^n\|_2^2 + \|\delta_t^{(1)}\varepsilon^n\|_2^2 \\ &\leq 2\|R^n\|_2^2 + 2C_0\left(\|\varepsilon^{n+1}\|_2^2 + \|\varepsilon^n\|_2^2\right) + \|\delta_t^{(1)}\varepsilon^n\|_2^2, \end{aligned} \quad (3.60)$$

whence the inequality (3.57) readily follows with $C_1 = \max\{4C'_0, 1\}$.

(c) Using the inequality (3.57) and the remarks at the beginning of the present section we obtain

that

$$\begin{aligned}
2\tau \sum_{n=1}^k \left| \langle R^n - \tilde{G}^n, \delta_t^{(1)} \varepsilon^n \rangle \right| &\leq 2\tau \sum_{n=1}^k \|R^n\|_2^2 + 2C_1\tau \left[\sum_{n=1}^{k+1} \|\varepsilon^n\|_2^2 + \sum_{n=1}^k \|\delta_t^{(1)} \varepsilon^n\|_2^2 \right] \\
&\leq 2\tau \sum_{n=0}^k \|R^n\|_2^2 \\
&\quad + 2C_1\tau \left[\sum_{n=1}^{k+1} \left(2\|\varepsilon^0\|_2^2 + 2T\tau \sum_{l=0}^{n-1} \|\delta_t^{(1)} \varepsilon^l\|_2^2 \right) + \sum_{n=1}^k \|\delta_t^{(1)} \varepsilon^n\|_2^2 \right] \\
&\leq 2\tau \sum_{n=0}^k \|R^n\|_2^2 + 4C_1T\|\varepsilon^0\|_2^2 + 2C_1(2T^2 + 1)\tau \sum_{n=0}^k \|\delta_t^{(1)} \varepsilon^n\|_2^2,
\end{aligned} \tag{3.61}$$

for each $k \in I_{N-1}$. The conclusion of this result follows for $C_2 = 4C_1T$ and $C_3 = 2C_1(2T^2 + 1)$.

(d) Note that (3.56) and the remarks at the beginning of this section imply that for each $k \in I_{N-1}$,

$$k\tau^2 \sum_{n=1}^k \|\tilde{G}^n\|_2^2 \leq 2C_0k\tau^2 \sum_{n=1}^{k+1} \|\varepsilon^n\|_2^2 \leq 2C_0T\tau \sum_{n=1}^{k+1} \left(2\|\varepsilon^0\|_2^2 + 2T\tau \sum_{l=0}^{n-1} \|\delta_t^{(1)} \varepsilon^l\|_2^2 \right), \tag{3.62}$$

whence the conclusion readily follows. \square

Let $G \in \mathcal{C}^2(\mathbb{R})$ and $G'' \in L^\infty(\mathbb{R})$, and suppose that $(u^n)_{n=0}^N$, $(v^n)_{n=0}^N$ and $(R^n)_{n=0}^N$ are sequences in \mathcal{V}_h . As in our last result, let $\varepsilon^n = v^n - u^n$ and $\tilde{G}^n = \delta_{v,t}G(v^n) - \delta_{w,t}G(w^n)$ for each $n \in \bar{I}_{N-1}$. Suppose also that

$$\mu_t \delta_t^2 \varepsilon^n - \sum_{i=1}^p \mu_t \delta_{x_i}^{(\alpha_i)} \varepsilon^n + \gamma \delta_t^{(1)} \varepsilon^n + \tilde{G}^n = R^n, \quad \forall n \in I_{N-1}. \tag{3.63}$$

Using this identity and mathematical induction it follows that

$$\delta_t^{(2)} \varepsilon^{k+1} = (-1)^k \delta_t^{(2)} \varepsilon^1 + \sum_{i=1}^p \delta_{x_i}^{(\alpha_i)} \varepsilon^{k+1} + (-1)^{k+1} \sum_{i=1}^p \delta_{x_i}^{(\alpha_i)} \varepsilon^1 + 2 \sum_{n=1}^k (-1)^n \left[\gamma \delta_t^{(1)} \varepsilon^n + \tilde{G}^n - R^n \right], \tag{3.64}$$

for each $k \in I_{N-2}$. Moreover, calculating the square of the Euclidean norm of $\delta_t^{(2)} \varepsilon^{k+1}$, using (3.55) and the inequalities at the beginning of this section, applying Lemma 3.12(a), multiplying by τ^2 and simplifying we readily obtain that

$$\begin{aligned}
\tau^2 \|\delta_t^{(2)} \varepsilon^{k+1}\|_2^2 &\leq 5\tau^2 \|\delta_t^{(2)} \varepsilon^1\|_2^2 + 5p\tau^2 g_h^{(\alpha)} \sum_{i=1}^p \|\Lambda_{x_i}^{(\alpha_i)} \varepsilon^1\|_2^2 + 5p\tau^2 g_h^{(\alpha)} \sum_{i=1}^p \|\Lambda_{x_i}^{(\alpha_i)} \varepsilon^{k+1}\|_2^2 \\
&\quad + 20\gamma^2 T\tau \sum_{n=1}^k \|\delta_t^{(1)} \varepsilon^n\|_2^2 + 40k\tau^2 \sum_{n=1}^k \left(\|\tilde{G}^n\|_2^2 + \|R^n\|_2^2 \right) \\
&\leq 160C_0T^2 \|\varepsilon^0\|_2^2 + 20\mu_t \|\delta_t^{(1)} \varepsilon^0\|_2^2 + 5p\tau^2 g_h^{(\alpha)} \sum_{i=1}^p \|\Lambda_{x_i}^{(\alpha_i)} \varepsilon^1\|_2^2 + 40T\tau \sum_{n=1}^k \|R^n\|_2^2 \\
&\quad + 5p\tau^2 g_h^{(\alpha)} \sum_{i=1}^p \|\Lambda_{x_i}^{(\alpha_i)} \varepsilon^{k+1}\|_2^2 + 20(8C_0T^2 + \gamma^2)T\tau \sum_{n=0}^k \|\delta_t^{(1)} \varepsilon^n\|_2^2.
\end{aligned} \tag{3.65}$$

This inequality will be used in the following section to establish the stability and the convergence of the finite-difference method (3.28).

The following result will be useful to prove the stability and convergence properties of (3.28). It is obviously a discrete version of the well-known Gronwall inequality.

Lemma 3.13 (Pen-Yu [77]). *Let $(\omega^n)_{n=0}^N$ and $(\rho^n)_{n=0}^N$ be finite sequences of nonnegative mesh functions, and suppose that there exists $C \geq 0$ such that*

$$\omega^k \leq \rho^k + C\tau \sum_{n=0}^{k-1} \omega^k, \quad \forall k \in I_{N-1}. \quad (3.66)$$

Then $\omega^n \leq \rho^n e^{Cn\tau}$ for each $n \in \bar{I}_N$. □

3.6 Numerical results

The main numerical properties of the finite-difference method (3.28) as well as some illustrative computational simulations are presented in this stage. Here we show that our scheme is a consistent, stable and convergent technique under suitable conditions on the parameters of the model. In a first stage, we show that (3.28) is a second-order consistent technique, and that the discrete energy density (3.46) also provides a consistent approximation to the continuous Hamiltonian (3.10). For practical purposes we define the following continuous and discrete functionals:

$$\mathcal{L}u(x, t) = \frac{\partial^2 u}{\partial t^2}(x, t) - \sum_{i=1}^p \frac{\partial^{\alpha_i} u}{\partial |x_i|^{\alpha_i}}(x, t) + \gamma \frac{\partial u}{\partial t}(x, t) + G'(u(x, t)), \quad \forall (x, t) \in \Omega, \quad (3.67)$$

$$Lu_j^n = \mu_t \delta_t^{(2)} u_j^n - \sum_{i=1}^p \mu_t \delta_{x_i}^{(\alpha_i)} u_j^n + \gamma \delta_t^{(1)} u_j^n + \delta_{u,t}^{(1)} G(u_j^n), \quad \forall (j, n) \in J \times I_{N-2}. \quad (3.68)$$

Theorem 3.14 (Consistency). *If $u \in C^5(\bar{\Omega})$ then there exist constants $C, C' > 0$ which are independent of h and τ such that for each $j \in J$ and each $n \in I_{N-2}$,*

$$|Lu_j^n - \mathcal{L}u(x_j, t_n)| \leq C(\tau^2 + \|h\|_2^2), \quad (3.69)$$

$$|Hu_j^n - \mathcal{H}u(x_j, t_n)| \leq C'(\tau + \|h\|_2^2). \quad (3.70)$$

Proof. We employ here the usual arguments with Taylor polynomials and the identity (3.26). Using the hypotheses of continuous differentiability, there exist constants $C_1, C_{2,i}, C_3, C_4 \in \mathbb{R}$ for $i \in I_p$ such that

$$\left| \mu_t \delta_t^{(2)} u_j^n - \frac{\partial^2 u}{\partial t^2}(x_j, t_{n+\frac{1}{2}}) \right| \leq C_1 \tau^2, \quad (3.71)$$

$$\left| \mu_t \delta_{x_i}^{(\alpha_i)} u_j^n - \frac{\partial^{\alpha_i} u}{\partial |x_i|^{\alpha_i}}(x_j, t_{n+\frac{1}{2}}) \right| \leq C_{2,i}(\tau^2 + h_i^2), \quad (3.72)$$

$$\left| \delta_t^{(1)} u_j^n - \frac{\partial u}{\partial t}(x_j, t_{n+\frac{1}{2}}) \right| \leq C_3 \tau^2, \quad (3.73)$$

$$\left| \delta_{u,t}^{(1)} G(u_j^n) - G'(u(x_j, t_{n+\frac{1}{2}})) \right| \leq C_4 \tau^2, \quad (3.74)$$

for each $j \in J$ and each $n \in I_{N-2}$. The first inequality in the conclusion of this theorem is readily reached using the triangle inequality and defining $C = \max\{C_1, \gamma C_3, C_4\} \vee \max\{C_{2,i} : i \in I_p\}$. To establish the second inequality, note that the consistency of the forward-difference operators, the Mean Value Theorem and the smoothness of the function u guarantee that there exists a constant C_5 independent of τ such that

$$\begin{aligned} \left| \delta_t^{(1)} u_j^n \delta_t^{(1)} u_j^{n-1} - \left(\frac{\partial u}{\partial t}(x_j, t_n) \right)^2 \right| &\leq \left| \delta_t^{(1)} u_j^{n-1} \right| \left| \delta_t^{(1)} u_j^n - \frac{\partial u}{\partial t}(x_j, t_n) \right| \\ &\quad + \left| \frac{\partial u}{\partial t}(x_j, t_n) \right| \left| \delta_t^{(1)} u_j^{n-1} - \frac{\partial u}{\partial t}(x_j, t_n) \right| \\ &\leq C_5 \tau, \end{aligned} \tag{3.75}$$

for each $j \in J$ and each $n \in I_{N-1}$. Likewise, there exist constants $C_{6,i}$ for each $i \in I_p$ such that

$$\left| u_j^n \delta_{x_i}^{(\alpha_i)} u_j^n - u(x_j, t_n) \frac{\partial^{\alpha_i} u}{\partial |x_i|^{\alpha_i}}(x_j, t_n) \right| \leq C_{6,i} h_i^2, \tag{3.76}$$

for each $j \in I$ and each $n \in I_{N-1}$. The second inequality of the conclusion follows again using the triangle inequality and letting $C' = \frac{1}{2}(C_5 \vee \max\{C_{6,i} : i \in I_p\})$. \square

We turn our attention to the stability and the convergence properties of (3.28). In the following, the constants C_1 , C_2 and C_3 are as in Lemma 3.12, and (ϕ_v, ψ_v) and (ϕ_w, ψ_w) will denote two sets of initial conditions of (3.3).

Theorem 3.15 (Stability). *Let $G \in C^2(\mathbb{R})$ and $G'' \in L^\infty(\mathbb{R})$, and suppose that τ and h satisfy*

$$\frac{5}{2} p \tau^2 g_h^{(\alpha)} < 1. \tag{3.77}$$

Let $\mathbf{v} = (v^n)_{n=0}^N$ and $\mathbf{w} = (w^n)_{n=0}^N$ be solutions of (3.28) for (ϕ_v, ψ_v) and (ϕ_w, ψ_w) , respectively, and let $\varepsilon^n = v^n - w^n$ for each $n \in \bar{I}_N$. Then there exist constants $C_4, C_5 \in \mathbb{R}^+$ and $0 < \eta_0 < 1$ independent of \mathbf{v} and \mathbf{w} such that, for each $n \in I_{N-1}$,

$$\frac{1}{2} \|\delta_t^{(2)} \varepsilon^n\|_2^2 + (1 - \eta_0) \sum_{i=1}^p \|\Lambda_{x_i}^{(\alpha_i)} \varepsilon^n\|_2^2 \leq C_4 \left(\|\varepsilon^0\|_2^2 + \mu_t \|\delta_t^{(1)} \varepsilon^0\|_2^2 + \sum_{i=1}^p \|\Lambda_{x_i}^{(\alpha_i)} \varepsilon^1\|_2^2 \right) e^{C_5 n \tau}. \tag{3.78}$$

Proof. Let η_0 satisfy $\frac{5}{2} p \tau^2 g_h^{(\alpha)} < \eta_0 < 1$. Obviously, the sequence $(\varepsilon^n)_{n=0}^N$ satisfies the initial-boundary-value problem

$$\begin{aligned} \mu_t \delta_t^{(2)} \varepsilon_j^n - \sum_{i=1}^p \mu_t \delta_{x_i}^{(\alpha_i)} \varepsilon_j^n + \gamma \delta_t^{(1)} \varepsilon_j^n + \delta_{v,t}^{(1)} G(v_j^n) - \delta_{w,t} G(w_j^n) &= 0, \quad \forall (j, n) \in J \times I_{N-2}, \\ \text{such that } \begin{cases} \varepsilon_j^0 = \phi_v(x_j) - \phi_w(x_j), & \forall j \in J, \\ \delta_t \varepsilon_j^0 = \psi_v(x_j) - \psi_w(x_j), & \forall j \in J, \\ \varepsilon_j^n = 0, & \forall (j, n) \in \partial J \times I_N. \end{cases} \end{aligned} \tag{3.79}$$

For the sake of convenience, let $\tilde{G}_j^n = \delta_{v,t}^{(1)} G(v_j^n) - \delta_{w,t} G(w_j^n)$ for each $j \in J$ and each $n \in \bar{I}_{N-1}$. From

the identities preceding Theorem 3.8 and those after the proof of Corollary 3.9, we readily obtain that

$$\begin{aligned} \langle \mu_t \delta_t^{(2)} \varepsilon^n, \delta_t^{(1)} \varepsilon^n \rangle &= \frac{1}{2} \delta_t^{(1)} \mu_t \|\delta_t^{(1)} \varepsilon^{n-1}\|_2^2 - \frac{\tau^2}{4} \delta_t^{(1)} \|\delta_t^{(2)} \varepsilon^n\|_2^2, \\ \langle -\mu_t \delta_{x_i}^{(\alpha_i)} \varepsilon^n, \delta_t^{(1)} \varepsilon^n \rangle &= \frac{1}{2} \delta_t^{(1)} \|\Lambda_{x_i}^{(\alpha_i)} \varepsilon^n\|_2^2, \quad \forall i \in I_{N-1}, \end{aligned} \quad (3.80)$$

$$|2\langle \tilde{G}^n, \delta_t^{(1)} \varepsilon^n \rangle| \leq C_1 \left(\|\varepsilon^{n+1}\|_2^2 + \|\varepsilon^n\|_2^2 + \|\delta_t^{(1)} \varepsilon^n\|_2^2 \right), \quad (3.81)$$

for each $n \in I_{N-1}$ and for some $C_1 \in \mathbb{R}^+$. Let $k \in I_{N-1}$. Taking the inner product of $\delta_t^{(1)} \varepsilon^n$ with both sides of the respective difference equation of (3.79), substituting the identities above, calculating then the sum of the resulting identity for all $n \in I_k$, multiplying by 2τ on both sides, applying Lemma 3.12 with $R^n = 0$ and simplifying algebraically yields

$$\begin{aligned} \frac{1}{2} \|\delta_t^{(1)} \varepsilon^{k+1}\|_2^2 + \sum_{i=1}^p \|\Lambda_{x_i}^{(\alpha_i)} \varepsilon^{k+1}\|_2^2 &\leq \mu_t \|\delta_t^{(1)} \varepsilon^0\|_2^2 + \sum_{i=1}^p \|\Lambda_{x_i}^{(\alpha_i)} \varepsilon^1\|_2^2 + \frac{\tau^2}{2} \|\delta_t^{(2)} \varepsilon^{k+1}\|_2^2 \\ &\quad + 2\tau \sum_{n=1}^k \left| \langle \tilde{G}^n, \delta_t^{(1)} \varepsilon^n \rangle \right| \\ &\leq \rho + \frac{5}{2} p \tau^2 g_h^{(\alpha)} \sum_{i=1}^p \|\Lambda_{x_i}^{(\alpha_i)} \varepsilon^{k+1}\|_2^2 + C_5 \tau \sum_{n=0}^k \|\delta_t^{(1)} \varepsilon^n\|_2^2 \\ &\leq \rho + \frac{5}{2} p \tau^2 g_h^{(\alpha)} \sum_{i=1}^p \|\Lambda_{x_i}^{(\alpha_i)} \varepsilon^{k+1}\|_2^2 + C_5 \tau \sum_{n=0}^k \omega^n, \quad \forall k \in I_{N-1}, \end{aligned} \quad (3.82)$$

where

$$C_4 = \max\{C_2 + 80C_0T^2, 11, 1 + \eta_0\}, \quad (3.83)$$

$$C_5 = 2C_3 + 20(8C_0T^2 + \gamma^2)T, \quad (3.84)$$

$$\rho = C_4 \left(\|\varepsilon^0\|_2^2 + \mu_t \|\delta_t^{(1)} \varepsilon^0\|_2^2 + \sum_{i=1}^p \|\Lambda_{x_i}^{(\alpha_i)} \varepsilon^1\|_2^2 \right), \quad (3.85)$$

$$\omega^n = \frac{1}{2} \|\delta_t^{(1)} \varepsilon^n\|_2^2 + (1 - \eta_0) \sum_{i=1}^p \|\Lambda_{x_i}^{(\alpha_i)} \varepsilon^n\|_2^2, \quad \forall n \in I_{N-1}. \quad (3.86)$$

Subtracting the second term on the right-hand side of (3.82) we note that the hypotheses of Lemma 3.13 are readily satisfied with $C = C_5$ and $\rho^k = \rho$ for each $k \in I_{N-1}$, whence the conclusion of Theorem 3.15 follows. \square

Note that the inequality (3.77) is satisfied for sufficiently small values of τ and of the components of h . Finally, we tackle the problem of the convergence of the numerical method (3.28). The proof of the following result is similar to that of Theorem 3.15. For that reason we provide only a sketch of the proof.

Theorem 3.16 (Convergence). *Let $u \in C^5(\bar{\Omega})$ be a solution of (3.3) with $G \in C^2(\mathbb{R})$ and $G'' \in L^\infty(\mathbb{R})$, and let $(v^n)_{n=0}^N$ be a solution of (3.28) for the initial conditions (ϕ, ψ) . Assume that $\varepsilon^n = v^n - u^n$ for each $n \in \bar{I}_N$. If (3.77) holds then the method (3.28) is convergent of order $\mathcal{O}(\tau^2 + \|h\|^2)$.*

Proof. Let η_0 be as in the proof of Theorem 3.15, and let R_j^n be the truncation error at the point

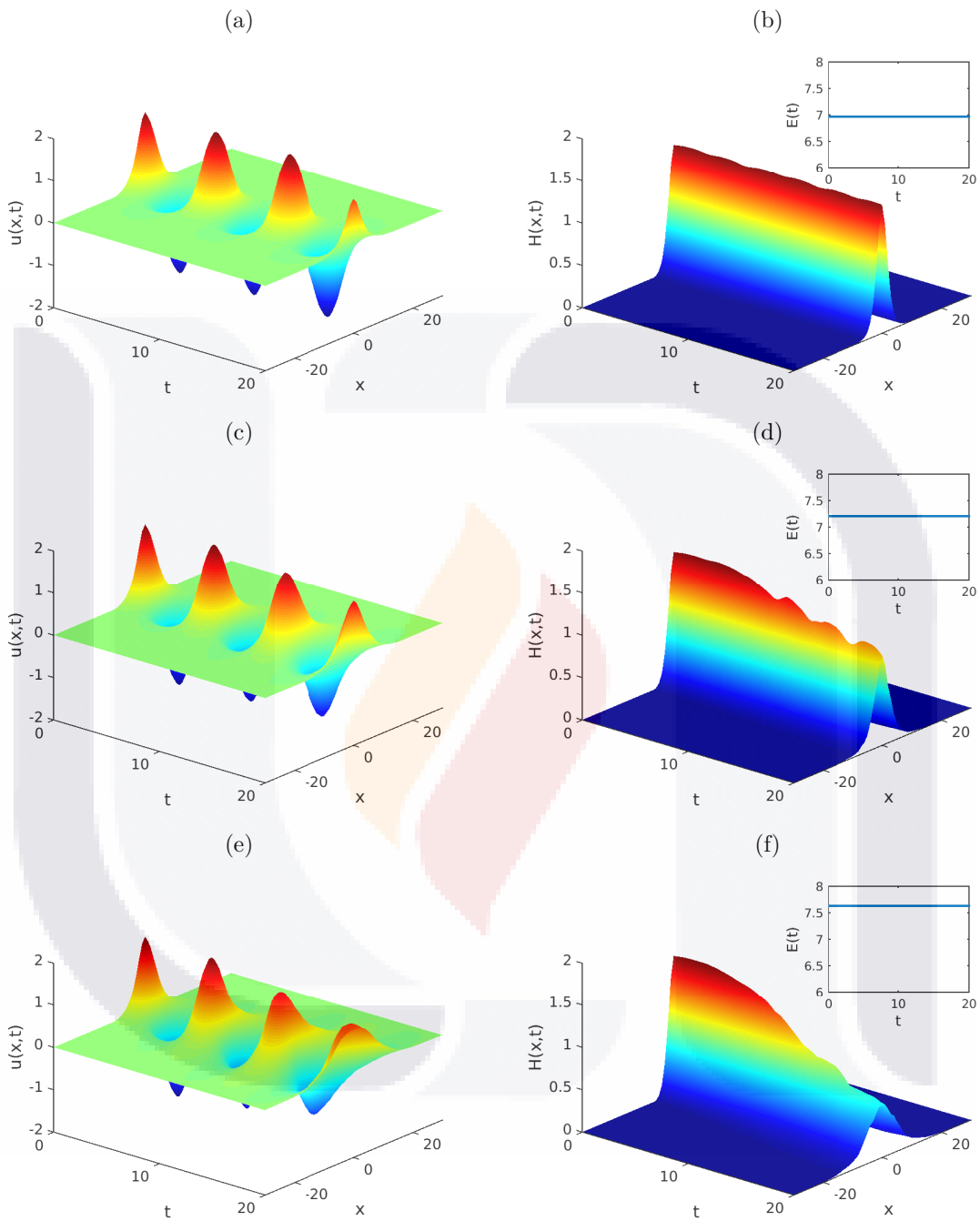


Figure 3.2: Graphs of the numerical solution (left column) and the associated energy density (right column) of the one-dimensional problem (3.3) with $G(u) = 1 - \cos u$ obtained using (3.28) and (3.46) on $\Omega = (-30, 30) \times (0, 100)$. The initial data were provided by (3.93) with $\omega = 0.9$, and the parameters employed were $\gamma = 0$, $h_1 = 0.5$ and $\tau = 0.05$. Various derivative orders were used, namely, $\alpha_1 = 2$ (top row), $\alpha_1 = 1.6$ (middle row) and $\alpha_1 = 1.2$ (bottom row). The insets of the graphs of the right column represent the discrete dynamics of the total energy (3.40) of the system.

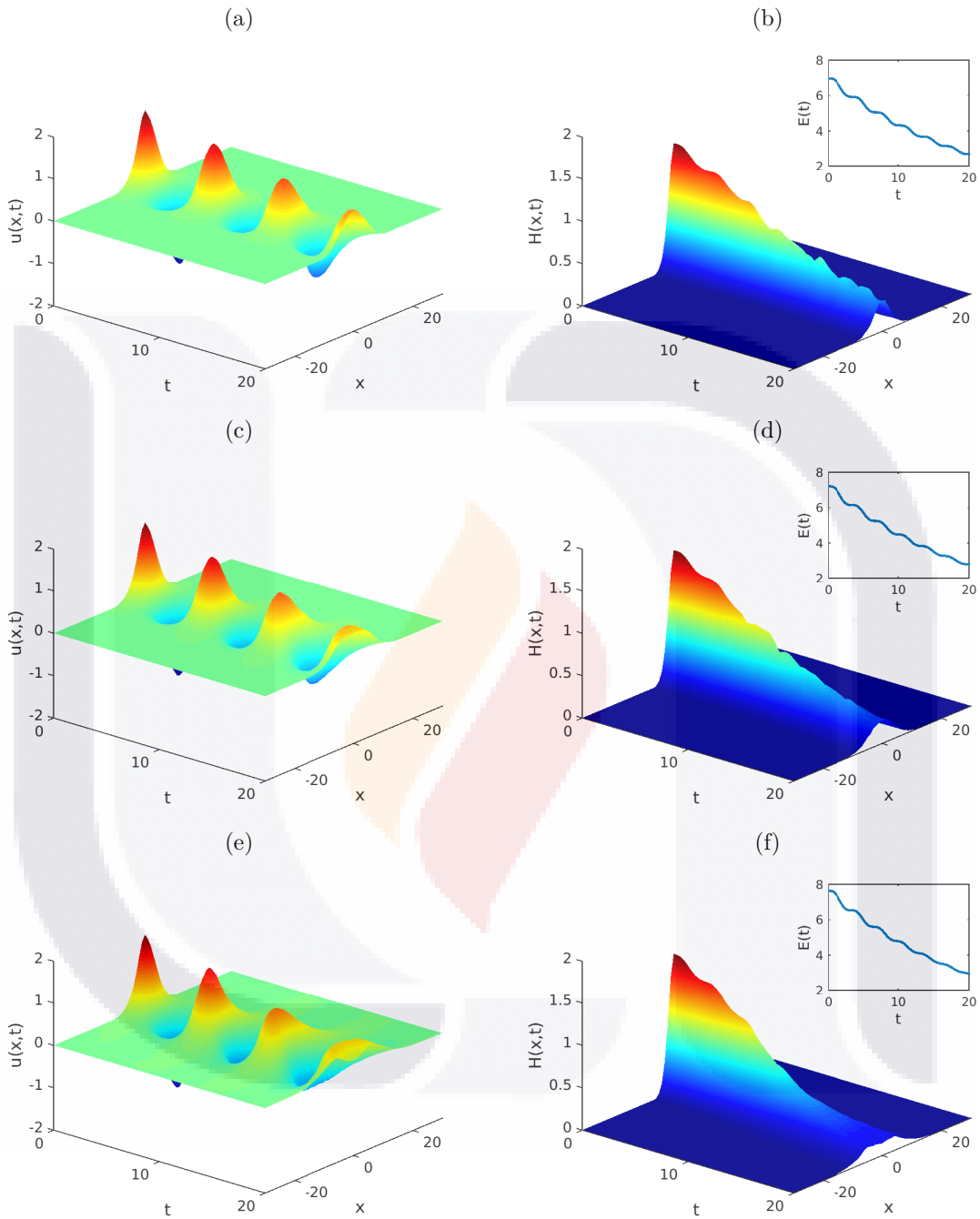


Figure 3.3: Graphs of the numerical solution (left column) and the associated energy density (right column) of the one-dimensional problem (3.3) with $G(u) = 1 - \cos u$ obtained using (3.28) and (3.46) on $\Omega = (-30, 30) \times (0, 100)$. The initial data were provided by (3.93) with $\omega = 0.9$, and the parameters employed were $\gamma = 0.05$, $h_1 = 0.5$ and $\tau = 0.05$. Various derivative orders were used, namely, $\alpha_1 = 2$ (top row), $\alpha_1 = 1.6$ (middle row) and $\alpha_1 = 1.2$ (bottom row). The insets of the graphs of the right column represent the discrete dynamics of the total energy (3.40) of the system.

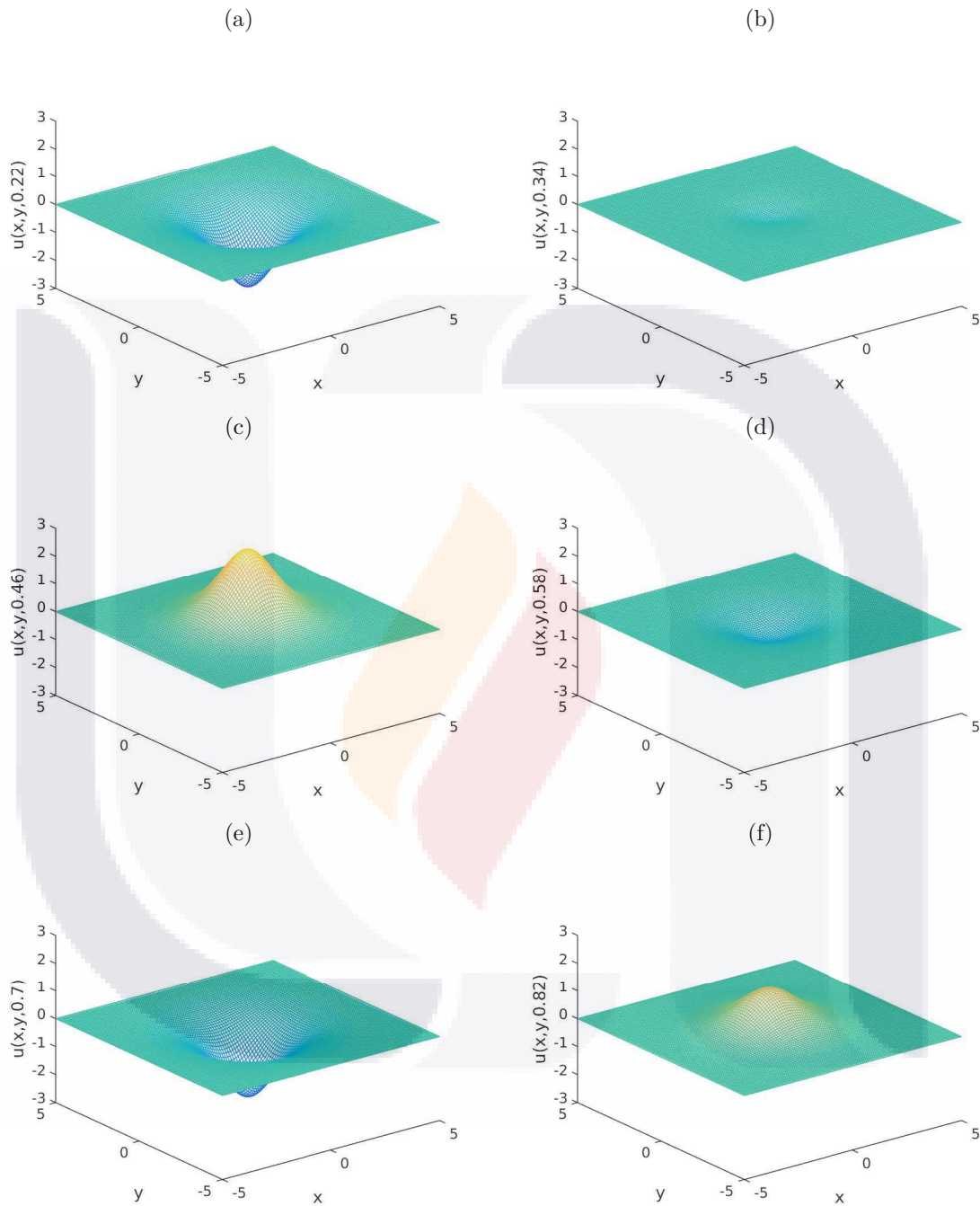


Figure 3.4: Graphs of the approximate solution of (3.3) in two spatial dimensions at the times (a) $t = 0.22$, (b) $t = 0.34$, (c) $t = 0.46$, (d) $t = 0.58$, (e) $t = 0.70$ and (f) $t = 0.82$. The model parameters employed were $\alpha_1 = 1.8$, $\alpha_2 = 1.6$, $\gamma = 0$, $G(u) = 1 - \cos u$, $B = (-5, 5) \times (-5, 5)$ and $T = 10$. Meanwhile, the initial conditions were provided by $\varphi(x^2 + y^2, t)$, where φ is given by (3.93) with $\omega = 0.8$. Numerically, we used the method (3.28) with $M_1 = M_2 = 100$ and $N = 500$.

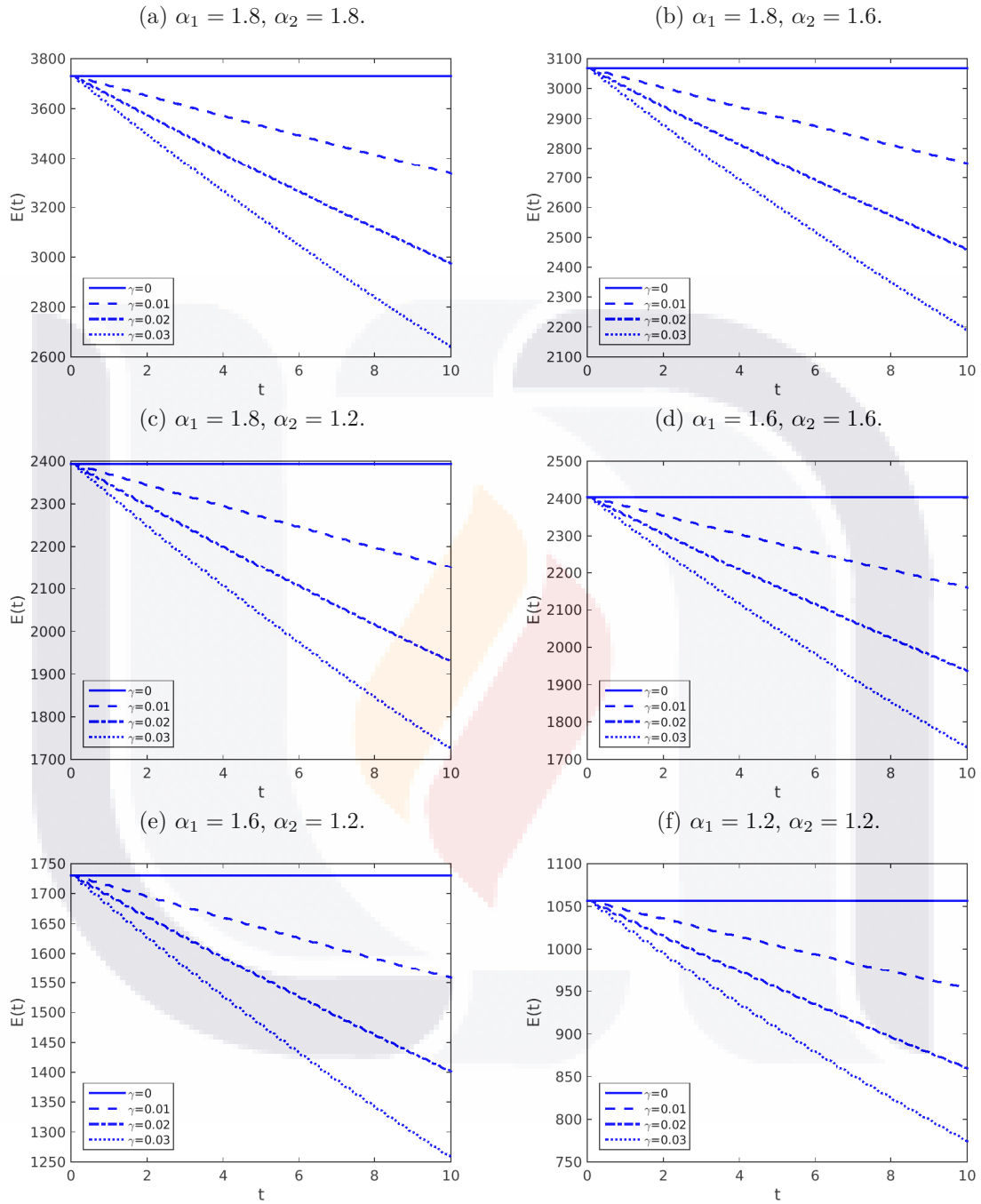


Figure 3.5: Graphs of the energy dynamics of the solution of (3.3) in two spatial dimensions using various sets of the parameters α_1 and α_2 , $G(u) = 1 - \cos u$, $B = (-5, 5) \times (-5, 5)$ and $T = 10$. The initial conditions were provided by $\varphi(x^2 + y^2, t)$, where φ is given by (3.93) with $\omega = 0.8$, and various damping coefficients were considered, namely, $\gamma = 0$ (solid), $\gamma = 0.01$ (dashed), $\gamma = 0.02$ (dashed-dotted) and $\gamma = 0.03$ (dotted). Numerically, we used the method (3.28) with $M_1 = M_2 = 100$ and $N = 500$.

(x_j, t_n) for each $j \in J$ and each $n \in \bar{I}_N$. Then $(\epsilon^n)_{n=0}^N$ satisfies

$$\begin{aligned} \mu_t \delta_t^{(2)} \epsilon_j^n - \sum_{i=1}^p \mu_t \delta_{x_i}^{(\alpha_i)} \epsilon_j^n + \gamma \delta_t^{(1)} \epsilon_j^n + \delta_{v,t}^{(1)} G(v_j^n) - \delta_{w,t} G(w_j^n) = R_j^n, \quad \forall (j, n) \in J \times I_{N-2}, \\ \text{such that } \begin{cases} \epsilon_j^0 = \delta_t \epsilon_j^0 = 0, & \forall j \in J, \\ \epsilon_j^n = 0, & \forall (j, n) \in \partial J \times I_N. \end{cases} \end{aligned} \quad (3.87)$$

Following the proof of Theorem 3.15, let $\tilde{G}_j^n = \delta_{v,t}^{(1)} G(v_j^n) - \delta_{w,t} G(w_j^n)$ for each $j \in J$ and each $n \in \bar{I}_{N-1}$. Proceeding as in the proof of that theorem, we readily obtain

$$\frac{1}{2} \|\delta_t^{(1)} \epsilon^{k+1}\|_2^2 + \sum_{i=1}^p \|\Lambda_{x_i}^{(\alpha_i)} \epsilon^{k+1}\|_2^2 \leq \rho^{k+1} + \frac{5}{2} p \tau^2 g_h^{(\alpha)} \sum_{i=1}^p \|\Lambda_{x_i}^{(\alpha_i)} \epsilon^{k+1}\|_2^2 + C_5 \tau \sum_{n=0}^k \omega^n, \quad \forall k \in I_{N-1}, \quad (3.88)$$

where C_5 is as before, and

$$C_4 = \max\{C_2 + 80C_0T^2, 11, 1 + \eta_0, 20T + 2\}, \quad (3.89)$$

$$\rho^k = C_4 \left(\|\epsilon^0\|_2^2 + \mu_t \|\delta_t^{(1)} \epsilon^0\|_2^2 + \sum_{i=1}^p \|\Lambda_{x_i}^{(\alpha_i)} \epsilon^1\|_2^2 + \tau \sum_{n=0}^{k-1} \|R^n\|_2^2 \right), \quad \forall k \in I_{N-1}, \quad (3.90)$$

$$\omega^k = \frac{1}{2} \|\delta_t^{(1)} \epsilon^k\|_2^2 + (1 - \eta_0) \sum_{i=1}^p \|\Lambda_{x_i}^{(\alpha_i)} \epsilon^k\|_2^2, \quad \forall k \in I_{N-1}. \quad (3.91)$$

Subtracting the second term of the right-hand side of (3.88) from both sides of that inequality assures that the hypotheses of Lemma 3.13 are satisfied. Using the conclusion of that result, the consistency property of our method and the homogeneous initial-boundary conditions of (3.87) we obtain that

$$\frac{1}{2} \|\delta_t^{(1)} \epsilon^k\|_2^2 + \sum_{i=1}^p \|\Lambda_{x_i}^{(\alpha_i)} \epsilon^k\|_2^2 \leq C_4 e^{C_5 k \tau} \tau \sum_{n=0}^{k-1} \|R^n\|_2^2 \leq C_6 (\tau^2 + \|h\|_2^2)^2, \quad \forall k \in I_{N-1}. \quad (3.92)$$

Here $C_6 = C_4 C^2 e^{C_5 T} T$ and C is the constant of Theorem 3.14. The conclusion of the theorem readily follows from the last inequality. \square

Finally, we provide some numerical approximations of the solution of problem (3.3) that show the capability of (3.28) to preserve the energy. The simulations were obtained using an implementation of our method in ©Matlab 8.5.0.197613 (R2015a) on a ©Sony Vaio PCG-5L1P laptop computer with Kubuntu 16.04 as operating system. In terms of computational times, we are aware that better results may be obtained with more modern equipment and more modest Linux/Unix distributions.

In a first stage, we consider undamped and damped one-dimensional forms of problem (3.3).

Example 3.17 (One-dimensional problem). Let $0 < \omega < 1$. In this example, we let $G(u) = 1 - \cos u$ for all $u \in \mathbb{R}$, and use the exact solution of the classical sine-Gordon equation described by

$$\varphi(x, t) = 4 \arctan \left(\frac{\sqrt{1 - \omega^2} \cos \omega t}{\omega \cosh \sqrt{1 - \omega^2} x} \right), \quad \forall (x, t) \in \mathbb{R} \times (\mathbb{R}^+ \cup \{0\}), \quad (3.93)$$

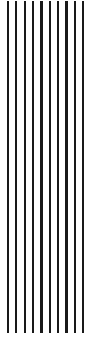
to prescribe the initial conditions. Computationally, we consider the domain $\Omega = (-30, 30) \times (0, 100)$,

$h_1 = 0.5$ and $\tau = 0.05$. Figure 3.2 shows the numerical solution (left column) and the associated energy density (right column) of the problem (3.3) obtained using (3.28) and (3.46), respectively, for $\omega = 0.9$ and $\gamma = 0$. Various derivative orders were used, namely, $\alpha_1 = 2$ (top row), $\alpha_1 = 1.6$ (middle row) and $\alpha_1 = 1.2$ (bottom row). The insets of the graphs of the right column represent the discrete dynamics of the total energy (3.40) of the system. The results show that the discrete total energy is conserved, in agreement with the theory established in this chapter and numerical results obtained through an implicit nonlinear numerical method [60]. We have used different computational parameters and the results (not presented here in view of their redundancy) show that the discrete total energy is likewise conserved. This qualitative behavior is in agreement with Theorem 3.8. \square

Example 3.18 (One-dimensional problem). Consider now the same problem as in Example 3.17, but letting $\gamma = 0.05$. The results of the simulations are shown in Figure 3.3. Obviously, in this case the quantities E^n are not conserved in view of the presence of a nonzero damping term. These results are in qualitative agreement with Theorem 3.8 and with the numerical simulations obtained in [60]. \square

We consider now the problem (3.3) in two spatial dimensions.

Example 3.19 (Two-dimensional problem). Let $\Omega = (-5, 5) \times (-5, 5) \times (0, 10)$, and define $G(u) = 1 - \cos u$ for each $u \in \mathbb{R}$. Consider the two-dimensional form of (3.3) with the initial conditions obtained using by $\varphi(x^2 + y^2, t)$, where φ is defined by (3.93) with $\omega = 0.8$. Under these circumstances, Figure 3.4 shows snapshots of the approximate solution of (3.3) at the times (a) $t = 0.22$, (b) $t = 0.34$, (c) $t = 0.46$, (d) $t = 0.58$, (e) $t = 0.70$ and (f) $t = 0.82$. The model parameters employed in this example were $\alpha_1 = 1.8$, $\alpha_2 = 1.6$ and $\gamma = 0$. Numerically, we used the method (3.28) with $M_1 = M_2 = 100$ and $N = 500$. The solutions appear to follow almost a periodic behavior. Moreover, Figure 3.5 shows the dynamics of the energy for various values of α_1 and α_2 , and different damping coefficients, namely, $\gamma = 0$ (solid), $\gamma = 0.01$ (dashed), $\gamma = 0.02$ (dashed-dotted) and $\gamma = 0.03$ (dotted). The results illustrate the fact that the total energy of the system is conserved in the case when $\gamma = 0$, while the system is dissipative if $\gamma \neq 0$. The results are in agreement with the theorems derived in this chapter. \square



Conclusions and discussions

Chapter 2 In this chapter, we considered a numerical method to approximate solutions of a semi-infinite nonlinear chain of coupled oscillators ruled by modified sine-Gordon equations harmonically driven at its end. The proposed finite-difference scheme is consistent order $\mathcal{O}(\Delta t)^2$ and we provided a necessary condition in order for the method to be stable order n . The process of nonlinear supratransmission for a coupled system of oscillators described by sine-Gordon equations was studied numerically under the scope of this numerical technique, and the dependence of supratransmission on damping was analyzed. Several conclusions can be drawn from our computational experiments on the sine-Gordon system of coupled oscillators (2.1). First of all, we have shown that the phenomenon of harmonic phonon quenching still appears in the presence of external and internal damping and that the discrepancy region due to phonon quenching is shortened as the external damping coefficient is increased, while it slightly widens as the internal damping coefficient increases. Second, the threshold value at which supratransmission first occurs for fixed frequencies outside the discrepancy region is seen to increase for both external and internal damping as the damping coefficient increases; both conclusions are clearly consequences of the dispersive and dissipative natures of the parameters β and γ , respectively.

It is worth noting that the bifurcation diagram for a value of the parameter β is approximately equal to the corresponding diagram for the undamped system shifted β horizontal units to the right. Likewise, a horizontal shift of $\sqrt{1+m^2}-1$ units in the bifurcation diagram of a sine-Gordon system of mass m with respect to the corresponding massless system is observed for small masses and frequencies outside the discrepancy region. At the same time, we have proposed a simple mathematical model to transmit binary information in discrete, semi-infinite chains of coupled oscillators using the process of nonlinear supratransmission. In the absence of dispersive and dissipative effects, our model (which is based on the modulation of amplitudes of source signals with constant frequency) has shown to be highly reliable for sufficiently long periods of single-bit generation, independently of the distance between the source of transmission and the point of reception.

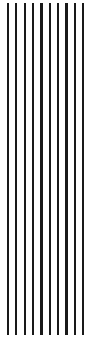
When weak damping is present the general picture does not change much. Stronger damping, however, manifests itself through a substantial decrease in the amplitude of the maximum local energy of the moving breathers with respect to the lattice site. In a forthcoming work, we will examine the possibility to overcome this problem via the concatenation of chain systems, where the driving at the beginning of each lattice will irradiate with an amplitude equal to a value just below its critical point

multiplied by the amplitude of the last site in the previous lattice. Finally, we wish to point out that the problem of determining whether it is possible to design a propagation system of binary signals in Josephson junction arrays still remains an open topic of research. Moreover, in view of the recently discovered phenomenon of nonlinear infratransmission (or lower-transmission, as named by the authors [47]), the problem of finding more efficient pathways to achieve signal transmission in other models is still an open question of general interest.

Chapter 3 In this chapter, we considered a damped fractional extension of the classical nonlinear wave equation in multiple spatial dimensions. The model under investigation is defined on a closed and bounded interval of the real line, and it considers the presence of a general nonlinear potential function that generalizes many particular models from mathematical physics, including the well-known sine-Gordon and Klein-Gordon equations from relativistic quantum mechanics. Moreover, in this paper we considered a space-fractional extension of the wave equation using Riesz fractional derivatives of orders in $(1, 2]$. We show here that the multidimensional model under investigation possesses energy functionals which are preserved under suitable assumptions on the boundary conditions and the parameters of the model. The exact resolution of the problem under study is a difficult mathematical task, so the design of numerical techniques that are capable of preserving discrete energy functions is a problem that merits further investigation.

Motivated by the analytical difficulties to provide exact solutions of our fractional wave equation, we designed an explicit finite-difference scheme to approximate its solutions. The numerical method is based on the use of fractional centered differences, which provide second-order consistent approximations of fractional-order derivatives. Using operator theory, we show that the multidimensional discrete fractional Laplacian is a positive and self-adjoint operator, whence the existence of a square root readily follows. This fact is employed then to propose a discrete energy functional of the numerical method which, under suitable conditions on the boundary conditions and the model parameters, is preserved at each discrete time. Additionally, the method is a second-order consistent discretization of the problem under investigation, and the simulations provided in this work show that the energy is conserved throughout time when the assumptions of the relevant theorems on energy preservation are satisfied. For the sake of convenience, a computer implementation of our method in the one-dimensional case is provided as an appendix.

This work was motivated by many seminal papers published by L. Vázquez and coworkers in the 1970s on the design of energy-preserving finite-difference schemes for nonlinear partial differential equations. Many nonlinear partial differential equations of integer order are known to possess energy functionals that are preserved under suitable boundary conditions, including models like the Schrödinger, the sine-Gordon and the nonlinear Klein-Gordon equations from relativistic quantum mechanics, just to mention some wave equations of physical relevance. Several groups of researchers have developed reliable numerical techniques to approximate the solutions of these and other nonlinear conservative systems as well as the constant energy functionals associated to them. On a personal note, the most notable contributions were the energy-preserving finite-difference methodologies proposed for the Schrödinger [99], the sine-Gordon [6, 26] and the nonlinear Klein-Gordon regimes [95]. Those works have been the sources of motivation for the numerical investigation carried out in the present manuscript. In many senses, these works constitute the formal birth of the discrete variational derivative method, whose use has been widely accepted in the specialized literature [31, 68, 32].



Bibliography

- [1] D. J.; Newell A. C. Ablowitz, M. J.; Kaup. Coherent pulse propagation, a dispersive, irreversible phenomenon. *J. Math. Phys.*, **15**:1852–1858, 1974.
- [2] Om P Agrawal. Formulation of Euler–Lagrange equations for fractional variational problems. *Journal of Mathematical Analysis and Applications*, 272(1):368–379, 2002.
- [3] S. Alexander, F. J.; Habib. Statistical Mechanics of Kinks in 1 + 1 Dimensions. *Phys. Rev. Lett.*, **71**:955–958, 1993.
- [4] Georgy Alifimov, Teresa Pierantozzi, and Luis Vázquez. Numerical study of a fractional sine-Gordon equation. In A. Le Mehuate, J. A. Tenreiro Machado, L. C. Trigeassou, and J. Sabatier, editors, *Fractional differentiation and its applications*, volume 4, pages 153–162, Bordeaux, France, July 2004. Proceedings of the IFAC-FDA Workshop.
- [5] F.; Magee C. J.; Scott A. C. Barone, A.; Esposito. Theory and Applications of the Sine-Gordon Equation. *Riv. Nuovo Cim.*, **1**:227–267, 1971.
- [6] Guo Ben-Yu, Pedro J Pascual, María J Rodriguez, and Luis Vázquez. Numerical solution of the sine-Gordon equation. *Applied Mathematics and Computation*, 18(1):1–14, 1986.
- [7] Fernanda PC Benetti, Ana C Ribeiro-Teixeira, Renato Pakter, and Yan Levin. Nonequilibrium stationary states of 3D self-gravitating systems. *Physical Review Letters*, 113(10):100602, 2014.
- [8] AH Bhrawy and MA Zaky. Highly accurate numerical schemes for multi-dimensional space variable-order fractional Schrödinger equations. *Computers & Mathematics with Applications*, 73(6):1100–1117, 2017.
- [9] T. Bishop, A. R.; Schneider, editor. *Solitons and Condensed Matter Physics*. Springer-Verlag, New York, 1981.
- [10] Matteo Bonforte and Juan Luis Vázquez. A priori estimates for fractional nonlinear degenerate diffusion equations on bounded domains. *Archive for Rational Mechanics and Analysis*, 218(1):317–362, 2015.
- [11] Alessandro Campa, Thierry Dauxois, and Stefano Ruffo. Statistical mechanics and dynamics of solvable models with long-range interactions. *Physics Reports*, 480(3):57–159, 2009.

- [12] M. C. Cattaneo. Sulla Conduzione de Calor. *Atti Sem. Matem. e Fis. Della U. Modena*, **3**:3, 1948.
- [13] Cem Çelik and Melda Duman. Crank–Nicolson method for the fractional diffusion equation with the Riesz fractional derivative. *Journal of Computational Physics*, 231(4):1743–1750, 2012.
- [14] Vasileios Chatziioannou and Maarten van Walstijn. Energy conserving schemes for the simulation of musical instrument contact dynamics. *Journal of Sound and Vibration*, 339:262–279, 2015.
- [15] Guangye Chen and Luis Chacon. A multi-dimensional, energy-and charge-conserving, nonlinearly implicit, electromagnetic vlasov–darwin particle-in-cell algorithm. *Computer Physics Communications*, 197:73–87, 2015.
- [16] Shiping Chen, Fawang Liu, and Kevin Burrage. Numerical simulation of a new two-dimensional variable-order fractional percolation equation in non-homogeneous porous media. *Computers & Mathematics with Applications*, 68(12):2133–2141, 2014.
- [17] Helen Christodoulidi, Tassos Bountis, Constantino Tsallis, and Lambros Drossos. Chaotic behavior of the Fermi–Pasta–Ulam β –model with different ranges of particle interactions. *Journal of Statistical Mechanics*, 12(12):123206, 2016.
- [18] Helen Christodoulidi, Constantino Tsallis, and Tassos Bountis. Fermi-Pasta-Ulam model with long-range interactions: Dynamics and thermostatics. *EPL (Europhysics Letters)*, 108(4):40006, 2014.
- [19] J. A.; Bishop A. R.; Trullinger S. E. Currie, J. F.; Krumhansl. Statistical Mechanics of One-Dimensional Solitary-Wave-Bearing Scalar Fields: Exact Results and Ideal-Gas Phenomenology. *Phys. Rev. B*, **22**:477–496, 1980.
- [20] Arturo de Pablo, Fernando Quirós, Ana Rodríguez, and Juan Luis Vázquez. A fractional porous medium equation. *Advances in Mathematics*, 226(2):1378–1409, 2011.
- [21] C.; Smereka P. Doering, C. R.; Mueller. Interacting Particles, the Fisher-Kolmogorov-Petrovsky-Piscounov Equation, and Duality. *Physica A*, **325**:243–259, 2003.
- [22] R. S. Drazin, P. G.; Johnson, editor. *Solitons: An Introduction*. Cambridge University Press, Cambridge, first edition, 1989.
- [23] Raffaele D’Ambrosio, Giuseppe De Martino, and Beatrice Paternoster. Numerical integration of Hamiltonian problems by G-symplectic methods. *Advances in Computational Mathematics*, 40(2):553–575, 2014.
- [24] Lukas Einkemmer and Matthias Wiesenberger. A conservative discontinuous galerkin scheme for the 2d incompressible navier–stokes equations. *Computer Physics Communications*, 185(11):2865–2873, 2014.
- [25] U.ENZ. Discrete Mass, Elementary Length, and a Topological Invariant as a Consequence of a Relativistic Invariant Variational Principle. *Phys. Rev.*, **131**:1392–1394, 1963.

- [26] Zhang Fei and Luis Vázquez. Two energy conserving numerical schemes for the sine-Gordon equation. *Applied Mathematics and Computation*, 45(1):17–30, 1991.
- [27] R. A. Fisher. The Wave of Advance of Advantageous Genes. *Annals of Eugenics*, 7:355–369, 1937.
- [28] J. B. J. Fourier, editor. *Théorie Analytique de la Chaleur*. Firmin Didot, Paris, 1822.
- [29] Avner Friedman. *Foundations of modern analysis*. Courier Corporation, New York, 1970.
- [30] Daisuke Furihata. Finite difference schemes for $\frac{\partial u}{\partial t} = \left(\frac{\partial u}{\partial t}\right)^\alpha \frac{\delta G}{\delta u}$ that inherit energy conservation or dissipation property. *Journal of Computational Physics*, 156(1):181–205, 1999.
- [31] Daisuke Furihata. Finite-difference schemes for nonlinear wave equation that inherit energy conservation property. *Journal of Computational and Applied Mathematics*, 134(1):37–57, 2001.
- [32] Daisuke Furihata and Takayasu Matsuo. *Discrete variational derivative method: A structure-preserving numerical method for partial differential equations*. CRC Press, New York, 2010.
- [33] Yali Gao, Liquan Mei, and Rui Li. A time-splitting galerkin finite element method for the davey–stewartson equations. *Computer Physics Communications*, 197:35–42, 2015.
- [34] J. Geniet, F.; Leon. Energy transmission in the forbidden band gap of a nonlinear chain. *Phys. Rev. Lett.*, 89:134102, 2002.
- [35] J. Geniet, F.; Leon. Nonlinear supratransmission. *J. Phys.: Condens. Matter*, 15:2933–2949, 2003.
- [36] I. N.; Moroz I. N. Gibbon, J. D.; James. The Sine-Gordon Equation as a Model for a Rapidly Rotating Baroclinic Fluid. *Phys. Script.*, 20:402–408, 1979.
- [37] Walter G Glöckle and Theo F Nonnenmacher. A fractional calculus approach to self-similar protein dynamics. *Biophysical Journal*, 68(1):46–53, 1995.
- [38] Rudolf Gorenflo, Francesco Mainardi, Daniele Moretti, Gianni Pagnini, and Paolo Paradisi. Discrete random walk models for space–time fractional diffusion. *Chemical physics*, 284(1):521–541, 2002.
- [39] F. Hasegawa, A.; Tappert. Transmission of stationary nonlinear optical pulses in dispersive dielectric fibers. i. anomalous dispersion. *Appl. Phys. Lett.*, 23:142–144, 1973.
- [40] Rudolf Hilfer. *Applications of fractional calculus in physics*. World Scientific, Singapore, 2000.
- [41] H. Hochstadt, editor. *The Functions of Mathematical Physics*. Dover Publications, Inc., New York, 1986.
- [42] Eleanor W Jenkins, Chris Paribello, and Nicholas E Wilson. Discrete mass conservation for porous media saturated flow. *Numerical Methods for Partial Differential Equations*, 30(2):625–640, 2014.

- [43] K Jörgens. Das Anfangswertproblem im Grossen für eine Klasse nichtlinearer Wellengleichungen. *Math. Zeit.*, **77**:295–308, 1961.
- [44] B. D. Josephson. PhD thesis, Cambridge University, Cambridge, England, 1964.
- [45] B. D. Josephson. Supercurrents Through Barriers. *Adv. Phys.*, **14**:419–451, 1965.
- [46] Hammad Khalil and Rahmat Ali Khan. A new method based on legendre polynomials for solutions of the fractional two-dimensional heat conduction equation. *Computers & Mathematics with Applications*, 67(10):1938–1953, 2014.
- [47] S.; Ruffo S. Khomeriki, R.; Lepri. Nonlinear supratransmission and bistability in the fermi-pasta-ulam model. *Phys. Rev. E*, **70**:066626, 2004.
- [48] RC Koeller. Applications of fractional calculus to the theory of viscoelasticity. *ASME, Transactions, Journal of Applied Mechanics(ISSN 0021-8936)*, 51:299–307, 1984.
- [49] I.; Piscounoff N. Kolmogorov, A.; Petrovsky. Étude de l'équations de la diffusion avec croissance de la quantité de matière et son application a un problème biologique. *Bull. Univ. Moskou, Ser. Internat.*, **1A**:1–25, 1937.
- [50] J. R. Krumhansl, J. A.; Schrieffer. Dynamics and Statistical Mechanics of a One-Dimensional Model Hamiltonian for Structural Phase Transitions. *Phys. Rev. B*, **11**:3535–3545, 1975.
- [51] G. L. Lamb Jr. Analytical Descriptions of Ultrashort Optical Pulse Propagation in a Resonant Medium. *Rev. Mod. Phys.*, **49**:99–124, 1971.
- [52] Nick Laskin. Fractional Schrödinger equation. *Physical Review E*, 66(5):056108, 2002.
- [53] H. M. Lieberstein. *Theory of Differential Equations*. Academic Press, New York, first edition, 1972.
- [54] Konstantin Lipnikov, Gianmarco Manzini, and Mikhail Shashkov. Mimetic finite difference method. *Journal of Computational Physics*, 257:1163–1227, 2014.
- [55] O. H.; Christiansen P. L. Lomdahl, P. S.; Soerensen. Soliton Excitations in Josephson Tunnel Junctions. *Phys. Rev. B*, **25**(9):5737–5748, 1982.
- [56] Yu Lu, An-kang Hu, and Ya-chong Liu. A finite pointset method for the numerical simulation of free surface flow around a ship. *Journal of Marine Science and Technology*, 21(2):190–202, 2016.
- [57] Yuesheng Luo, Xiaole Li, and Cui Guo. Fourth-order compact and energy conservative scheme for solving nonlinear Klein-Gordon equation. *Numerical Methods for Partial Differential Equations*, in press:doi:10.1002/num.22143, 2017.
- [58] A. Macías-Díaz, J. E.; Puri. A numerical method for computing radially symmetric solutions of a dissipative nonlinear modified klein-gordon equation. *Num. Meth. Part. Diff. Eq.*, **21**:998–1015, 2005.

- [59] A. Macías-Díaz, J. E.; Puri. An energy-based computational method in the analysis of the transmission of energy in a chain of coupled oscillators. *Appl. Num. Anal. & Comp. Math.*, , 2006. submitted.
- [60] J E Macías-Díaz. *Journal of Computational Physics*, submitted for publication, 2017.
- [61] J E Macías-Díaz. Existence and uniqueness of positive and bounded solutions of a discrete population model with fractional dynamics. *Discrete Dynamics in Nature and Society*, 2017, 2017.
- [62] J E Macías-Díaz. Numerical study of the process of nonlinear supratransmission in Riesz space-fractional sine-Gordon equations. *Communications in Nonlinear Science and Numerical Simulation*, 46:89–102, 2017.
- [63] J E Macías-Díaz. Persistence of nonlinear hysteresis in fractional models of Josephson transmission lines. *Communications in Nonlinear Science and Numerical Simulation*, 53:31–43, 2017.
- [64] J E Macías-Díaz. Numerical simulation of the nonlinear dynamics of harmonically driven Riesz-fractional extensions of the Fermi–Pasta–Ulam chains. *Communications in Nonlinear Science and Numerical Simulation*, 55:248–264, 2018.
- [65] J E Macías-Díaz and J Villa-Morales. A deterministic model for the distribution of the stopping time in a stochastic equation and its numerical solution. *Journal of Computational and Applied Mathematics*, 318:93–106, 2017.
- [66] V. G. Makhanov, A. R. Bishop, and D. D. Holm, editors. *Nonlinear Evolution Equations and Dynamical Systems Needs '94; Los Alamos, NM, USA 11-18 September '94: 10th International Workshop*. World Scientific Pub. Co. Inc., Singapore, first edition, 1995.
- [67] W. P. Mason, editor. *Physical Acoustics, Vol. III*. Academic Press, New York, first edition, 1966.
- [68] Takayasu Matsuo and Daisuke Furihata. Dissipative or conservative finite-difference schemes for complex-valued nonlinear partial differential equations. *Journal of Computational Physics*, 171(2):425–447, 2001.
- [69] E. L. McCall, S. L.; Hahn. Self-induced transparency. *Phys. Rev.*, **183**:457–485, 1969.
- [70] J.; McGee, H.; McInerney and A. Harrus. The Virtual Cook: Modeling Heat Transfer in the Kitchen. *Physics Today*, **52**:30–36, 1999.
- [71] Adriana Miele and Job Dekker. Long-range chromosomal interactions and gene regulation. *Molecular biosystems*, 4(11):1046–1057, 2008.
- [72] L. F. Mollenauer, R. H. Stolen, and J. P. Gordon. Experimental observation of picosecond pulse narrowing and solitons in optical fibers. *Phys. Rev. Lett.*, **45**:1095–1098, 1980.
- [73] W. A. Morawetz, C. S.; Strauss. Decay and scattering of solutions of a nonlinear relativistic wave equation. *Comm. Pure and Appl. Math.*, **25**:1–31, 1972.

- [74] Victor Namias. The fractional order Fourier transform and its application to quantum mechanics. *IMA Journal of Applied Mathematics*, 25(3):241–265, 1980.
- [75] Hosein Nasrolahpour. A note on fractional electrodynamics. *Communications in Nonlinear Science and Numerical Simulation*, 18(9):2589–2593, 2013.
- [76] A. H. Nayfeh. *Perturbation Methods*. Wiley and Sons, New York, NY, first edition, 1993.
- [77] Kuo Pen-Yu. Numerical methods for incompressible viscous flow. *Scientia Sinica*, 20:287–304, 1977.
- [78] T. H. Perring, K. K.; Skyrme. A Model Uniform Field Equation. *Nucl. Phys.*, **31**:550–555, 1962.
- [79] V. G. Pimenov, A. S. Hendy, and R. H. De Staelen. On a class of non-linear delay distributed order fractional diffusion equations. *Journal of Computational and Applied Mathematics*, 318:433–443, 2017.
- [80] Luís Pinto and Ercília Sousa. Numerical solution of a time-space fractional Fokker Planck equation with variable force field and diffusion. *Communications in Nonlinear Science and Numerical Simulation*, 50:211–228, 2017.
- [81] V. F. Polyanin, A. D.; Zaitsev. *Handbook of Nonlinear Partial Differential Equations*. Chapman & Hall CRC Press, Boca Raton, Fla., first edition, 2004.
- [82] YZ Povstenko. Theory of thermoelasticity based on the space-time-fractional heat conduction equation. *Physica Scripta*, 2009(T136):014017, 2009.
- [83] E. I. Rashba and M. D. Sturge, editors. *Excitons*. North Holland, Amsterdam, 1982.
- [84] S Saha Ray. A new analytical modelling for nonlocal generalized Riesz fractional sine-Gordon equation. *Journal of King Saud University-Science*, 28(1):48–54, 2016.
- [85] M. Remoissenet. *Waves Called Solitons*. Springer-Verlag, New York, third edition, 1999.
- [86] H. Royden. *Real Analysis*. Prentice Hall, New York, third edition, 1988.
- [87] S Sahoo and S Saha Ray. Improved fractional sub-equation method for $(3+ 1)$ -dimensional generalized fractional KdV–Zakharov–Kuznetsov equations. *Computers & Mathematics with Applications*, 70(2):158–166, 2015.
- [88] Alberto Sapora, Pietro Cornetti, and Alberto Carpinteri. Wave propagation in nonlocal elastic continua modelled by a fractional calculus approach. *Communications in Nonlinear Science and Numerical Simulation*, 18(1):63–74, 2013.
- [89] Enrico Scalas, Rudolf Gorenflo, and Francesco Mainardi. Fractional calculus and continuous-time finance. *Physica A: Statistical Mechanics and its Applications*, 284(1):376–384, 2000.
- [90] I. E. Segal. The Global Cauchy problem for a relativistic scalar field with power interaction. *Bull. Soc. Math. Fr.*, **91**:129–135, 1963.

- [91] J. D. Sherratt, J. A.; Murray. Models of Epidermal Wound Healing. *Proc. Biol. Sci.*, **241**(1300):29–36, 1990.
- [92] T. H. R. Skyrme. A Nonlinear Theory of Strong Interactions. *Proc. Roy. Soc. London*, **A247**:260–278, 1958.
- [93] T. H. R. Skyrme. Particle States of a Quantized Meson Field. *Proc. Roy. Soc. London*, **A262**:237–245, 1961.
- [94] L. Strauss, W. A.; Vázquez. Numerical Solution of a Nonlinear Klein-Gordon Equation. *J. Comput. Phys.*, **28**:271–278, 1978.
- [95] Walter Strauss and Luis Vázquez. Numerical solution of a nonlinear Klein-Gordon equation. *Journal of Computational Physics*, 28(2):271–278, 1978.
- [96] Ninghu Su, Paul N. Nelson, and Sarah Connor. The distributed-order fractional diffusion-wave equation of groundwater flow: Theory and application to pumping and slug tests. *Journal of Hydrology*, 529, Part 3:1262–1273, 2015.
- [97] M. Tabor. *Chaos and Integrability in Nonlinear Dynamics: An Introduction*. John Wiley and Sons, New York, 1989.
- [98] William T Taitano, Luis Chacón, AN Simakov, and K Molvig. A mass, momentum, and energy conserving, fully implicit, scalable algorithm for the multi-dimensional, multi-species Rosenbluth–Fokker–Planck equation. *Journal of Computational Physics*, 297:357–380, 2015.
- [99] Y-F Tang, L Vázquez, F Zhang, and VM Pérez-García. Symplectic methods for the nonlinear Schrödinger equation. *Computers & Mathematics with Applications*, 32(5):73–83, 1996.
- [100] Vasily E Tarasov. Fractional generalization of gradient and Hamiltonian systems. *Journal of Physics A: Mathematical and General*, 38(26):5929, 2005.
- [101] Vasily E Tarasov. Continuous limit of discrete systems with long-range interaction. *Journal of Physics A: Mathematical and General*, 39(48):14895, 2006.
- [102] Vasily E Tarasov and Elias C Aifantis. Non-standard extensions of gradient elasticity: Fractional non-locality, memory and fractality. *Communications in Nonlinear Science and Numerical Simulation*, 22(1):197–227, 2015.
- [103] Vasily E Tarasov and George M Zaslavsky. Fractional dynamics of coupled oscillators with long-range interaction. *Chaos: An Interdisciplinary Journal of Nonlinear Science*, 16(2):023110, 2006.
- [104] Vasily E Tarasov and George M Zaslavsky. Fractional dynamics of systems with long-range interaction. *Communications in Nonlinear Science and Numerical Simulation*, 11(8):885–898, 2006.
- [105] Vasily E Tarasov and George M Zaslavsky. Conservation laws and Hamilton’s equations for systems with long-range interaction and memory. *Communications in Nonlinear Science and Numerical Simulation*, 13(9):1860–1878, 2008.

- [106] J. W. Thomas. *Numerical Partial Differential Equations*. Springer-Verlag, New York, first edition, 1995.
- [107] Philipp Trisjono, Seongwon Kang, and Heinz Pitsch. On a consistent high-order finite difference scheme with kinetic energy conservation for simulating turbulent reacting flows. *Journal of Computational Physics*, 327:612–628, 2016.
- [108] A. V. Ustinov. Solitons in josephson junctions. *Physica D*, 123:315–329, 1998.
- [109] J.; Oboznov V. A. Ustinov, A. V.; Mygind. Phase-locked flux-flow josephson oscillator. *J. Appl. Phys.*, 72:1203–1205, 1992.
- [110] J.; Pedersen N. F.; Oboznov V. A. Ustinov, A. V.; Mygind. Millimeter-wave-induced fluxon pair creation in flux-flow josephson oscillators. *Phys. Rev. B*, 46:578–580, 1992.
- [111] M.; Duwel A. E. Trias E.; Orlando T. P.; Watanabe S.; Strogatz S. van der Zant, H. S. J.; Barahona. Dynamics of one-dimensional josephson-junction arrays. *Physica D*, 119:219–226, 1998.
- [112] Juan Luis Vázquez. Nonlinear diffusion with fractional Laplacian operators. In *Nonlinear partial differential equations*, pages 271–298. Springer, 2012.
- [113] D. Vvedensky. *Partial Differential Equations with Mathematica*. University Press, Cambridge, Great Britain, first edition, 1993.
- [114] P. R. Wallace. *Mathematical Analysis of Physical Problems*. Dover, New York, first edition, 1984.
- [115] Dongling Wang, Aiguo Xiao, and Xueyang Li. Parametric symplectic partitioned runge–kutta methods with energy-preserving properties for hamiltonian systems. *Computer Physics Communications*, 184(2):303–310, 2013.
- [116] Pengde Wang and Chengming Huang. An energy conservative difference scheme for the nonlinear fractional Schrödinger equations. *Journal of Computational Physics*, 293:238–251, 2015.
- [117] Peicheng Yu, Xinlu Xu, Adam Tableman, Viktor K Decyk, Frank S Tsung, Frederico Fiuza, Asher Davidson, Jorge Vieira, Ricardo A Fonseca, Wei Lu, et al. Mitigation of numerical cerenkov radiation and instability using a hybrid finite difference-fft maxwell solver and a local charge conserving current deposit. *Computer Physics Communications*, 197:144–152, 2015.
- [118] M. D. Zabusky, N. J.; Kruskal. Interaction of Solitons in a Collisionless Plasma and the Recurrence of the Initial State. *Phys. Rev. Lett.*, 15:240–243, 1965.
- [119] Li Zhu and Qibin Fan. Numerical solution of nonlinear fractional-order Volterra integro-differential equations by SCW. *Communications in Nonlinear Science and Numerical Simulation*, 18(5):1203–1213, 2013.
- [120] D. Zwillinger. *Handbook of Differential Equations*. Academic Press, Boston, MA, third edition, 1997.